International
WOCE
Newsletter

Number 37 ISSN 1029-1725 December 1999

IN THIS ISSUE

News from the WOCE IPO

W. John Gould, Director, WOCE IPO and ICPO, Southampton Oceanography Centre, UK. john.gould@soc.soton.ac.uk

WOCE → CLIVAR → GOOS/GCOS

A number of meetings over the past months have demonstrated the clear transition that is now going on from the undoubted success of WOCE to the broader new WCRP project CLIVAR and ultimately towards a new concept for most researchers-sustained activities needed to provide operational observations (and modelling) of the ocean. This transition is evident in the content and outcome of a series of meeting that have been held in the past 2 months.

The WOCE SSG met in La Jolla, California, in mid-October. The venue gave the SSG a chance to hear at first hand about the activities of the WOCE Hydrographic Programme Office that is compiling the WOCE One-Time and Repeat Hydrography into a readily available, high quality data set. The report of the SSG meeting is about to be published. The following are action items that you should be immediately aware of. It is planned to produce a series of hard copy (and electronic) atlases of WOCE hydrographic data to be freely available to researchers and libraries. The production is already partially funded but additional funding is being sought. If anyone knows of organisations that are likely to be receptive to bids for the printing of the Atlases please let me know.

The SSG was happy with the progress of the WOCE workshops – a report of the N. Atlantic one and the announcement of the variability/representativeness one are in this issue. Planning will start for a global workshop on oceanic fluxes in 2001 and consideration is being given to holding one on bottom-induced mixing.

About WOCE

The World Ocean Circulation Experiment (WOCE) is a component of the World Climate Research Programme (WCRP), which was established by WMO and ICSU, and is carried out in association with IOC and SCOR.

WOCE is an unprecedented effort by scientists from more than 30 nations to study the large-scale circulation of the ocean. In addition to global observations furnished by satellites, conventional in-situ physical and chemical observations have been made in order to obtain a basic description of the physical properties and circulation of the global ocean during a limited period.

The field phase of the project lasted from 1990–1997 and is now being followed by Analysis, Interpretation, Modelling and Synthesis activities. This, the AIMS phase of WOCE, will continue to the year 2002.

The information gathered during WOCE will provide the data necessary to make major improvements in the accuracy of numerical models of ocean circulation. As these models improve, they will enhance coupled models of the ocean/atmosphere circulation to better simulate – and perhaps ultimately predict – how the ocean and the atmosphere together cause global climate change over long periods.

WOCE is supporting regional experiments, the knowledge from which should improve circulation models, and it is exploring design criteria for long-term ocean observing system.

The scientific planning and development of WOCE is under the guidance of the Scientific Steering Group for WOCE, assisted by the WOCE International Project Office (WOCE IPO):

- W. John Gould, *Director*
- Peter M. Saunders, *Staff Scientist*
- N. Penny Holliday, *Project Scientist*
- Roberta Boscolo, *Project Scientist*
- Sheelagh Collyer, *Publication Assistant*
- Jean C. Haynes, *Administrative Assistant*

For more information please visit:
http://www.soc.soton.ac.uk/OTHERS/woceipo/ipo.html

WOCE → CLIVAR → GOOS/GCOS (continued)

The SSG were informed about the progress on the compilation of the WOCE Conference Book. Since contributions are still being received the Editors and publisher feel that it is still to early to advertise the book so please be patient.

Shortly after SSG meeting I attended the Ocean Observing System for Climate (usually known as OceanObs'99) meeting in St Raphael. It considered the case and observational strategies for a wide variety sustained ocean observations. I presented a paper co-authored by John Toole and 16 other contributors on sustained deep ocean hydrography. This triggered substantial discussion about the need for such measurements in the deep Pacific. The OceanObs organisers are working on a conference statement that will summarise the meeting's conclusions. A draft is available at http://www.bom.gov.au/OceanObs99 as are the texts of the invited papers.

The Saturday following OceanObs (and incidentally the first day that week that it had not poured with rain) the CLIVAR Data Task Team met. Again the final outcome of the meeting is being agreed but one key action was that the DTT provided support for many elements of the existing WOCE data system since they saw these as the most effective means of handling many types of ocean data in CLIVAR. The DTT (and WOCE SSG) was concerned that the mechanisms for handling the profile and trajectory data from the increasing numbers of profiling floats were still unclear and this matter requires attention.

In this issue

We have been gratified with the large number of contributions we have received that came from the N. Atlantic Workshop. You will see that they cover a wide range of topics and areas – modelling and observations, tropics to subpolar. Fritz Schott has kindly summarised the outcome of the workshop. Of course there is lots of other science in this issue and I especially draw your attention to the announcement about the next workshop in Kyushu in October 2000.

A task for WOCE will be to document what was measured, where, when and by whom. The collection and checking of this information is a huge task and an announcement explains what is involved.

And finally…

All of us in the WOCE IPO send you our best wishes for Christmas and for the coming year. We will soon find out whether we are Y2K compliant!

Mode waters in the subpolar North Atlantic in historical data and during the WOCE period

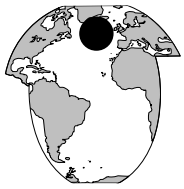

Lynne D. Talley, Scripps Institution of Oceanography, USA. lynne@gyre.ucsd.edu

A principal focus of observational upper ocean work in the subpolar North Atlantic is the transformation of inflowing warm, saline subtropical waters into the precursors of intermediate water formed in the Labrador Sea and deep water formed in the Nordic Seas. This constitutes the local upper ocean limb of the meridional overturning circulation whose amplitude is calculated variously at about 15 to 20 Sv. This is the surface layer whose characteristics directly influence the atmosphere, and thus whose transformation is directly relevant to climate.

Conventional circulation analyses show a branching of the Gulf Stream and North Atlantic Current feeding the cyclonic subpolar circulation, which is sometimes depicted with broad northward flow in the eastern subpolar region, splitting into surface flow into the Norwegian Sea and westward flow along the northern margin and into the Irminger Current which feeds into the Labrador Sea. Ample evidence for incursion of lower latitude properties has been demonstrated. Mass, heat and salt budgets for the transformation of upper ocean waters around the subpolar gyre have been computed (e.g. McCartney and Talley, 1984). However, the seasonal transformation with careful local flux budgets, and description of the actual transformation process as tied to the fluxes and local circulation has not heretofore been accomplished and is a goal of the WOCE Atlantic Circulation and Climate Experiment (ACCE).

The upper ocean waters of the subpolar gyre are characterised by thick layers of low stability (Subpolar Mode Water – SPMW), assumed to originate as deep mixed layers in winter. In general these layers are more than 400 m thick, ranging up to more than 600 m, and then to 1500 during intermediate depth convection in the Labrador Sea (McCartney and Talley, 1982). The SPMW was depicted therein as moving smoothly eastward and then northward and thence cyclonically around the subpolar gyre into the Labrador Sea, with an initial potential temperature and density of 14°C and 26.9 σ_θ just south of the North Atlantic Current loop, varying smoothly around the gyre to

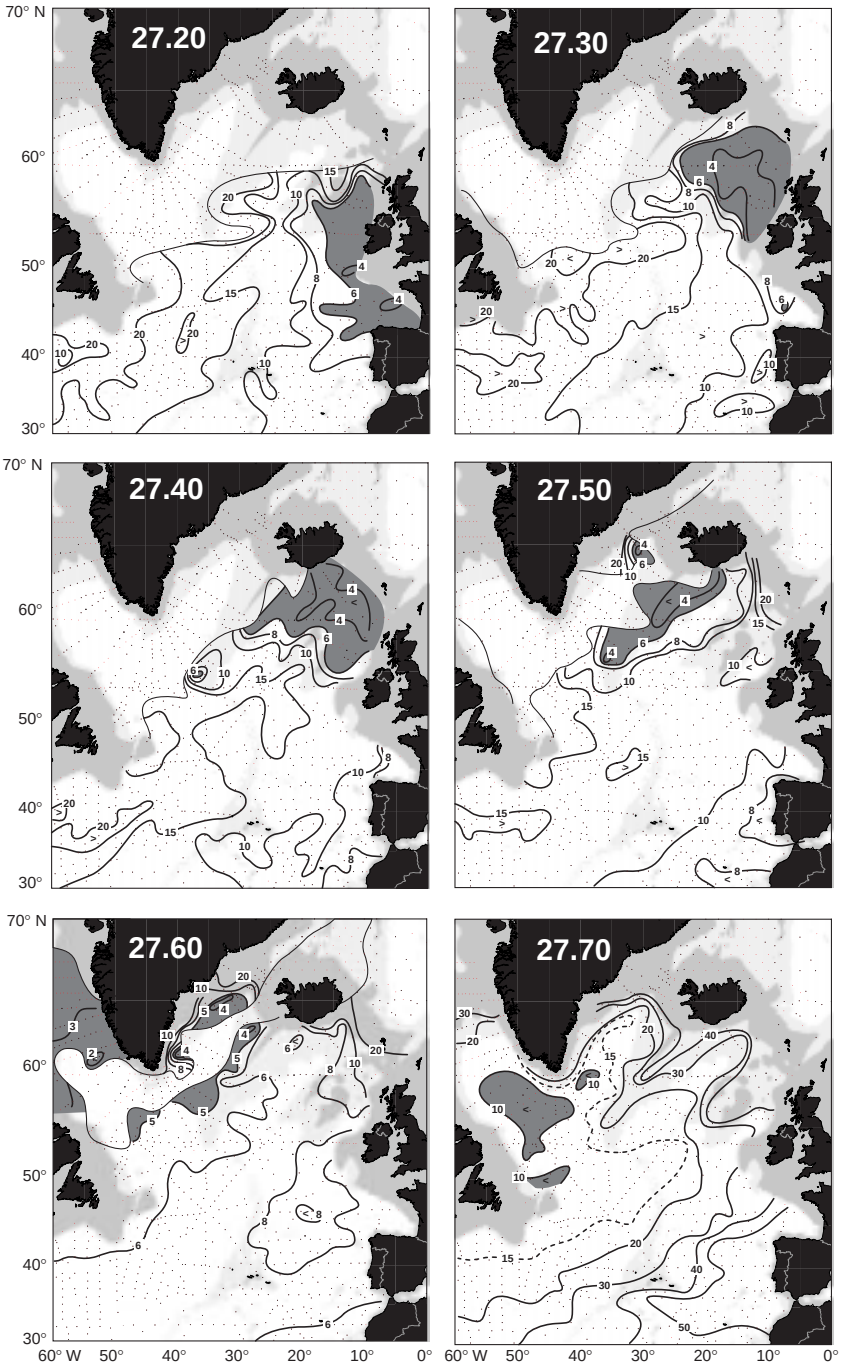

Figure 1. Isopycnic potential vorticity ($\times 10^{-13}$ cm^{-1} sec^{-1}) based on the Reid (1994) data set, most of which was collected in the late 1950s and 1960s, during a period of low North Atlantic Oscillation index. PV less than 4×10^{-13} cm^{-1} sec^{-1} at 27.2 to 27.5 σ_θ is darker shaded; each of these isopycnals has a similar range of PV. The shaded region at 27.6 σ_θ is less than 5×10^{-13} cm^{-1} sec^{-1}, since PV is somewhat higher on this isopycnal. The shaded region at 27.7 σ_θ is less than 1×10^{-13} cm^{-1} sec^{-1} since PV is generally lower at this density, which lies at the top of the Labrador Sea Water layer.

finally arrive at the Labrador Sea Water (LSW) properties of about 3°C/27.84 σ_θ. The North Atlantic Current jet was the fulcrum of this cyclonic movement. Southward subduction of the 27.1 and 27.2 σ_θ waters of the eastern region into the subtropical gyre is also observed.

The preliminary analysis of SPMW presented here, using both historical and recent WOCE data, contradicts this smooth picture of SPMW property distribution and advection. Further analysis combining additional hydrography, float observations, satellite and surface flux fields is being pursued to clarify the transformation and circulation of SPMW. This preliminary work is presented because the new maps of SPMW distribution provide a rather different view of SPMW than earlier work. Because of significant temporal variations in surface and water mass properties, linked to the North Atlantic Oscillation, data must be sorted in time. The analysis below uses historical data collected during the 1950s and 1960s for comprehensive mapping of the SPMW. WOCE data collected during the summer of 1997 are then used to show greater detail within highly-resolved vertical sections; SPMW properties are contrasted with those of the low NAO 1950s/1960s period.

Subpolar Mode Water using historical hydrographic data

Subpolar Mode Water (SPMW) for the 1950s and 1960s is mapped here using data assembled by Reid (1994). During that time, the NAO was in a protracted low phase, and so it is expected that the data set, while covering many years, is reasonably uniform. It was relatively easy to create maps from the data set, suggesting that the data set is internally consistent. This data set has much better spatial resolution than the more limited data set used in McCartney and Talley (1982) who first described the SPMW; the more limited data set is included in the Reid data set.

Isopycnic potential vorticity ($f\partial\rho / \rho\partial z$) was calculated from the historical bottle data as outlined first in Talley and McCartney (1982). PV was mapped on isopycnals at every 0.1 σ_θ from 26.8 to 27.7 σ_θ. Maps for 27.2 to 27.7 σ_θ are shown in Fig. 1. Low PV indicates a relatively thick layer. On all isopycnals, low potential vorticity occurs near the isopycnal surface outcrop, and hence is bounded by a high lateral gradient of PV on the outcrop margin. The thickest layers proceed from the Bay of Biscay at 27.2 σ_θ, to Rockall Trough/Plateau at 27.3 σ_θ, to the south side of the Iceland–Scotland Ridge at 27.4 σ_θ, to along the Reykjanes Ridge at 27.5 σ_θ, around the perimeter of the outcrop in the Irminger Basin at 27.6 σ_θ, to the central Labrador Sea at 27.7 σ_θ. The last distribution is very similar to that of the denser LSW (Talley and McCartney, 1982). In contrast to the smooth, wide SPMW distribution shown in McCartney and Talley (1982), these maps show that the deep mixed layers are strongly confined to the boundary regions. The most extreme low PV is mostly associated with topography – the shelf around the UK, Rockall Plateau/Hatton Bank, the Iceland–Scotland Ridge, the Reykjanes Ridge and the Greenland Shelf. This could be due variously to strong eddies forming near the margins, sluggish circulation in these regions, or enhanced mixing over topography, possibly due to large tidal dissipation. Measurements do not extend up on to the shelves in general in this data set and so the importance of mixing on the shelves was not evaluated.

The density of the SPMW potential vorticity minimum (Fig. 2) shows the tight North Atlantic Current, turning northward after crossing the Reykjanes Ridge, and a fanning of isopycnals from this tight feature. In contrast to the picture of McCartney and Talley (1982), this more detailed view suggests that the warmer mode waters south of 50°N (27.0 to 27.15 σ_θ or so) are mainly associated with the subtropical circulation and move southward, as described in McCartney (1982). The SPMW that proceeds into NADW formation more likely originates directly from the North Atlantic Current waters. Little SPMW is found between 27.2 and 27.3 σ_θ; this is likely the primary bifurcation density between the subtropical and subpolar circulations. A large area of SPMW around 27.4 σ_θ is found in the northeast, and a large area of density 27.5 σ_θ is located over the western flank of the Reykjanes Ridge and most of the Irminger Basin. The very lowest potential vorticity at the minimum is shaded in the figure, and shows the importance of the ridge complexes.

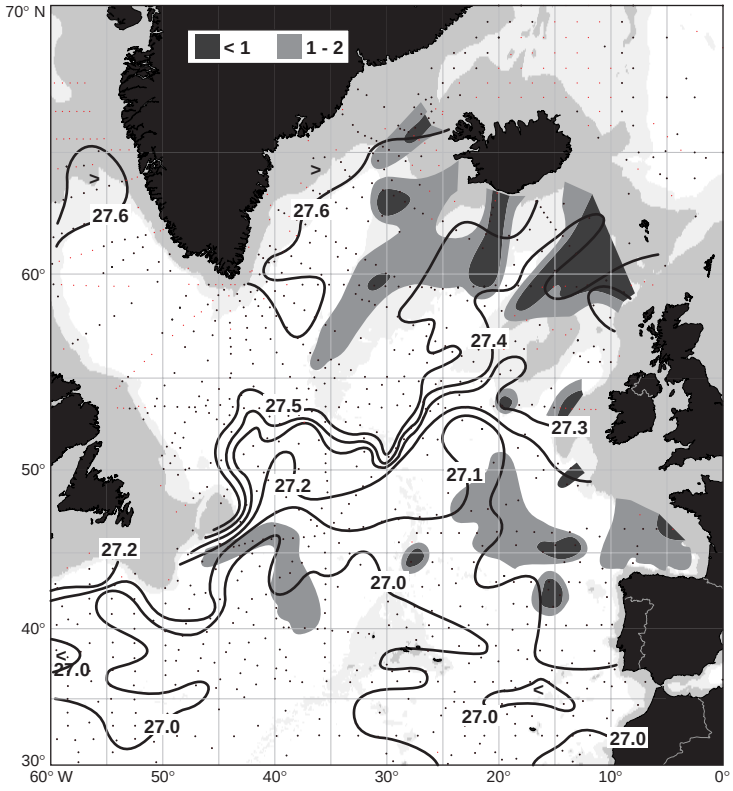

Figure 2. Potential density σ_θ at the absolute potential vorticity minimum (for densities less than 27.65 σ_θ), using the Reid (1994) data set. Regions of potential vorticity of less than 1 and 2×10^{-13} cm^{-1} sec^{-1} are shaded (dark and light, respectively).

Subpolar Mode Water in summer 1997

SPMW in May–August 1997 was mapped using WOCE hydrographic section data (Fig. 3). (Data from: WOCE A24 [Talley/Knorr], AR19 [Koltermann, Meteor], AR7W [Schott, Meteor], A25 [Bacon, Discovery], Zenk [Meteor].) This year followed a protracted period of high NAO, although the NAO during 1997 was low. Compared with the historical data examined above, freshening of waters by about 0.01 psu at 27.5 to 27.7 σ_θ in the Labrador and Irminger basins is apparent. Salinity at 27.3 to 27.5 was higher in the eastern boundary region in 1997, suggesting increased flow of saline waters from the south.

The lowest potential vorticity, indicating a nearby outcrop, for each of the isopycnals is shown in Figs. 3a and b. As with the earlier data, the importance of the boundary regions and ridges is clear, especially in the extension of the 27.5 σ_θ SPMW southward along the Reykjanes Ridge. In comparison with the 1950s/1960s, the SPMW in the eastern subpolar region is somewhat denser, with the 27.3 and 27.4 isopycnals outcropping several degrees of latitude farther south in 1997. Irminger and Labrador Sea SPMW centres are similar in the two time periods, although the 27.7 σ_θ mode extends more clearly into the Irminger Sea in 1997. This is presumably associated with the average circulation defined by the Labrador Sea PALACE floats, as described above.

Examination of PV along the individual, highly-resolved WOCE shows that in general there are large regions of coherently low PV with very slowly varying density, terminating abruptly and switching to another density. An example of this blocky structure is shown in Fig. 4 (page 11) which is the WOCE A24 section from Greenland to the United Kingdom (summer 1997). A break in mode water potential vorticity and density is evident at the subarctic front located at 22–23°W. It is difficult to depict this type of structure on a contoured horizontal map. Fig. 3c shows the regions as indicated by these sections, with the average densities of the SPMWs in each region listed. There clearly were not enough data to completely map the features, but the continuity of mode water properties from one section to another within a region supports the suggestion that the properties change nearly discontinuously and that they are nearly uniform over mappable areas.

Prominent in this SPMW distribution based on WOCE data is the North Atlantic Current and its northward extension in the subarctic front, as defined on each section by at least two stations. Within this feature there is no SPMW (Fig. 4). South and east of the front, SPMWs fall into separate density classes, which appear nearly discontinuous. It is not claimed herein that these exact density classes would be found in each year, but the general increase in density towards the north is a robust feature of all data sets, while the probability of quantisation within this general increase is very likely for periods, and should be pursued with data sets from other years. In the southern region, south of about 47°N, the mode waters are broken up by an eddy field. (This impression of eddy domination in this region in comparison with the rest of the subpolar gyre corresponds well to results from recent subsurface float data from the subpolar and northern subtropical gyre – Davis, Owens and Lavender, pers. comm.) Data along the Iceland–Scotland Ridge from this period were not available to me and so mapping of the northern SPMW is not included.

West of the subarctic front, in the eastern Irminger Basin and along the Reykjanes Ridge, the SPMW density is remarkably uniform, centred at 27.52 σ_θ, with none of the progression of densities observed east of the front.

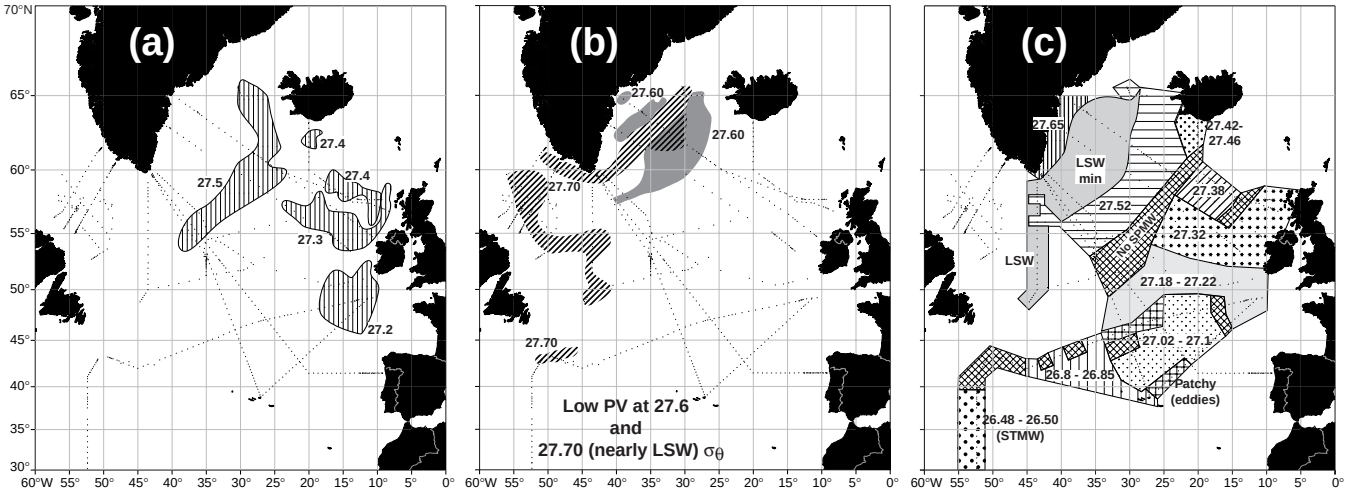

Figure 3. (a) Areas of potential vorticity less than 4×10^{-13} cm^{-1} sec^{-1} for isopycnals 27.2 to 27.5 σ_θ, based on WOCE hydrographic sections collected in May–August 1997. Data were smoothed CTD profiles, and so the potential vorticity numbers are not precisely comparable with those calculated from bottle data, as were used in Figs. 1 and 2. (b) Potential vorticity less than 6×10^{-13} cm^{-1} sec^{-1} at 27.6 and less than 3×10^{-13} cm^{-1} sec^{-1} at 27.7, for the same data set. (c) Density of the potential vorticity minimum in the SPMW in May–August 1997. Shaded regions indicate where a clear SPMW potential vorticity minimum is not present. Potential density values listed in the various regions are the average SPMW density for that region, about which there is only small variation.

Modes at a density of 27.65 σ_θ are found at the few stations in Denmark Strait and along the Greenland shelf, and appear to be associated with thick mixed layers formed locally there. The central Irminger Basin is dominated by Labrador Sea Water, and so identification of an SPMW there is not sensible in this data set.

In summary, this initial view of the SPMW distribution based on more detailed analysis of the 1950s/1960s data and WOCE data from summer 1997, suggests major refinements to previous ideas: boundary intensification of the low potential vorticity areas, association of the major SPMW modes with topographic features, a clear demarcation between SPMWs east and west of the subarctic front, quantisation of SPMW densities, with SPMW west of the subarctic front being of nearly uniform density. Much further analysis is required to pursue these SPMW features, to attempt to identify specific formation sites or regions for each SPMW "type" and the connections between them, and hopefully to identify the processes producing such remarkably thick mixed layers. Important adjunct data sets are the floats for the circulation and eddy field, surface fluxes, and high resolution SST and altimetry to better define the horizontal structures and relation to the eddy field and fronts.

Acknowledgements

WOCE data sets collected during summer 1997 were graciously supplied by Sheldon Bacon, Fritz Schott, Walter Zenk, Peter Koltermann, and for the Labrador Sea from winter 1997 by Bob Pickart. The summer 1997 WOCE cruise on the RV Knorr was supported by the National Science Foundation OCE9529584.

References

McCartney, M. S., 1982: The subtropical circulation of mode waters. J. Mar. Res., 40(suppl.), 427–464.

McCartney, M. S., and L. D. Talley, 1982: The subpolar mode water of the North Atlantic Ocean. J. Phys. Oceanogr., 12, 1169–1188.

McCartney, M. S., and L. D. Talley, 1984: Warm water to cold water conversion in the northern North Atlantic Ocean. J. Phys. Oceanogr., 14, 922–935.

Reid, J. L., 1994: On the total geostrophic circulation of the North Atlantic Ocean: flow patterns, tracers and transports. Prog. Oceanogr., 33, 1–92.

Talley, L. D., and M. S. McCartney, 1982: Distribution and circulation of Labrador Sea Water. J. Phys. Oceanogr., 12, 1189–1205.

WOCE Global Data on CD-ROMs (Version 2) to be issued mid-2000

The WOCE Data Assembly Centres (DACs) are already in the process of finalising data sets and associated metadata that will be included on the second version of the WOCE Global Data CDs. The new issue will be a significant upgrade from Version 1.0 which included data that were submitted by early 1998, before the field programme was completed and well before the basic 2 year PI proprietary period had passed for many data sets. It appears at present that none of the CDs will contain all WOCE data of a specific type (current meter, hydrography etc.) for the entire WOCE observational period (1990–98) but a few will be close and could be complete with help from PIs. The Data Information Unit, NASA/JPL and IFREMER are also preparing updates of their CDs for inclusion with the new issue. The final version of the WOCE Global Data (Version 3.0) will be issued in 2003 at the time of the final WOCE Conference.

The schedule for production and delivery of Version 2.0 is as follows:

April 2000	Data delivered to DACs and CD contents finalised
June 2000	Master copies of the CDs go to US-NODC for reproduction
Aug./Sept. 2000	CD-ROM sets distributed to the community

Around 80% of WOCE data have been submitted to the DACs, which means of course, that another 20% still reside with PIs. Some data already submitted are not yet public and can only be released with the permission of the PI concerned. The DACs and DIU are working with PIs to arrange delivery and to obtain authority to release their data in time to meet the above schedule. Anyone uncertain about how to submit data can contact the DIU (woce.diu@diu.cms.udel.edu, http://diu.cms.udel.edu/woce/, Tel (+1) 302-645-4278, Fax (+1) 302-645-4007) or any of the DACs. Anyone holding data should expect to be contacted very soon if they haven't been already.

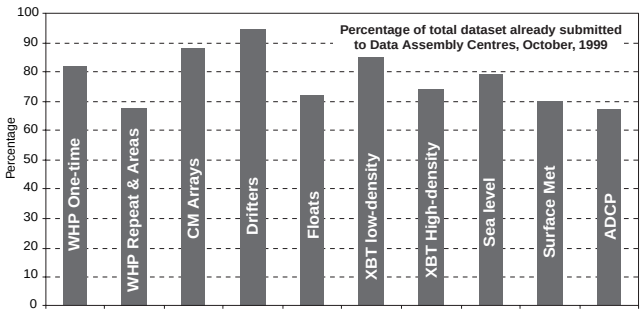

Deep Water Variability in the subpolar North Atlantic

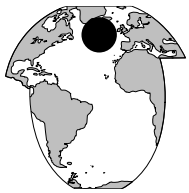

Monika Rhein, Friedrich Schott, Lothar Stramma, Jürgen Fischer, and Christian Mertens, Institut für Meereskunde Kiel, Germany*
** now at Institut für Ostseeforschung Warnemünde, Germany.*
mrhein@ifm.uni-kiel.de, monika.rhein@io-warnemuende.de

The subpolar North Atlantic is an important region for the formation and modification of the components of the North Atlantic Deep Water (NADW). These deep water masses leave the subpolar gyre mainly in the Deep Western Boundary Current and are part of the cold limb of the thermohaline circulation. The WOCE repeat sections (AR7, A2) showed that this region is subject to significant interannual changes, which might influence the exchange of mass and heat between the subpolar and the subtropical gyre. In 1996, the IfM Kiel established a special research programme, (SFB 460), entitled "Dynamics of the Thermohaline Circulation Variability", that has a multi-year perspective. The main objectives are the variability in deep water mass formation and transports in the subpolar North Atlantic and the role of these variabilities on the thermohaline overturning and on the oceanic uptake of CO_2. The programme includes modelling efforts, shipboard measurements (hydrography, nutrients, velocity measurements with lowered ADCP, shipboard-ADCP, chlorofluorocarbons, CO_2 system), moorings (measuring velocities and stratification) and floats (PALACE and RAFOS) as well as acoustic tomography and inspection of historical data. Here we present results from four hydrographic cruises which had been carried out in the western subpolar North Atlantic since 1996 (Fig. 1, Table 1). Related posters at the WOCE North Atlantic Workshop in Kiel, August. 1999, reported on the boundary current variability in the Labrador Sea (Fischer et al., 1999), on vertical currents and convection in the Labrador Sea (Mertens et al., 1999), on the variability of the geostrophic boundary current transports from historical data (Kieke and Rhein, 1999), and on the formation rates and spreading of Labrador Sea Water (Rhein et al., 1999).

Table 1. Cruises, 1996-1999, western North Atlantic

Ship	Cruise	Date
RV Valdivia	161	18 July-18 August 1996
RV Meteor	39/4	06 July-11 August 1997
RV Valdivia	172	04 July-12 August 1998
RV Meteor	45/3	11 July-10 August 1999

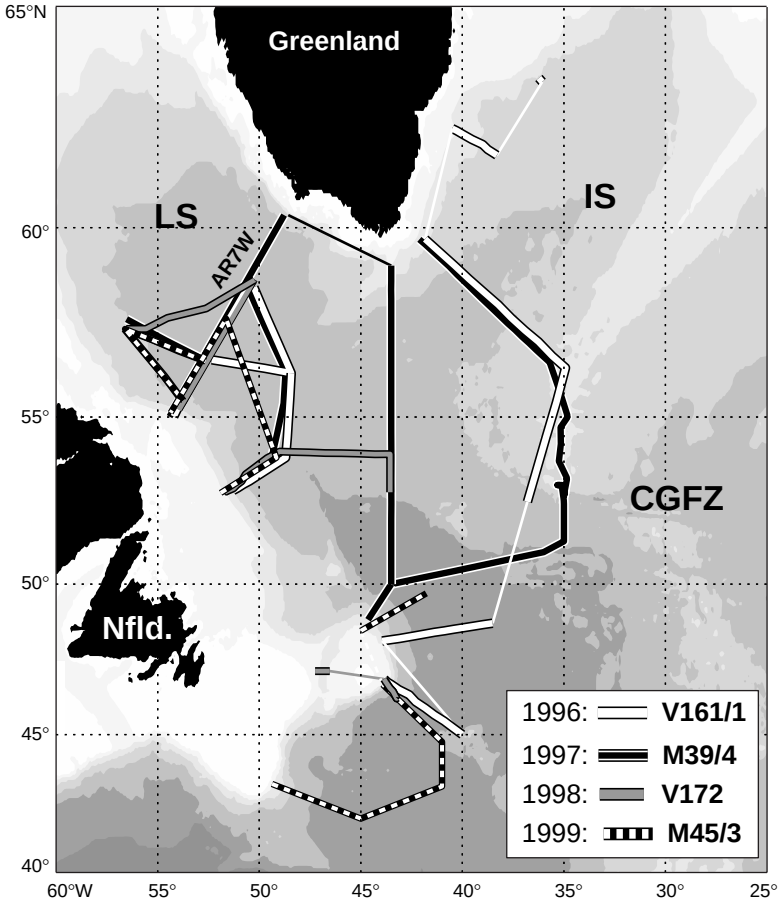

Figure 1. Cruise map of the SFB 460 hydrographic cruises in the western subpolar North Atlantic. IS: Irminger Sea; LS: Labrador Sea; CGFZ: Charlie Gibbs Fracture Zone; Nfld: Newfoundland; AR7W: WOCE section AR7W.

Deep water masses in the subpolar North Atlantic

The three main deep water mass components in the subpolar North Atlantic are depicted in the salinity sections (Fig. 2) along the south-western part of the WOCE line AR7W (for location see Fig. 1). The Labrador Sea Water (LSW) defined between the isopycnals σ_θ 27.74–80 is characterised by a temperature and salinity minimum and formed by deep convection in the Labrador Sea. After formation, LSW flows north-eastward into the Irminger Sea (time scale 6 months, Sy et al., 1997), eastward into the north-east Atlantic (time scale 2–3 years), and LSW is also exported southward with the Deep Western Boundary Current (DWBC).

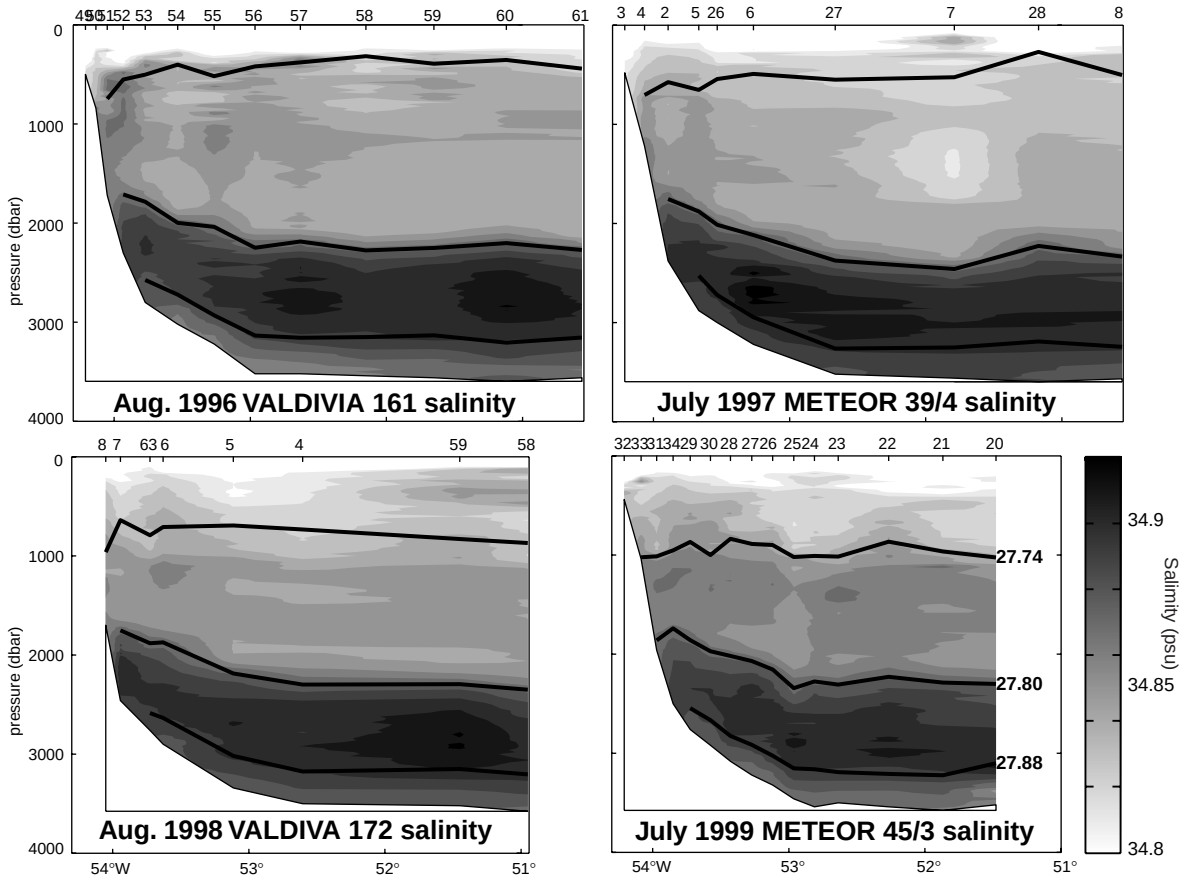

Figure 2. Salinity along the south-western WOCE AR7W line in the Labrador Sea, 1996–1999. The thick lines are the isopycnals σ_θ 27.74, 27.80, 27.88, which separate the water masses Labrador Sea Water (LSW), Gibbs Fracture Zone Water (GFZW) and Denmark Strait Overflow Water (DSOW).

The Gibbs Fracture Zone Water (GFZW) bounded by σ_θ 27.80–88 is marked by a salinity maximum. This water mass is a mixture of the water spilling over the sills between Iceland and Scotland and ambient north-east Atlantic water. It enters the western Atlantic through the Charlie Gibbs Fracture Zone. The usually westward flow of GFZW in the fracture zone is occasionally reversed by deep-reaching northward excursions of the North Atlantic Current, as observed during our cruise in 1997 and also seen in historical data (Schott et al., 1999). In the western Atlantic, the GFZW is believed to circulate in the Irminger Sea in a cyclonic fashion and then flow along the Greenland continental slope south and west into the Labrador Sea (Dickson and Brown, 1994).

The deepest water mass (below σ_θ 27.88) is the Denmark Strait Overflow Water (DSOW), which, after passing the Denmark Strait, sinks to the bottom and flows as a deep boundary current along Greenland into the Labrador Sea. DSOW is also modified by entrainment and is colder and less saline than GFZW. Both, the LSW and the DSOW exhibit maxima in CFCs and anthropogenic CO_2 (Koertzinger et al., 1999), caused by their recent contact with surface water.

Deep water variability, 1996–1999

The major impact of the ceasing convection activity in the Labrador Sea since 1995 is the decrease of the LSW thickness in the central Labrador Sea from about 2000 m in 1996 to about 1300 m in 1999 (Fig. 3a, page 12). The reduced thickness is caused by the deepening of the upper boundary of LSW, the isopycnal σ_θ 27.74. The location of the lower boundary (σ_θ 27.80) remained essentially constant (Fig. 2). In the same time period, the water above the LSW became more stable, such that deep convection in the winter 2000 will require higher buoyancy losses than for instance in 1996. The prominent LSW salinity minimum at $\sigma_\theta = 27.78$, which is present in the whole subpolar North Atlantic, became saltier and warmer since 1996, as no deep convection ventilated this density layer in the period thereafter.

In 1997 we observed one profile which was ventilated to a density of $\sigma_\theta = 27.765$, the ventilated water was fresher and colder than the ambient LSW (station 7, see Fig. 2b). Note that in Fig. 2b due to the coarse station spacing outside the boundary current the salinity minimum in the LSW layer observed at station 7 is smoothed over

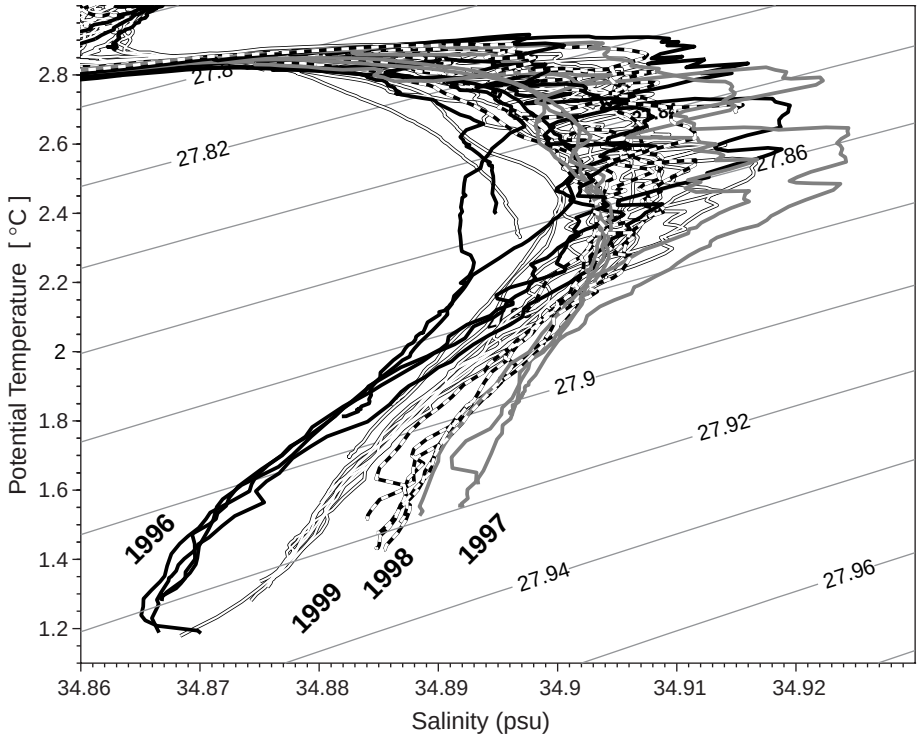

Figure 4. $\theta - S$ plot for GFZW and DSOW, south-western WOCE AR7W section, 1996–1999.

much of the central Labrador Sea. However, the eddies there are fairly small, with diameters in the range of a few kilometres, and we have no data to estimate the real extent of the ventilated water.

The mean salinity distribution of GFZW ($\sigma_\theta = 27.80 - 88$) in the four realisations (Fig. 3b) show higher salinities and therefore purer GFZW in the southern and central Labrador Sea than in the deep boundary currents. This indicates westward spreading of GFZW from the Charlie Gibbs Fracture Zone towards the Labrador Sea rather than a cyclonic boundary circulation around the Irminger Sea, as previously concluded. The thickness of the GFZW layer remained fairly constant. Variability of water mass characteristics, however, was observed. The potential temperature and salinity in 1999 at the WOCE AR7W section was lower than in 1997 (Fig. 4), opposite to the changes in the LSW.

On the way from the northern Irminger Sea to the Labrador Sea the DSOW becomes warmer and more saline (Fig. 3c) by mixing with the GFZW. We observed in both, the Irminger Sea and the Labrador Sea a significant large scale interannual DSOW variability. The DSOW warmed from 1996 to 1997, and cooled in 1998 and in 1999 (Figs. 3c, 4). The time scale of these changes could not be investigated with our data alone (one survey per year). Combining them with data from other programmes in this region like VEINS and Nordic WOCE one might be able to evaluate the role of variability in the water mass characteristics north of Iceland and in the entrainment south of the Denmark Straits on the observed large scale changes.

Summarising, we observed that the thickness of LSW decreased from 1996 to 1999, with the LSW becoming warmer and saltier, accompanied by an increase in upper layer stability. The GFZW spreads directly westward west of the Charlie Gibbs Fracture Zone, and DSOW became warmer from 1996 to 1997 followed by subsequent cooling in 1998 and in 1999. In 1996–1998, the focus of our studies was the region north of Newfoundland. In the following years, the mooring programme and the shipboard measurements will be extended southward to the Grand Banks in order to quantify the deep water export out of the subpolar gyre and to study the transport variability and associated water mass characteristics.

Acknowledgements

This research is funded by the Deutsche Forschungsgemeinschaft. We thank A. Sy (BSH, Germany) for providing the RV Meteor 39/5 hydrographic data and D. Kieke for help with the figures.

References

Dickson, R. R., and J. Brown, 1994: The production of North Atlantic Deep Water: Sources, rates, and pathways. J. Geophys. Res., 99, 12319–12341.

Fischer, J., F. Schott, C. Mertens, F. Morsdorf, P. Rhines, and J. R. N. Lazier, 1999: Boundary current variability in the Labrador Sea, 1996–1999. The WOCE North Atlantic Workshop, Kiel, August 1999.

Kieke, D., and M. Rhein, 1999: Geostrophic boundary current transports in the subpolar North Atlantic. The WOCE North Atlantic Workshop, Kiel, August 1999.

Koertzinger, A., M. Rhein, and L. Mintrop, 1999: Anthropogenic CO_2 and CFCs in the North Atlantic Ocean – a comparison of man-made tracers. Geophys. Res. Lett., 26, 2065–2068.

Mertens, C., F. Schott, J. Fischer, and U. Send, 1999: Observations of vertical currents and convection. The WOCE North Atlantic Workshop, Kiel, August 1999.

Rhein, M., J. Fischer, C. Mertens, D. H. Min, A. Putzka, W. Roether, W. M. Smethie, D. Smythe-Wright, A. Sy, and R. F. Weiss, 1999: Estimates of LSW formation rates by the CFC inventory in the subpolar North Atlantic, 1997. The WOCE North Atlantic Workshop, Kiel, August 1999.

Sy, A., M. Rhein, J. R. N. Lazier, K. P. Koltermann, J. Meincke, A. Putzka, and M. Bersch, 1997: Surprisingly rapid spreading of newly formed intermediate waters across the North Atlantic Ocean. Nature, 386, 675–679.

Schott, F., L. Stramma, and J. Fischer, 1999: Interaction of the North Atlantic Current with the deep Charlie Gibbs Fracture Zone throughflow. Geophys. Res. Lett., 26, 369–372.

Effects of an improved model representation of overflow water on the subpolar North Atlantic

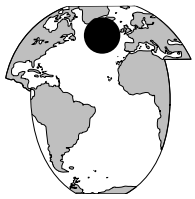

Joachim Dengg, Claus Böning, and Ute Ernst, Institut für Meereskunde, Kiel, Germany; Rene Redler, GMD SCAI, Sankt Augustin, Germany; and Aike Beckmann, AWI, Bremerhaven, Germany. jdengg@ifm.uni-kiel.de

Overflows of dense water masses across the sills in the subpolar North Atlantic have been shown to make an important contribution to the observed water properties in the core of the Deep Western Boundary Current (e.g. Doney and Jenkins, 1994). There is also evidence from model studies for a strong influence on the meridional overturning in ocean general circulation models (Döscher et al., 1994) and its response to changes in high-latitude buoyancy forcing (e.g. Böning et al., 1996, and Lohmann, 1998). However, in recent model intercomparisons (DYNAMO Group, 1997; Winton et al., 1998) it has become apparent that z-coordinate ocean models (i.e. discretisations that use the geopotential as vertical coordinate) have a tendency to erase these dense overflow signals due to excessive artificial mixing at their characteristic step-like topography. To overcome this problem, a number of new parameterisations for bottom boundary layer (BBL) processes have been suggested and tested in idealised model configurations (Beckmann and Döscher, 1997; Campin and Goosse, 1999; Gnanadesikan et al., 1999; Killworth and Edwards, 1999; Song and Chao, 1999).

In this brief report, we will demonstrate some of the effects of including one such scheme (in our case Beckmann and Döscher, 1997, as implemented by Döscher and Beckmann, 1999) into an eddy-permitting OGCM simulation of the North Atlantic. For the purposes of this analysis, we concentrate on the properties and the spreading of Denmark Strait Overflow Water (DSOW), since this is where the largest impact of an improved representation of overflows is to be expected for the large-scale circulation. Results are compared to a non-eddy resolving version of the same model code to address the sensitivity to the choice of horizontal grid spacing.

Without going into the theory of the parameterisation (which may be found in Beckmann and Döscher, 1997), we would just point out that this particular BBL scheme is basically re-directing the flow of dense water down the gradients of the topography. This is achieved by allowing a direct communication between the deepest grid boxes at each horizontal grid point, which is not included in the standard z-coordinate formulation with step-like representation of the bathymetry. Beyond that, there is no claim to an accurate representation of the detailed dynamics of overflows in the Beckmann and Döscher (1997) parameterisation. However, as will be shown below, this rather crude method already has several important effects on the large-scale circulation, thus confirming the need for a suitable and maybe dynamically more consistent parameterisation (as proposed in some of the other schemes listed above).

The circulation model used here is the FLAME configuration (Family of Linked Atlantic Model Experiments; Redler et al., 1998; Redler and Dengg, 1999) of the GFDL MOM2.1 code (Pacanowski, 1995). The two model versions presented in this report employ an isotropic horizontal grid with $\frac{1}{3}°$ and $\frac{4}{3}°$ resolution respectively, i.e. approximately 14 km and 57 km grid spacing in the Denmark Strait. Vertical resolution in both model configurations varies with depth, increasing from 10 m at the surface to 75 m at the sill depth and 250 m below 2000 m. Both models use isopycnal Laplacian lateral mixing. The models were initialised with the climatology of Levitus and Boyer (1994) and spun up for 15 years without the BBL scheme, after which the process studies presented here ran for another 10 years.

Fig. 1 (page 23) shows the effect of the BBL-parameterisation on the temperature distribution at the bottom of the northern North Atlantic: The climatology of Reynaud (Reynaud et al., 1998) has temperatures below 2.5°C in the deep Irminger Sea and below 2.0°C in the Labrador Sea. Note that these climatological data are already warmer than the minimum found in synoptic data (cf. Fig. 3), probably due to lower resolution in the deep boundary currents and more smoothing by the objective interpolation. The Levitus data that were used for

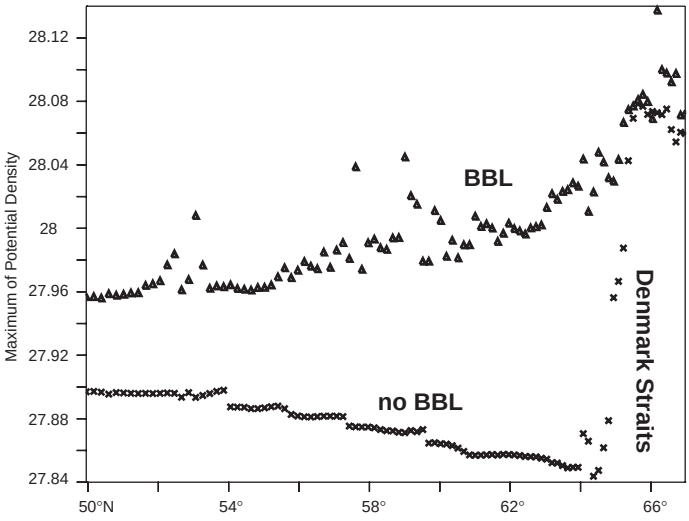

Figure 2. Zonal maximum (between 55°W and 25°W) of potential density σ_0 at the bottom as a function of latitude south of Denmark Straits. The upper curve (triangles) is from the $\frac{1}{3}°$ model with BBL, the lower (crosses) from the corresponding run without it.

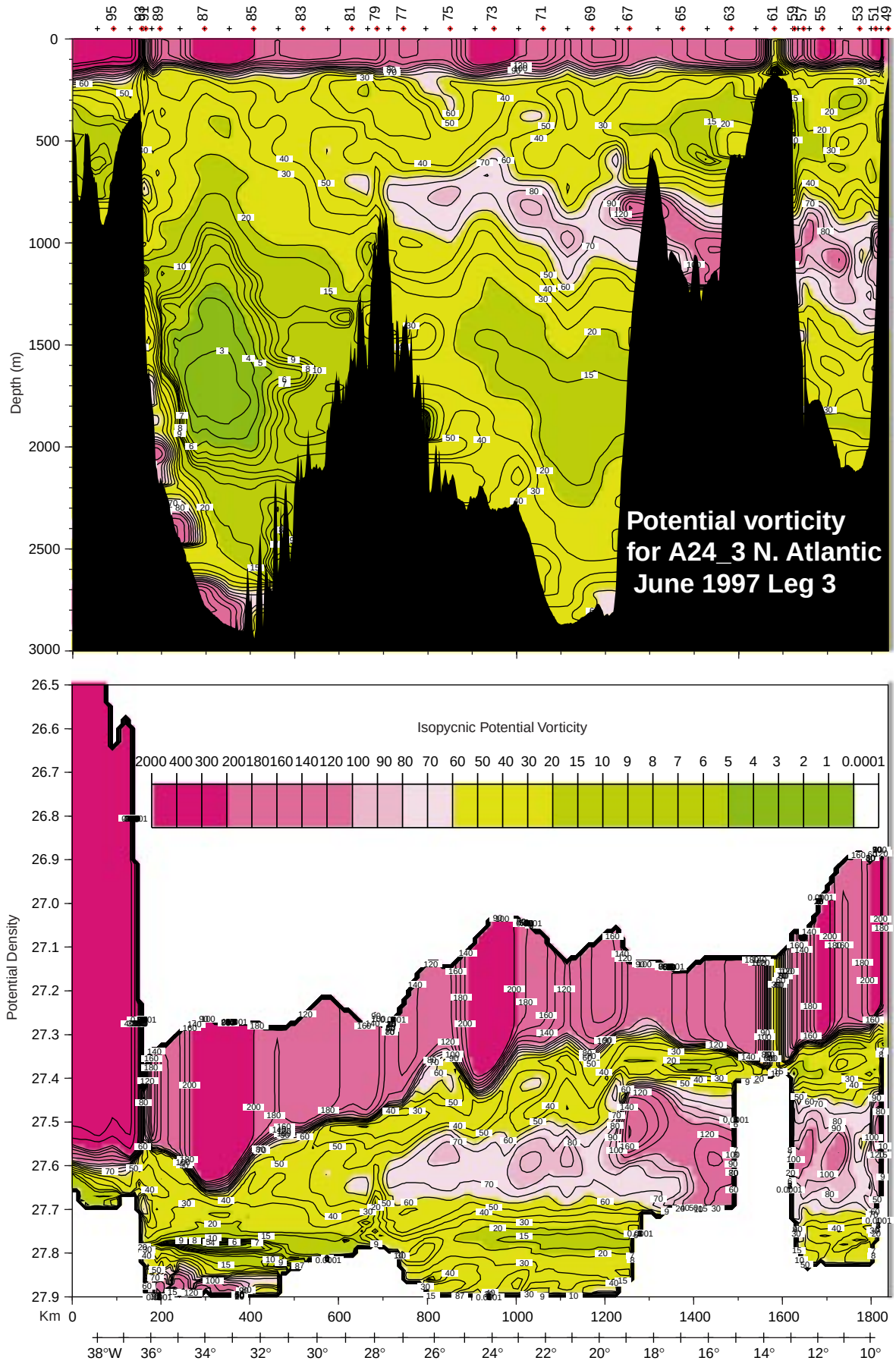

Talley, page 3, *Figure 4. (a) Isopycnic potential vorticity ($f\partial\rho / \rho\partial z$) along WOCE section A24 from Greenland to the United Kingdom, and (b) the same as a function of potential density σ_θ. The section is from the RV Knorr in summer 1997.*

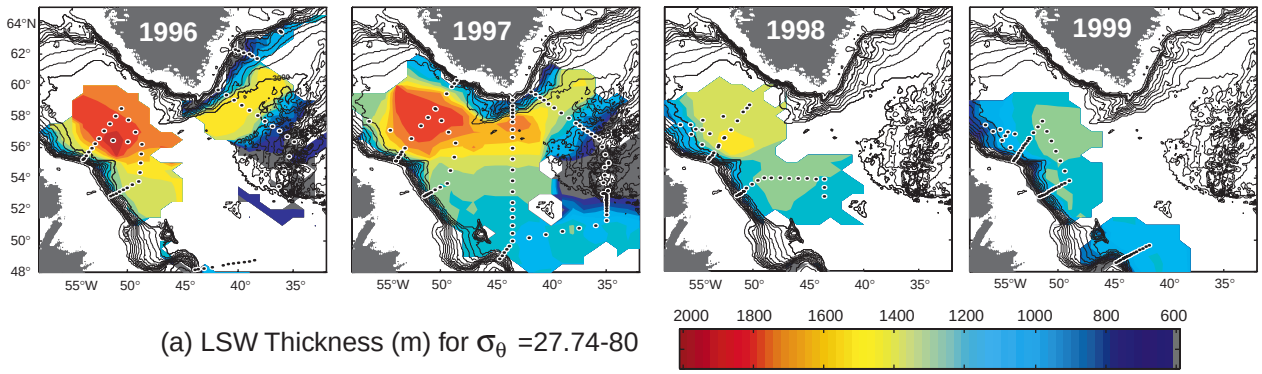

(a) LSW Thickness (m) for σ_θ =27.74-80

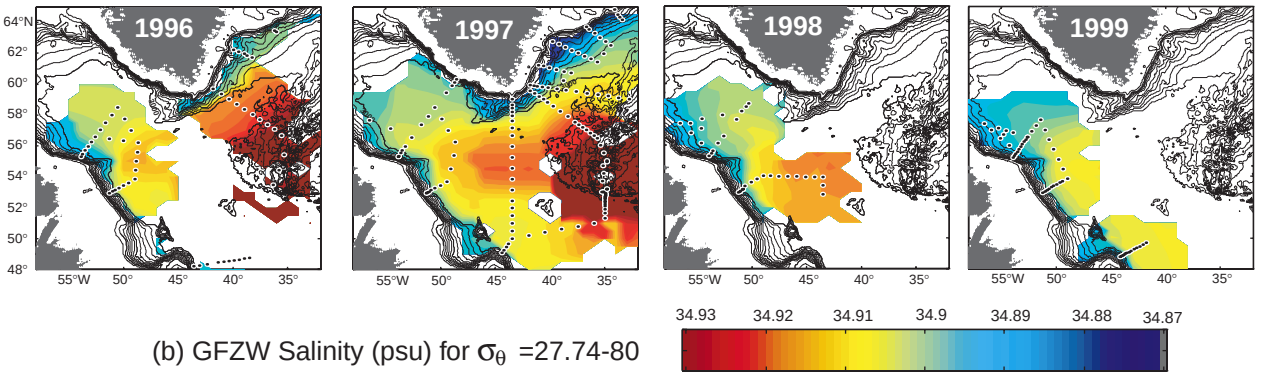

(b) GFZW Salinity (psu) for σ_θ =27.74-80

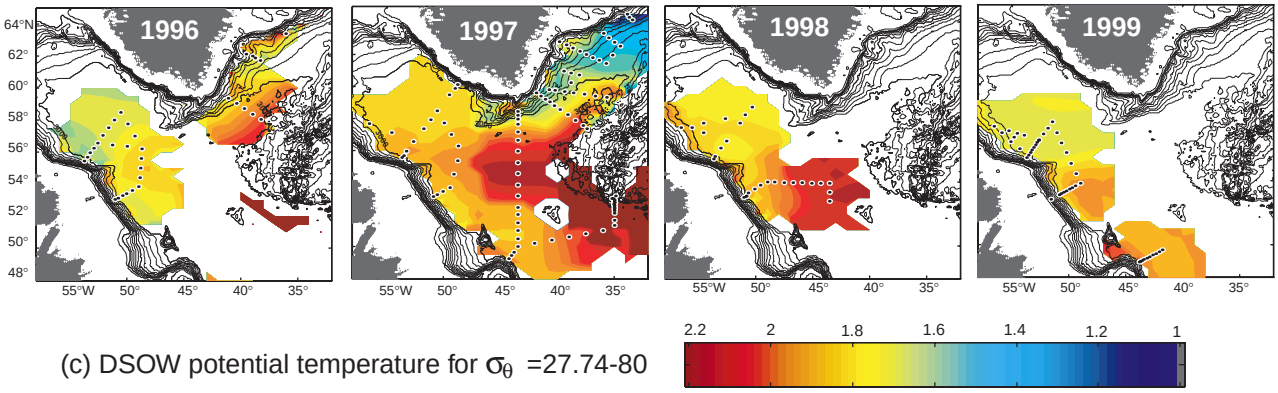

(c) DSOW potential temperature for σ_θ =27.74-80

Rhein et al., page 7, *Figure 3. (a) Distribution of LSW thickness (σ_θ = 27.74 – 80), 1996–1999; (b) Distribution of mean salinity of GFZW, 1996–1999; (c) Distribution of mean potential temperature of DSOW. The RV Meteor 39/5 data east of Greenland (September 1997) kindly provided by A. Sy (BSH, Germany) are included in the 1997 maps. The maps are drawn with a topography following interpolation scheme (Rhein et al., 1999).*

initialisation are affected even more by these effects. The model without an explicit BBL sub-model is not able to reproduce the observed cold bottom temperatures (neither at 4/3° nor at 1/3° resolution). Throughout the region, the model is at least 0.5°C warmer than the climatological data by Reynaud. In contrast, with the BBL code, both the coarser resolution model and the high resolution version have prominent signals of cold overflows in the bottom temperatures in the DSOW and also in the Iceland–Scotland overflow. At the higher resolution, the very cold overflow water is quite realistically confined to narrow bands along the shelf edge (which are not resolved in the climatological data). At 4/3° resolution this cold water spreads over too wide a region, putting this result at odds with the climatological data; possibly, a more appropriate choice of parameters in the BBL code might improve this. Experiments are underway.

It should be noted that – although not explicitly prescribed by a local restoring – the source water in the Denmark Strait is the same in the model with and without a BBL. However, within a few grid points from the exit of the Strait, the effect of the mixing at topographic steps dilutes this water in the model without the BBL sub-code. This may be seen in Fig. 2, where the zonal maximum of density is shown as a function of latitude for both runs. With the BBL (upper curve) the mixing is very gradual and density decreases slowly with distance from the Strait. Without the BBL parameterisation there is an abrupt drop in maximum density immediately south of the sill, with a slight increase towards the south where the densest waters are formed in this experiment.

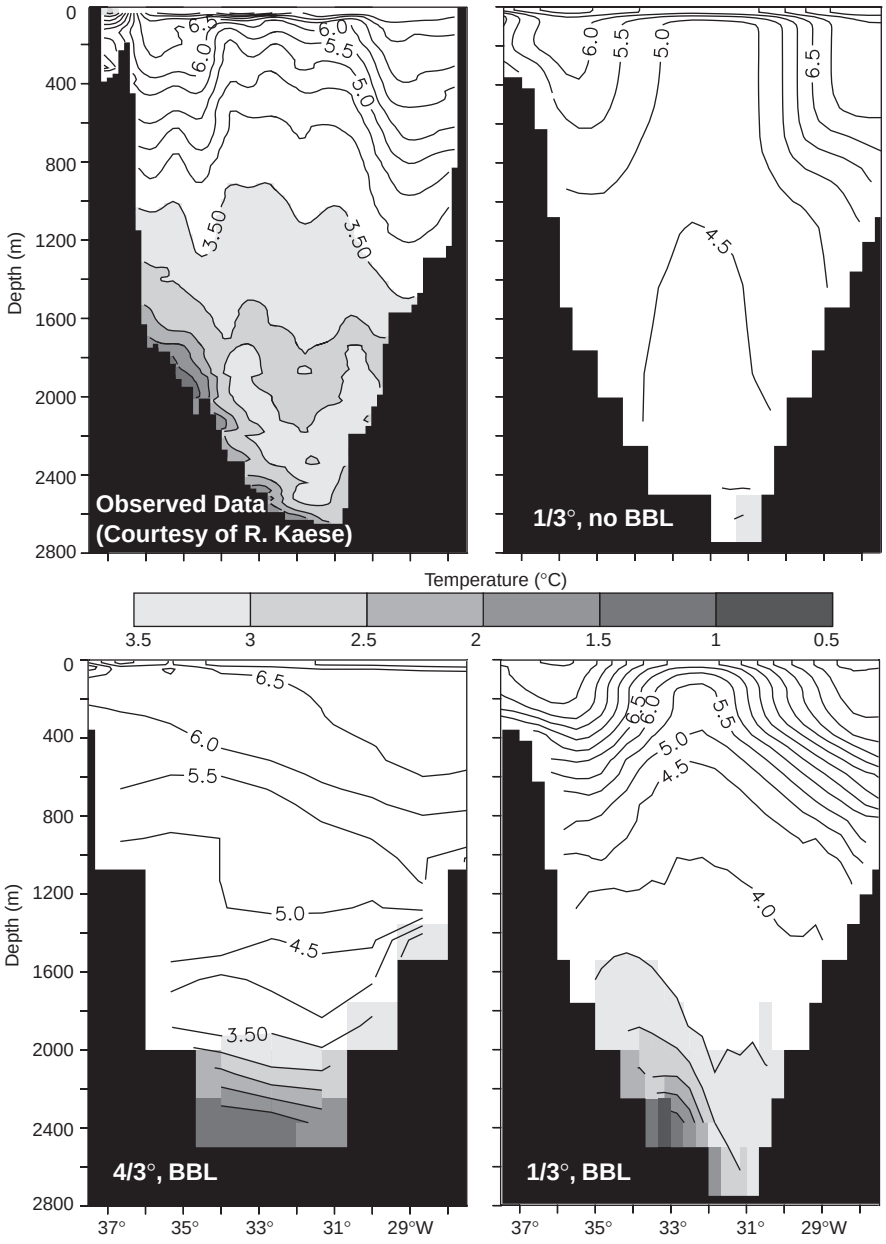

Figure 3. Zonal sections of temperature at 64°N. Top left: composite of synoptic observations, Poseidon cruises in 1996/97 (courtesy R. Käse, IfM Kiel), other figures as in Fig. 1. Temperatures colder than 3.5°C shaded.

Along a section at 64°N (Fig. 3), more differences between model realisations and observations become apparent: an analysis of section data with high spatial resolution obtained with RV Poseidon in 1996 and 1997 (R. Käse, pers. comm.) displays a very thin layer of overflow water that has not yet made it far down the continental slope. Those models that have the overflow signal at all (i.e. those with BBL) show a much thicker layer that resides at greater depths. With the BBL parameterisation used here, the thickness of the overflow plume is ultimately determined by the vertical grid spacing of the lowest grid box, in our case 250 m at depths below 2500 m. Therefore, this aspect of the solution should improve with an increase in vertical resolution. The vertical position of the overflow at the slope of the Greenland shelf, however, is determined by other factors, one of which is horizontal resolution: as was discussed in the context of Fig. 1, in the lower resolution version of the model the overflow water already fills the deepest regions of the basin, while at higher horizontal resolution it is able to retain a semblance of a boundary current structure at the shelf edge, although at too great a depth.

The change in deep water properties has consequences for the meridional overturning in the models. Fig. 4 shows the overturning stream function in the higher resolution model without and with a BBL. While the amplitude of the overturning hardly

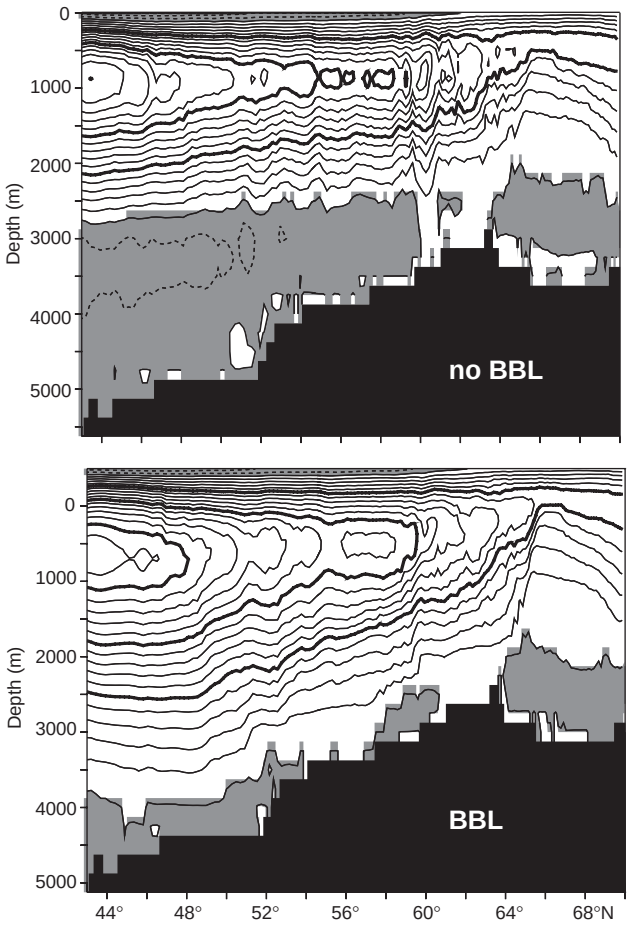

Figure 4. Stream function of zonally integrated meridional volume transport (Sv) in the ⅓° model. Contour interval 1 Sv, bold contours every 5 Sv, negative values with darker shading. Top: without BBL code, bottom: with a BBL.

changes at all (15 Sv for the run without BBL, 16 Sv with BBL), the vertical structure displays a downward shift of the southward return flow from about 1500–2000 m to 2000–3500 m in the BBL-case. The latter is expected from the Community Modelling Effort (CME) results (Döscher et al., 1994), but the lack of an increase in overturning amplitude is not. Whether this is a property of the particular BBL scheme used, or whether indeed the presence of an overflow does not affect the amplitude of the overturning remains under investigation at this time.

The change of the vertical structure of the overturning is immediately reflected in the spreading of tracers. Fig. 5 displays the example of an artificial age tracer (defined as zero age in the Denmark Strait with "ageing" setting in away from the source region). Without the BBL code, this tracer initially sinks to about 1500-2000 m after leaving the Denmark Strait and then spreads horizontally at about this depth horizon. With a BBL, it descends to successively deeper levels on its way south, in much better agreement with tracer observations in the deep western boundary current.

To sum up, at this point a first evaluation of the results with this simple BBL scheme would be:

- Pronounced influences of the presence of DSOW on the water mass and tracer distribution and on the overturning in the subpolar North Atlantic have been identified.
- For large-scale circulation and climate models, this affirms the necessity of introducing an appropriate representation of this water and its evolution downstream of the source region.
- Once the spurious elimination of DSOW at the exit of the Denmark Strait has been prevented by a suitable parameterisation, the dynamics of its southward spreading as a DWBC begin to matter. These are resolution dependent, however, and could not be addressed by the BBL scheme employed here. Whether other BBL parameterisations will be able to tackle this issue, particularly at the coarse resolutions commonly used in climate models, remains to be seen.

Acknowledgements

We gratefully acknowledge contributions by Thierry Reynaud (climatological data) and Rolf Käse (synoptic observations), as well as the work by the Ferret team at PMEL for providing the plot software.

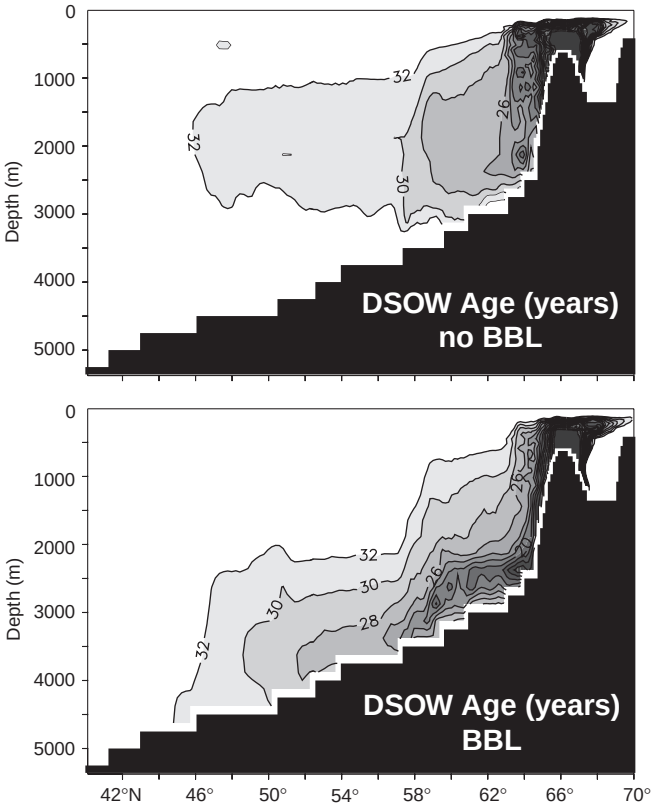

Figure 5. Meridional distributions of the zonal minimum of an artificial age tracer (years), defined as 0 years ("new" overflow water) in the Denmark Strait, with a background age of 35 years. Top: without BBL code, bottom: with a BBL.

References

Beckmann, A., and R. Döscher, 1997: A method for improved representation of dense water spreading over topography in geopotential-coordinate models. J. Phys. Oceanogr., 27, 581–591.

Böning, C. W., F. O. Bryan, W. R. Holland, and R. Döscher, 1996: Deep-water formation and meridional overturning in a high-resolution model of the North Atlantic. J. Phys. Oceanogr., 26, 1142–1164.

Campin, J.-M., and H. Goosse, 1999: Parameterization of density-driven downsloping flow for a coarse-resolution ocean model in z-coordinate. Tellus, 51A, 412–430.

Doney, S. C., and W. J. Jenkins, 1994: Ventilation of the deep western boundary current and abyssal western North Atlantic: estimates from tritium and ^{3}He distributions. J. Phys. Oceanogr., 24, 638–659.

Döscher, R., and A. Beckmann, 1999: Effects of a bottom boundary layer parameterization in a coarse resolution model of the North Atlantic Ocean. J. Atmos. Oceanic Technol., in press.

Döscher, R., C. W. Böning, and P. Herrmann, 1994: Response of circulation and heat transport in the North Atlantic to changes in thermohaline forcing in northern latitudes: a model study. J. Phys. Oceanogr., 24, 2306–2320.

DYNAMO Group, 1997: DYNAMO. Dynamics of North Atlantic Models: Simulation and assimilation with high resolution models. Technical Report 294, Institut für Meereskunde, Kiel, Germany.

Gnanadesikan, A., R. Pacanowski, and M. Winton, 1999: Representing the bottom boundary layer in the GFDL ocean model: Model framework, dynamical impacts, and parameter sensitivity. J. Phys. Oceanogr., submitted.

Killworth, P. D., and N. R. Edwards, 1999: A turbulent bottom boundary layer code for use in numerical ocean models. J. Phys. Oceanogr., 29, 1221–1238.

Levitus, S., and T. P. Boyer, 1994: World Ocean Atlas 1994. Volume 4: Temperature. NOAA Atlas NESDIS 4, NOAA, Washington, DC.

Lohmann, G., 1998: The influence of a near-bottom transport parameterization on the sensitivity of the thermohaline circulation. J. Phys. Oceanogr., 28, 2095–2103.

Pacanowski, R. C., 1995: MOM 2 Documentation, User's Guide and Reference Manual. Technical Report 3, GFDL Ocean Group.

Redler, R., K. Ketelsen, J. Dengg, and C. Böning, 1998: A high-resolution numerical model for the circulation of the Atlantic Ocean. In: Proceedings of the Fourth European SGI/CRAY MPP Workshop, H. Lederer and F. Hertweck (eds.), pp. 95–108 Max-Planck-Institut für Plasmaphysik.

Redler, R., and J. Dengg, 1999: Spreading of CFCs in numerical models of differing resolution. Int. WOCE Newsl., 35, 12–14, unpubl. manuscript.

Reynaud, T., P. LeGrand, H. Mercier and B. Barnier (1998): A new analysis of hydrographic data in the Atlantic and its application to an inverse modelling study. Int. WOCE Newsl., 32, 29-31, unpubl. manuscript.

Song, Y. T., and Y. Chao, 1999: An embedded bottom boundary layer formulation for z-coordinate ocean models. J. Atmos. Oceanic Technol., in press.

Winton, M., R. Hallberg, and A. Gnanadesikan, 1998: Simulation of density-driven frictional downslope flow in z-coordinate ocean models. J. Phys. Oceanogr., 28, 2163–2174.

Meridional distribution of CFCs in the western subtropical Atlantic Ocean

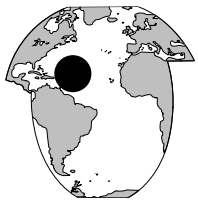

William M. Smethie, Jr., Lamont-Doherty Earth Observatory of Columbia University, Palisades, NY, USA. bsmeth@ldeo.columbia.edu

During July and August of 1997, hydrographic/tracer sections were run along 52° and 66°W in the western subtropical Atlantic Ocean (Fig. 1) as part of the Atlantic Circulation and Climate Experiment. This experiment was the US contribution to the WOCE North Atlantic programme and these two lines are designated as WOCE lines A20 (52°W) and A22 (66°W). The northern and southern ends both lines cross the western boundary flow regime. Chlorofluorocarbons (CFCs) 11,12 and 113 were measured along these lines and the CFC-11 distributions are shown in Fig. 2 (page 24). The CFC-12 and CFC-113 distributions are similar, but CFC-113 has not penetrated as far into the Atlantic as CFC-11 and CFC-12 because of its shorter input history (Walker et al., 1999).

There are three distinct subsurface CFC maxima. The shallowest maxima is centred at about 300 m depth and extends from about 16°N to 39°N. This feature is not observed at the northern or southern boundaries and is not associated with the flow of western boundary currents. It is associated with the subtropical mode water mass, Eighteen Degree Water, and the CFC maxima has a potential temperature very close to 18°C (Fig. 3). The underlying CFC minimum is associated with Upper Circumpolar Water, which is far from its source region and hence has a low CFC concentration. This minimum is strongest in the southern half of the 52°W section. The higher CFC concentration in the Upper Circumpolar Water depth range observed along the southern half of the 66°W section may be the result of diapycnal mixing with the overlying and underlying CFC maxima.

The two deeper maxima are intensified at the boundaries. Both maxima represent recently formed components of North Atlantic Deep Water (NADW) that are transported equatorward in the Deep Western Boundary Current

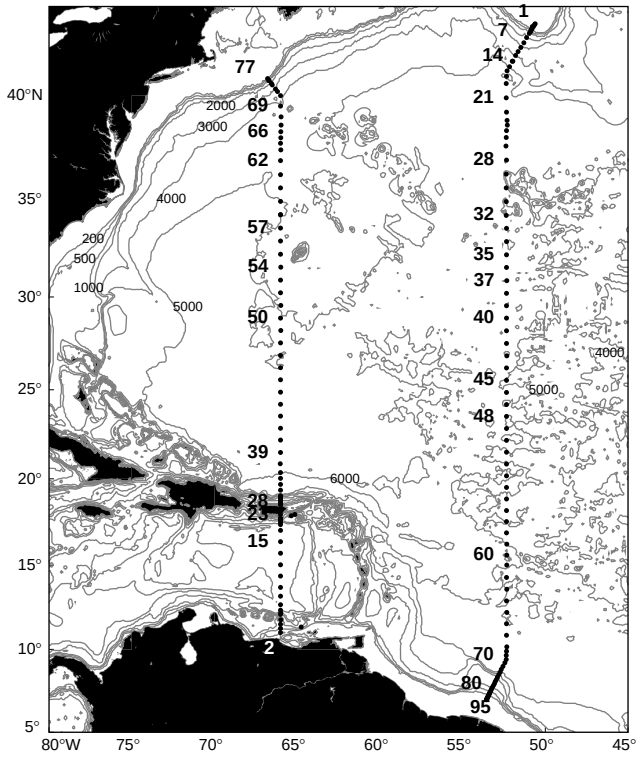

Figure 1. Station location map for the WOCE A20 (52°W) and A22 (66°W) lines.

(DWBC). The CFC concentrations of both maxima decrease in the downstream direction of the DWBC, from the northern end of the 52°W section, to the northern end of the 66°W section, to the southern end of the 66°W section, to the southern end of the 52°W section (Figs. 2 and 4).

The upper of the two deeper maxima has a density range of $\sigma_{1.5} = 34.5$ to 34.7 (Fig. 2). It has two sources, Upper Labrador Sea Water (ULSW) and Classical Labrador Sea Water (CLSW) (Pickart and Smethie, 1998; Smethie et al., 1999). Separate maxima occur for these two sources at the northern end of the 52°W section where the ULSW and CLSW maxima have core densities of $\sigma_{1.5} = 34.56$ and 34.66 respectively. These maxima merge into a broad single maximum that extends along the entire length of both sections with concentration generally decreasing in the southward direction and then increasing at the southern boundary in the DWBC. Relatively high CFC concentrations extend southward from the northern boundaries of both sections to about 34°N, well seaward of the DWBC. This southern extension of the CFC maximum demonstrates the importance of deep recirculation gyres associated with the Gulf Stream in transporting water away from the DWBC into the interior. There are also separate lobes of high CFC water farther south along both sections between 30 and 32°N. The CFC concentration is highest in the 66°W lobe suggesting flow from the western boundary to the interior, but this appears to be south of the Gulf Stream recirculation region. The CLSW CFC signal is thought to have originated from the increased production of CLSW associated with the high NAO index in the late 1980s and early 1990s (Dickson et al., 1996; Smethie et al., 1999). This CLSW can be identified as a low salinity feature in potential temperature/salinity plots from stations at the northern end of the sections (Fig. 4). However this low salinity feature is not observed in the DWBC at the southern end of the sections, although salinity is lower than in the interior. This indicates that only a small amount, if any, of the recently formed CLSW reached these locations by mid-1997. Therefore the CFC signal at the southern ends of the sections is derived primarily from ULSW. Potential temperature/salinity plots for stations located in the Gulf Stream recirculation region and in the high CFC feature at 30–32°N (Fig. 5) do have the low salinity feature indicating that recently formed CLSW is a component of these waters.

The deepest CFC maximum is derived from a mixture of overflow waters, Denmark Strait Overflow Water (DSOW) and Iceland–Scotland Overflow Water (ISOW) and has a core density of about $\sigma_4 = 45.88$. Previous work has shown that ISOW contributes the most water to this mixture but DSOW contributes most of the CFC signal (Smethie, 1993; Smethie et al., 1999). As for the Labrador Sea Water maximum, the deep maximum extends well south of the DWBC indicating recirculation of the deep water in the Gulf Stream recirculation region. The potential temperature of the deep CFC maximum is about 2.1°C which lies just above the break in the potential/salinity diagram that occurs at 2°C (Fig. 4).

The lowest CFC concentrations (less than 0.01 pmol/kg) are found in the interior along the 52°W section. Here the bottom water contains a large fraction of Antarctic Bottom Water that was formed prior to sig-

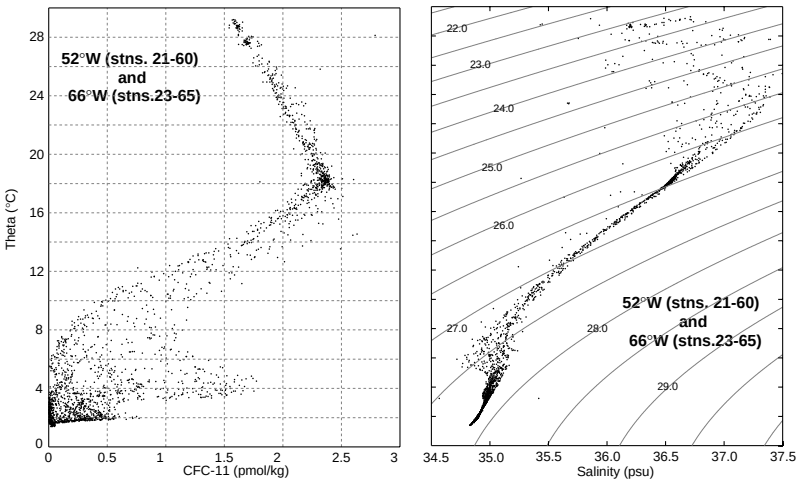

Figure 3. Potential temperature/CFC-11 and potential temperature/salinity plots for stations 21–60 along the 52°W line and stations 23–65 along the 66°W line. See Fig. 1 for station locations. Lines of constant σ_θ are included on the potential temperature/salinity plot. CFC maxima are located at about 18°C (Eighteen Degree Water), 3.5–4.5°C (ULSW and CLSW), and 2°C (Overflow waters).

nificant input of CFCs into the ocean (prior to 1950). The overlying NADW also must have formed prior to significant CFC input.

Water entering the Caribbean Sea from the subtropical North Atlantic has a density of about $\sigma_{1.5} = 34.60$ which lies within the density range of the middle CFC maximum (Fig. 2b). The CFC concentration is relatively high along the slope just south of Puerto Rico indicating that North Atlantic water enriched in CFCs flows down the Greater Antilles Slope to the bottom. As discussed previously, the source of the CFC signal at the southern end of the 66°W section is USLW so the deep water of the Caribbean Sea is renewed by ULSW. In the bottom of the basin, higher CFC concentrations are observed along the boundary suggesting a deep boundary current circulation around the basin.

Acknowledgements

I would like to thank H. Lee and E. Gorman for preparation of the data and figures. This work was supported by NSF Grant OCE 95-31864.

References

Dickson, R. R., J. R. N. Lazier, J. Meincke, P. Rhines, and J. Swift, 1996: Long-term coordinated changes in the convective activity of the North Atlantic. Prog. Oceanogr., 38, 241–295.

Pickart, R. S., and W. M. Smethie, Jr., 1998: Temporal evolution of the Deep Western Boundary Current where it enters the sub-tropical domain. Deep-Sea Res., I(45), 1053–1084.

Smethie, W. M., Jr., 1993: Tracing the thermohaline circulation in the western North Atlantic using chlorofluorocarbons. Prog. Oceanogr., 31, 51–99.

Smethie, W. M., Jr., R. A. Fine, A. Putzka, and E. P. Jones, 1999: Tracing the flow of North Atlantic Deep Water using chlorofluorocarbons. J. Geophys. Res., in press.

Walker, S. J., R. F. Weiss, and P. K. Salameh, 1999: Reconstructed histories of the annual mean atmospheric mole fractions for the halocarbons CFC-11, CFC-12, CFC-113 and carbon tetrachloride. J. Geophys. Res., in press.

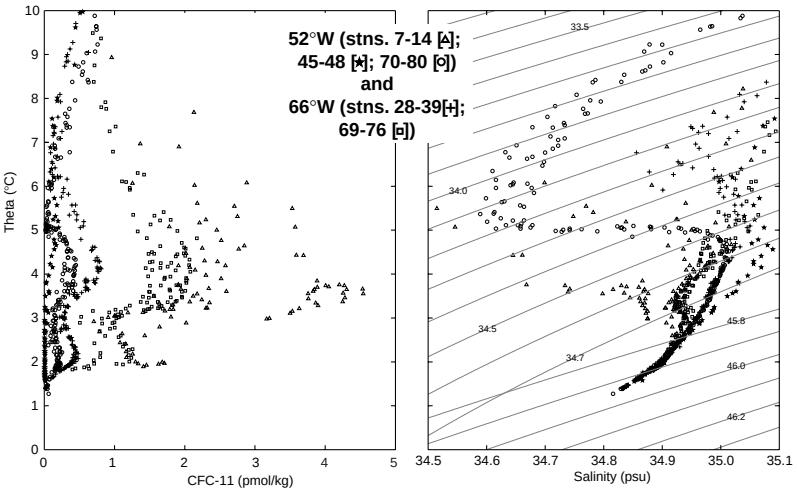

Figure 4. Potential temperature/CFC-11 and potential temperature/salinity plots for stations from the DWBC at the northern (52°W stations 7–14, 66°W stations 69–76) and southern (52°W stations 70–80, 66°W stations 28–39) ends of the meridional lines and from the centre of the 52°W line (stations 45–48). See Fig. 1 for station locations. Lines of constant $\sigma_{1.5}$ and σ_4 are included on the potential temperature/salinity plot.

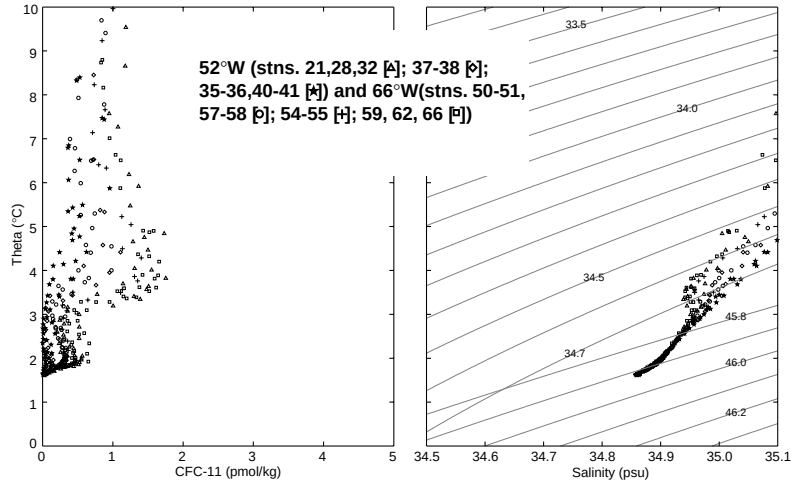

Figure 5. Potential temperature/CFC-11 and potential temperature/salinity plots for select stations from the Gulf Stream recirculation region (52°W stations 21, 28, 32 and 66°W stations 59, 62, 66), the high CFC feature south of the Gulf Stream recirculation region (52°W stations 37–38 and 66°W stations 54–55), and the interior (52°W stations 35–36, 40–41 and 66°W stations 50–51, 57–58). See Fig. 1 for station locations. Lines of constant $\sigma_{1.5}$ and σ_4 are included on the potential temperature/salinity plot.

Atlantic inflow to the Nordic Seas in the Svinøy section

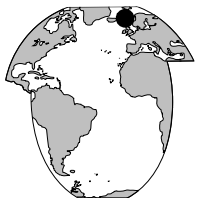

Kjell Arild Orvik, Øystein Skagseth, and Martin Mork, Geophysical Institute, University of Bergen, Norway. skagseth@gfi.uib.no

The Atlantic inflow (AI) of heat to the Nordic Seas (Norwegian, Greenland and Iceland Seas) and its extension northward to higher latitudes is an important factor for climate and biological production in Northern Europe. Consequences of a disruption of the North Atlantic circulation are still under debate, and numerous attempts have been made to estimate the AI. This presentation deals accordingly with the AI to the Norwegian Sea in the Svinøy section. The Svinøy section (Fig. 1, page 23) runs north-westwards from the Norwegian coast at 62°N and cuts through the AI just to the north of the Faroe–Shetland Channel. Based on moored current records 1995–1999, and observations from CTD-casts, SeaSoar-CTD and VM-ADCP, long-term transport estimates and structure of the AI will be described.

Fig. 1 outlines the large scale current pattern of the AI to the Nordic Seas, entering the Norwegian Sea mainly through two pathways; through the Faroe–Shetland Channel (SST: 8–9°C) and over the Faroe–Iceland Ridge (SST: 6–7°C). The Faroe–Iceland inflow has a complex structure, but due to the established Faroe–Iceland Front running eastwards with a meandering and unstable frontal jet (Read and Pollard, 1992), the major inflow must occur close to Iceland. This frontal jet continues eastwards and farther north-eastwards into the Norwegian Sea after passing to the north of the Faroes. It passes through the Svinøy section as the western branch of the Norwegian Atlantic Current (NAC) and tends to follow the topographic slope of the Vøring plateau (Poulain et al., 1996). A topographically trapped current as well, continues eastwards along the northern slope of the Faroe Plateau. Then it partly relaxes from the topographic steering and continues into the Faroe–Shetland Channel, retroflects and merges with the AI through the Faroe–Shetland Channel. This AI occurs along the slope north-west of Shetland as a barotropic current. It partly branches into the North Sea and continues northwards through isobathic confluence towards the Svinøy section as the eastern branch of the NAC. Different branches of the topographically trapped NAC merge in the Svinøy section and the western branch is intercepted as well. This makes the Svinøy section a key area for monitoring the Atlantic inflow to the Nordic Seas.

Measurements

The Svinøy section monitoring programme was initiated in April 1995 and funded by the Norwegian Research Council. Since 1997 it has been run as a part of the EU-MAST, VEINS (Variability of Exchanges In the Northern Sea) programme, which will continue until year 2000. 9 Aanderaa current meters on 3 moorings were deployed, and since 1996 the monitoring programme has been extended to a 4 mooring current meter array, S1, S2, SE1 and SE2, in the shelf break area between depths of 490–880 m with some additional measurements, S3, farther offshore at 2000 m bottom depth (Figs. 1–2). Moored records are supplemented with observations from CTD/SeaSoar-CTD and VM-ADCP along the Svinøy section.

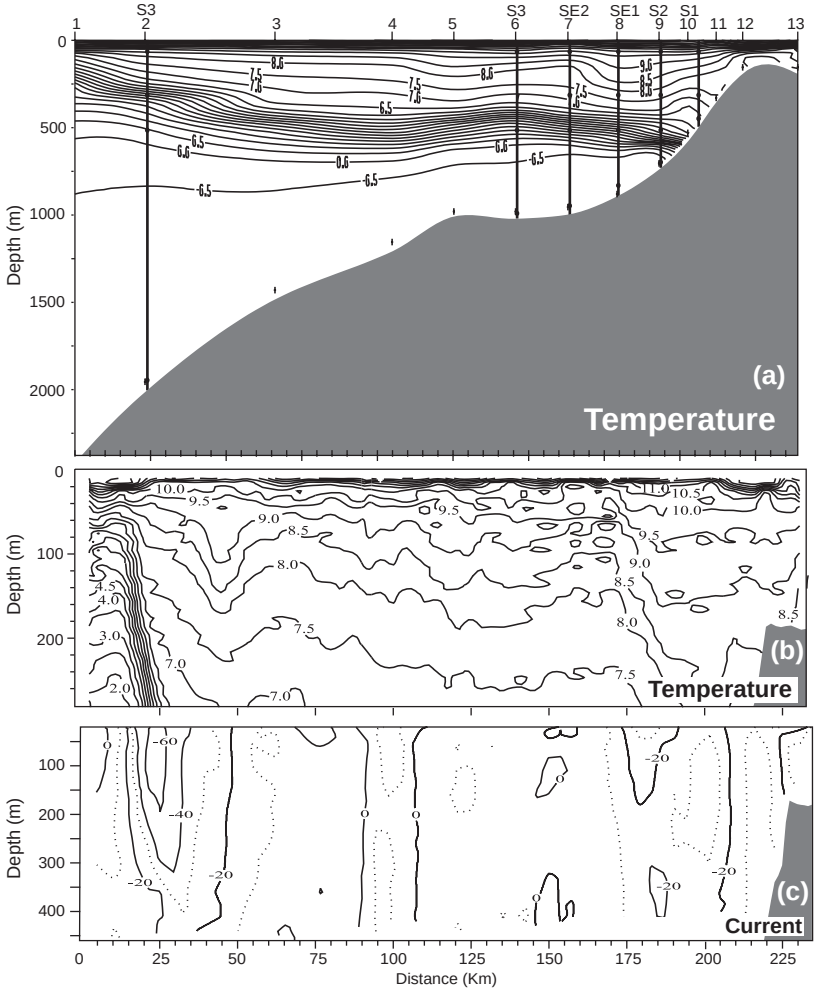

Figure 2. (a) CTD, (b) SeaSoar-CTD, and (c) ADCP section along the Svinøy section, August 1997. Mooring lines and current meter depths are indicated.

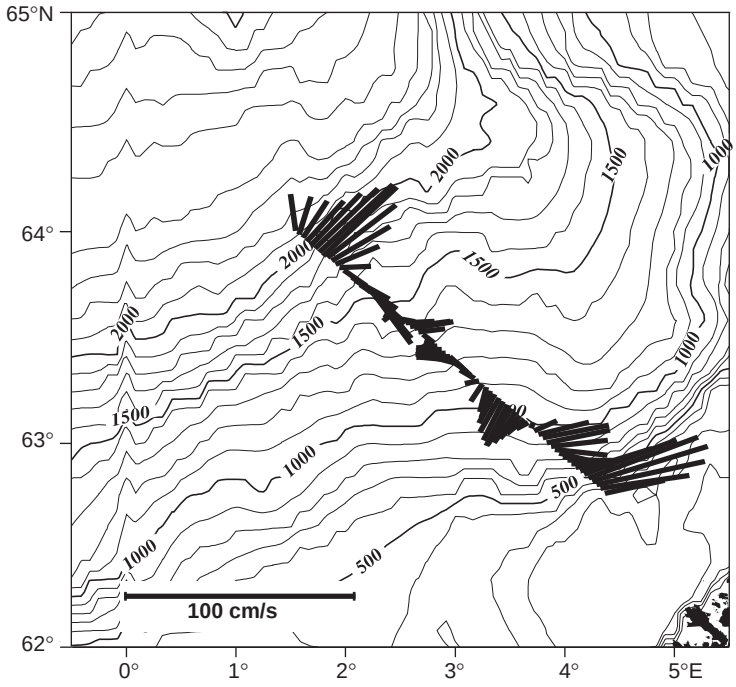

Figure 3. ADCP current plots, 5 min averaged, along the Svinøy section at 100 m depth, April 1997.

Atlantic inflow in the Svinøy section

The hydrography along the Svinøy section shows the extension of the AI as a wide, warm and saline wedge, extending more than about 300 km north-westwards from the shelf break (Fig. 2). This hydrography mirrors a wide and wedge-shaped baroclinic current consistent with the historical view of the AI. In Fig. 1 we have outlined the NAC as a two-branch current as indicated from surface Lagrangian drifters by Poulain et al., 1996. The VM-ADCP transect from April 1997 (Fig. 3) presented as current stick plots at 100 m depth, are the first Eulerian identification of the two-branch NAC; a western branch and an eastern branch.

Western branch

Fig. 2 shows contoured sections of standard CTD (temperature), SeaSoar-CTD (temperature) and VM-ADCP in August 1997. The SeaSoar-CTD transect was subsequently followed by the CTD section and demonstrates the improved horizontal resolution obtained by using SeaSoar-CTD compared with standard hydrography. The observations identify for the first time the western branch of the NAC as a 400 m deep and 30–50 km wide frontal jet, located just above the 2000 m isobath. The striking current jet with max. speed of 80 cm/s, coincides with the Polar Front in a meandering and unstable pattern.

Eastern branch

In the slope area, contoured mean currents 1997–1998 (Fig. 4) reveal the eastern branch as a 30–50 wide current with a significant barotropic component. The current shows evidence of topographic trapping over the slope, and the core of the flow is located between depths of 200 m and 800 m with an annual mean of 30 cm/s and maximum of 117 cm/s. The core shows a barotropic structure, while on the deeper side the baroclinicity is significant.

Flux estimates

Based on our current meter array, the volume flux of the AI in the eastern branch has been calculated. We define the AI as water with salinity above 35.0 psu, corresponding to temperatures above 5°C. For the two-year period August 1996 to October 1998, the estimates of the volume transport on a daily time scale ranges from -2.2 Sv ($1\text{Sv} = 10^6\ \text{m}^3\ \text{s}^{-1}$) to 11.8 Sv, and between 0.1 Sv and 8.0 Sv on a monthly time scale, respectively. The annual mean AI in this eastern branch is estimated as 4.4 Sv.

The sparse, current observations of the western branch preclude reliable, direct transport calculations. Therefore the baroclinic transport of AI to the west of SE2 (Fig. 3), is inferred from hydrography in a presumed geostrophical balance. When a certain density corresponds to a zero velocity reference interface outcrops the surface, the vertical density profile from one CTD station, will be sufficient to calculate the baroclinic volume transport (Jakhelln, 1936). We have used 33 CTD-casts from SE2 for the period 1995–1998 and the estimated volume transport of AI ranges from 1.3 Sv to 5.6 Sv, with

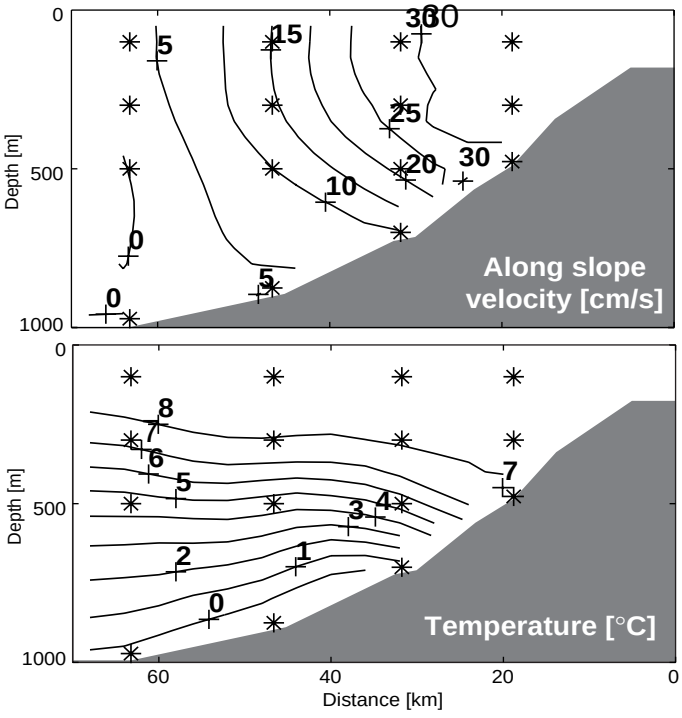

Figure 4. Current and temperature contours. Data from April 1997 to April 1998.

an overall mean of 3.4 Sv. Thus our investigations to date indicate a yearly mean AI of 7.8 in the Svinøy section.

Seasonality

The nearly four-year current time series from mooring S1 in the core of the AI (100 m depth) from April 1995 to February 1999 is presented in Fig. 5 together with the NAO (North Atlantic Oscillation) index (Jones et al., 1997) as 3-month low pass filtered records. Fig. 5 shows a strong connection between the NAO index and the eastern branch of the NAC from April 1996 to February 1999, where a high inflow coincides with a high NAO index. This indicates that the variabilities of the AI are strongly related to the westerlies in the North Atlantic. A high NAO index reflects a strong Icelandic low with a corresponding strong cyclonic wind stress curl forcing a large northward Sverdrup transport in the North Atlantic and a subsequent strong AI to the Norwegian Sea. Low index cases will reflect a different meteorological pattern with northerly winds over the eastern Norwegian Sea. However, the high summer inflow in 1995 and the subsequent winter maximum in 1996, both coincide with a low index. Thus, the AI is also influenced by other types of atmospheric modes .

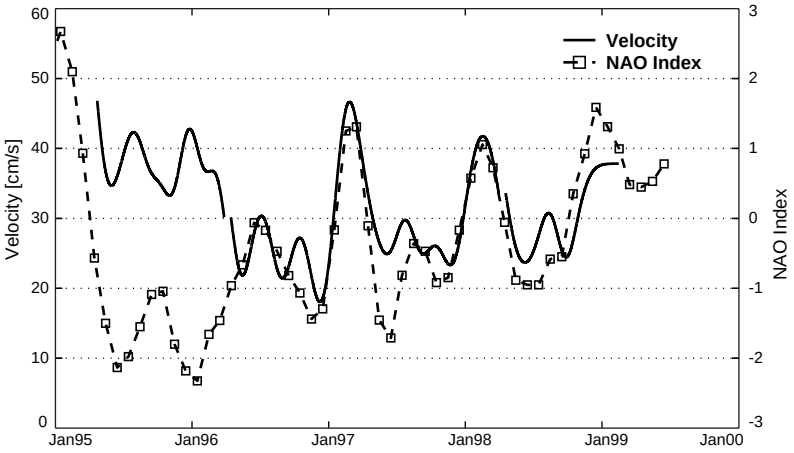

Figure 5. Current time series from April 1995 to February 1999 at 100 m depth on mooring S1 (full line) against the NAO index (dashed line) in terms of three months low pass filtered data.

Fig. 5 shows no systematic seasonal signal for the year 1995–1996, while the four consecutive years 1996, 1997, 1998 and 1999 show evidence of winter maxima and summer minima, i.e. a systematic annual cycle. Thus, the first monitoring year shows properties which are not representative to date, after four years of moored records. The offshore baroclinic volume fluxes show large variability within each month, but indicate a seasonal cycle.

The nearly four-year time series has made it feasible to resolve seasonality, and our findings show evidence of a systematic annual cycle. Our monitoring programme to date, has not exhibited any inter-annual or long term trends in the Atlantic inflow. In order to resolve decadal climate variations, the monitoring programme must be extended considerably.

References

Jakhelln, A., 1936: The water transport of gradient currents. Goefys. Publ., XI(11).

Jones, P. D., T. Jonsson, and D. Webber, 1997: Extension to the North Atlantic Oscillation using early instrumental pressure observations from Gibraltar and south-west Iceland. Int. J. Climatol., 17(13), 1433–1450.

Poulain, P.-M., A. Warn-Varnas, and P. P. Niiler, 1996: Near-surface circulation of the Nordic Seas as measured by Lagrangian drifters. J. Geophys. Res., 101(C8), 18237–18258.

Read, J. F., and R. T. Pollard, 1992: Water masses in the region of the Iceland-Faroes Front. J. Phys. Oceanogr., 22, 1365–1378.

MEETING TIMETABLE 2000

January 24–28	AGU Ocean Sciences Meeting	San Antonio, TX, USA
February 20–24	SOLAS Open Science Conference	Kiel, Germany
March 13–17	JSC Annual Meeting	Tokyo, Japan
April 3–7	Southern Hemisphere Meteorology and Oceanography	Santiago de Chile, Chile
April 5–7	WOCE Data Products Committee DPC–13	College Station, TX, USA
April 13–17	JGOFS 2nd Open Science Conference "Ocean Biogeochemistry: A New Paradigm"	Bergen, Norway
April 25–29	EGS General Assembly	Nice, France
May 1–5	CLIVAR SSG 9th Session	Honolulu, HI, USA
May 30–June 3	AGU Spring Meeting	Washington, DC, USA
June 27–30	2000 Western Pacific Geophysics Meeting	Tokyo, Japan
October 24–27	WOCE/CLIVAR Representativeness and Variability Workshop	Fukuoka, Japan
October 30–31	WOCE–27	Fukuoka, Japan
December 15–19	AGU Fall Meeting	San Francisco, CA, USA

Circulation and mode waters of the North Atlantic subpolar gyre in 1996

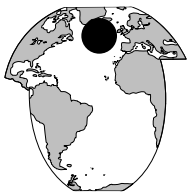

Raymond Pollard, Jane Read, and Penny Holliday Southampton Oceanography Centre, UK; and Harry Leach, University of Liverpool, UK. r.pollard@soc.soton.ac.uk

In October/November 1996 the second Vivaldi survey was undertaken as a UK contribution to WOCE. These surveys differed from most WOCE hydrography in that the full depth CTDs were widely spaced in order to survey in between them, underway at 8 knots, profiling to 400 m every few km with a CTD mounted on SeaSoar. Vivaldi '91 surveyed south of 54°N (Pollard et al., 1996), while Vivaldi '96 extended the survey northwards across the subpolar gyre (Fig. 1). However, the cruise began with closely spaced CTDs across the regularly occupied Rockall Trough section (Holliday et al., 1999) which was extended to Iceland for the first time. Here we show the upper layer circulation (Fig. 2) and the distribution and structure of Subpolar Mode Waters (SPMW) (Fig. 3, page 26).

Taking 1400 m as the zero velocity reference level, we have calculated the transport above that level between many CTD station pairs. We have confidence in this choice, as currents are mostly small at this depth and more careful inversions (van Aken and Becker, 1996; Bacon, 1997) (hereinafter AB and SB) yield similar depths of no motion. Where the CTD grid was not eddy resolving, SeaSoar data (Fig. 3) have been used to give confidence in the transport pathways sketched on Fig. 2. An equivalent figure is given by AB, the difference being that our data are close to synoptic while theirs is a mean over several years.

The easiest pathways to sketch were those for the Irminger Current flowing up the west flank of the Reykjanes Ridge. 10 Sv crosses our southern line (54°N) west of 25°W (between stations 02 and 05), half of it between CTDs 04 and 05 (25–30°W). All of this transport can be accounted for flowing northwards in the Irminger Basin, with 9 Sv passing between CTDs 88 and 89. These transports compare well with SB's 9 Sv and Krauss' (1995) 9.6 Sv west of the Ridge, while AB estimates 13 Sv turning back to cross the Reykjanes Ridge. Thus northward transport of 10 Sv in the Irminger Basin is well established. Isopycnic salinity maps (Fig. 3) indicate that most of this flow does not penetrate far into the Iceland Basin, being strongly steered back west round the Reykjanes Ridge in the vicinity of 57°N. Indeed, a possible interpretation of Figs. 2 and 3 is that as much as 5 Sv of the NAC may not cross the Ridge at all, branching south of Greenland to cross the Ridge at about 55°N, 40°W.

East of 25°W a further 17 Sv passes between CTDs 05 and 18. Of this, 14 Sv crosses the entrance to the Rockall Trough and is turned sharply north-west to pass to the south and west of the Rockall and Hatton Banks. The remaining 3 Sv passes through the Rockall Trough (compare Holliday et al., 1999). The transport across 54°N is in good agreement with Vivaldi '91 (Pollard et al., 1996) and with SB who shows 16 Sv of upper layer flow west of Hatton Bank. By 60°N the 14 Sv has reduced to about 12 Sv, which splits into two equal branches. 6 Sv passes north-eastwards both north and south of Lousy Bank (Fig. 2). We suspect that this enters the Norwegian Sea south and east of the Faroes but cannot be sure. The other 6 Sv turns towards Iceland so must turn north-east again along the Iceland Shelf before

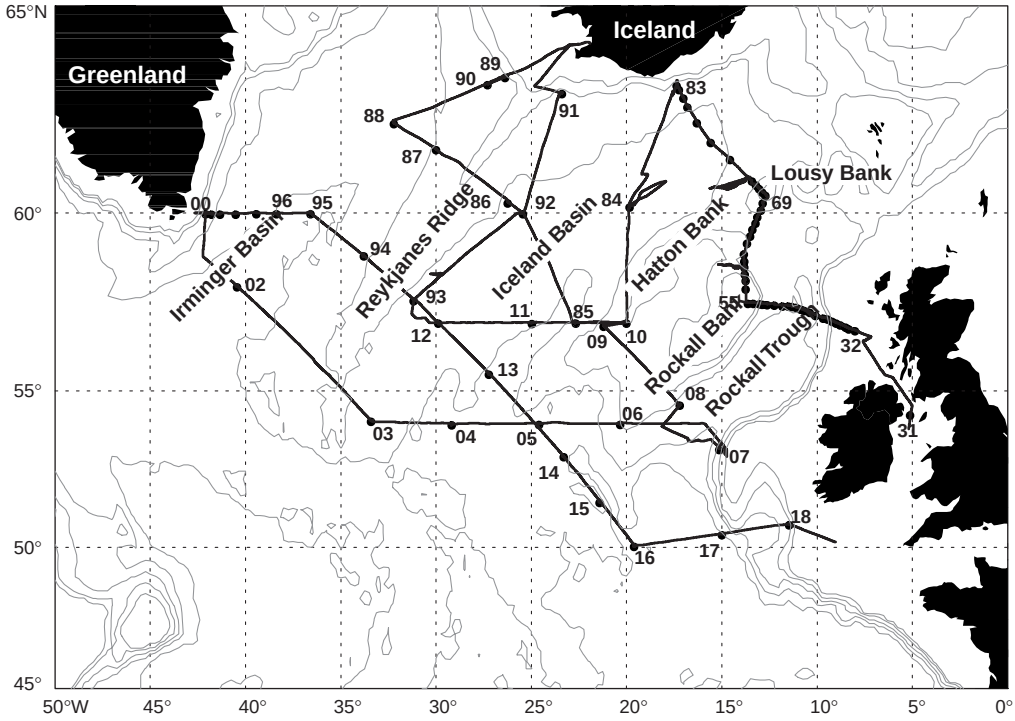

Figure 1. Track plot for Discovery Cruise 223, 28 September – 19 November 1996. All full depth CTDs are marked by dots. For some CTDs the last two digits of the Discovery station number are shown, starting with 31 (12931) and ending with 18 (13018).

turning east along the Iceland–Faroes Front (Read and Pollard, 1992; Krauss, 1995). We can be sure that the northward flow through the Iceland Basin did not turn west and cross the Reykjanes Ridge north of 60°N in 1996 because the transport between CTDs 91 and 92 (Fig. 1) was only 0.5 Sv and was eastwards. Nor could much of it have turned south to circulate cyclonically round the Iceland Basin, as the transport between CTDs 84 and 92 was only 1.1 Sv to the south. The reduction in transport between 50°N and the Iceland–Scotland section of 3 Sv from 17 Sv to 14 Sv (Fig. 2) is similar to that found by AB, who accounted for it by conversion of surface to intermediate waters.

It is also relevant to note the two areas of anticyclonic circulation in Fig. 2. Anticyclonic circulation of the upper layer is well documented in the Rockall Trough (Arhan et al., 1994; Bacon, 1997; Holliday et al., 1999). On the eastern flank of the Reykjanes Ridge we found southward flow of 2.5 Sv between each of station pairs 86–92 and 93–12. The property distributions between those station pairs on isopycnals (Fig. 3) match those further west over the Ridge and differ from those to the east in the Iceland Basin. This, together with the weak eastward transport between CTDs 91 and 92 mentioned above, shows that the southward flow must be part of anticyclonic circulation over the Ridge rather than cyclonic circulation round the Iceland Basin.

We are now in a position to refine the description of Subpolar Mode Water formation and circulation given by McCartney and Talley (1982), starting with the lightest SPMW ($\sigma_0 = 27.2\,\mathrm{kg\,m^{-3}}$, Fig. 3) in the south-east corner of the survey area. East of 25°W there is a marked change in stratification on 27.2, with saline water and weak stratification clearly indicating Eastern North Atlantic Water (ENAW), which is SPMW formed by winter mixing west of the Bay of Biscay (Pollard et al., 1996). A tongue of ENAW is transported north-west across the entrance to the Rockall Trough and the south-west flanks of the Rockall and Hatton Banks. High salinities extend well into the northern Rockall Trough, showing that ENAW is found everywhere east of 25°W, covering the Rockall and Hatton Banks and the whole of the Rockall Trough up to the Wyville-Thomson Ridge. On 27.3 the mode water extends round the west and north flanks of Hatton Bank into the Rockall Trough.

The effect of winter mixing is most striking on the 27.4 surface in the north Rockall Trough, where thicknesses reach over 160 dbar ($pv < 0.15 * 10^{-10}\ \mathrm{m^{-1}\,s^{-1}}$), over twice as high as on any other surface, and the depth of 27.4 (not shown) is over 700 dbar. Indeed, 27.4 is also over 700 dbar deep at CTDs 07 and 08 at the south end of the Rockall Trough, but thicknesses are much less, showing clearly that deep winter mixing in situ has penetrated down to the 27.4 density in the north Rockall Trough, and that water has not been replaced by advection from the south since the end of winter. Given that the highest salinities are at the surface (maximum over 35.5 on 27.2 south of Ireland), we infer that ENAW is mixed down to provide the high salinities on 27.4 in the north Rockall Trough.

Another striking feature is the apparent cyclonic progression of the saline, low potential vorticity 27.4 water round the northern end of the Iceland Basin and down the eastern flank of the Reykjanes Ridge. There is an enigma here, as westward flow south-east of Iceland is perpendicular to the transport pathways of Fig. 2. A possible explanation is that currents in the north Iceland Basin are relatively weak and may switch between eastward flow past Lousy Bank and northward flow to the Iceland Shelf (before turning east in the Iceland Faroes Current, e.g. Read and Pollard, 1992). This mechanism would shed eddies (like that at 62°N, 16°W, Fig. 2) which would transfer water westwards.

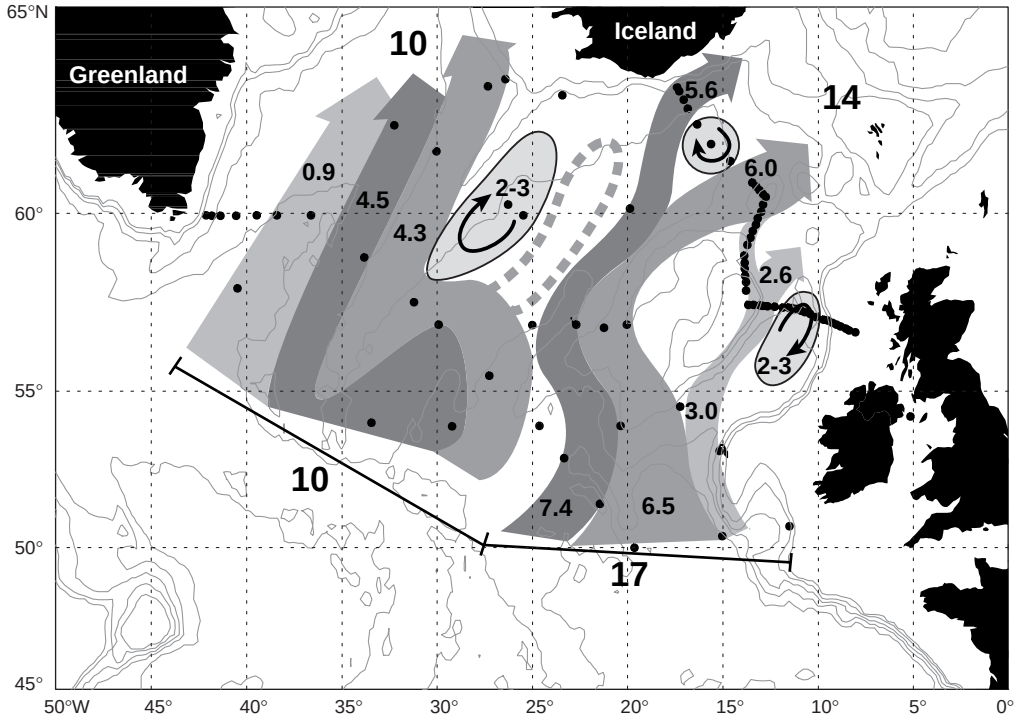

Figure 2. Pathways are sketched for transport (in Sv) of the flow above 1400 m relative to 1400 m. The wide, elongated arrows are bounded by streamlines, so that the numbers give the transport between pairs of streamlines.

On 27.5 the most weakly stratified water is found on the western flank of the Reykjanes Ridge,

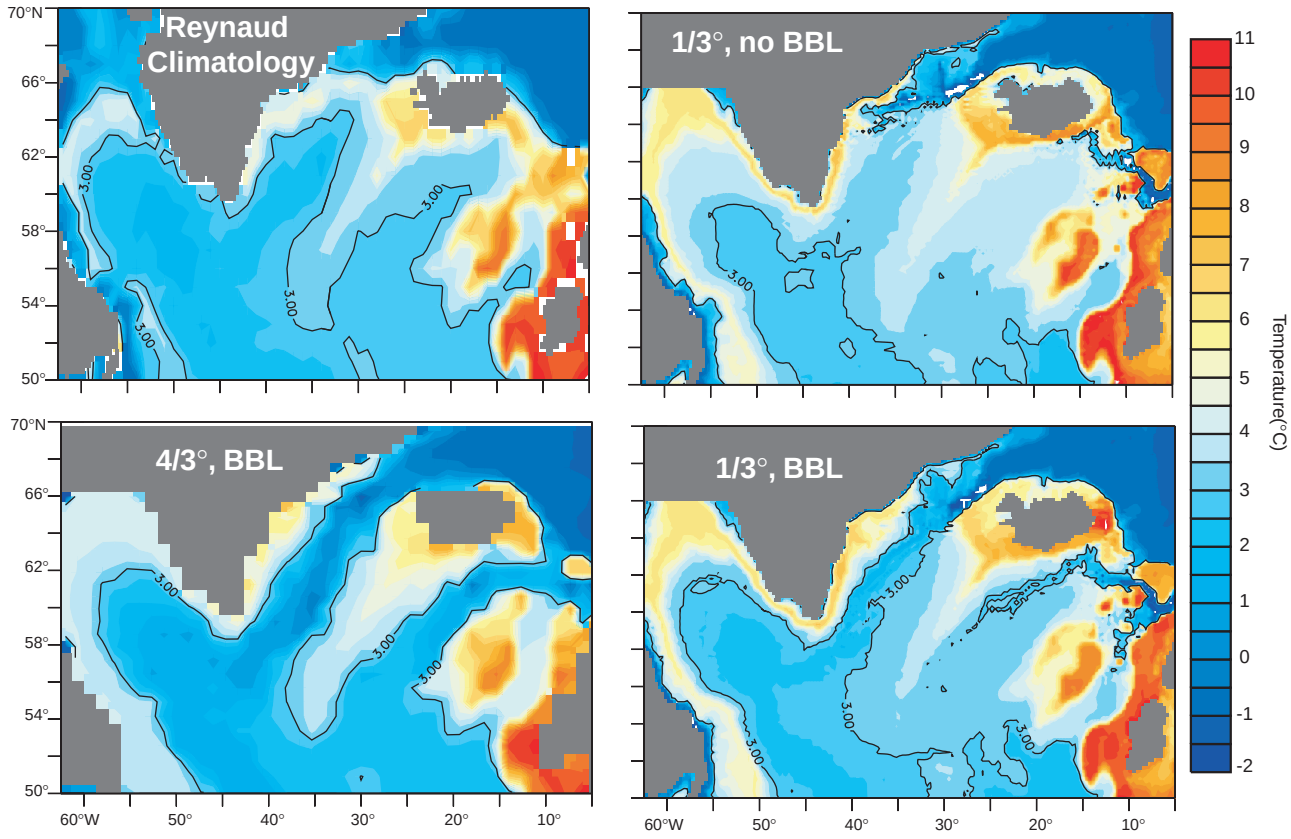

Dengg et al., page 10, *Figure 1. Annual mean potential temperature (°C) at the bottom of the ocean. Top left: climatology by Reynaud, top right: ⅓° model without BBL, bottom left: ⅘° model with BBL, and bottom right: ⅓° model with BBL. 3.0°C contour shown as solid line to facilitate comparison.*

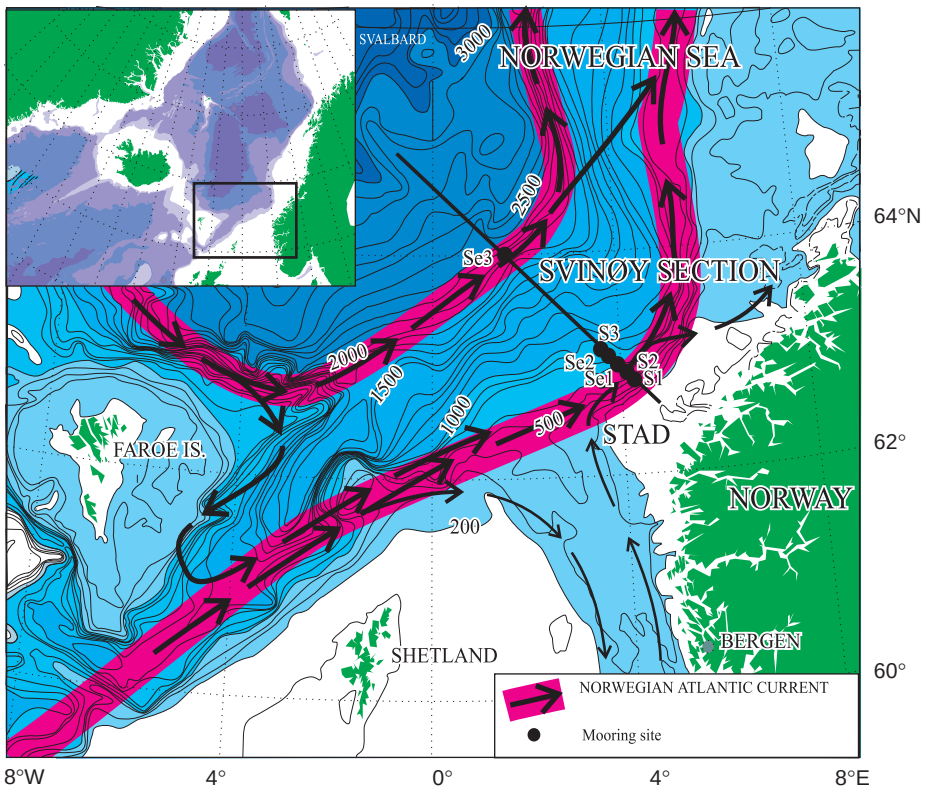

Orvik et al., page 18, *Figure 1. Schematic of surface currents showing the Atlantic inflow to the Norwegian Sea. Svinøy section with mooring sites is indicated as a full line.*

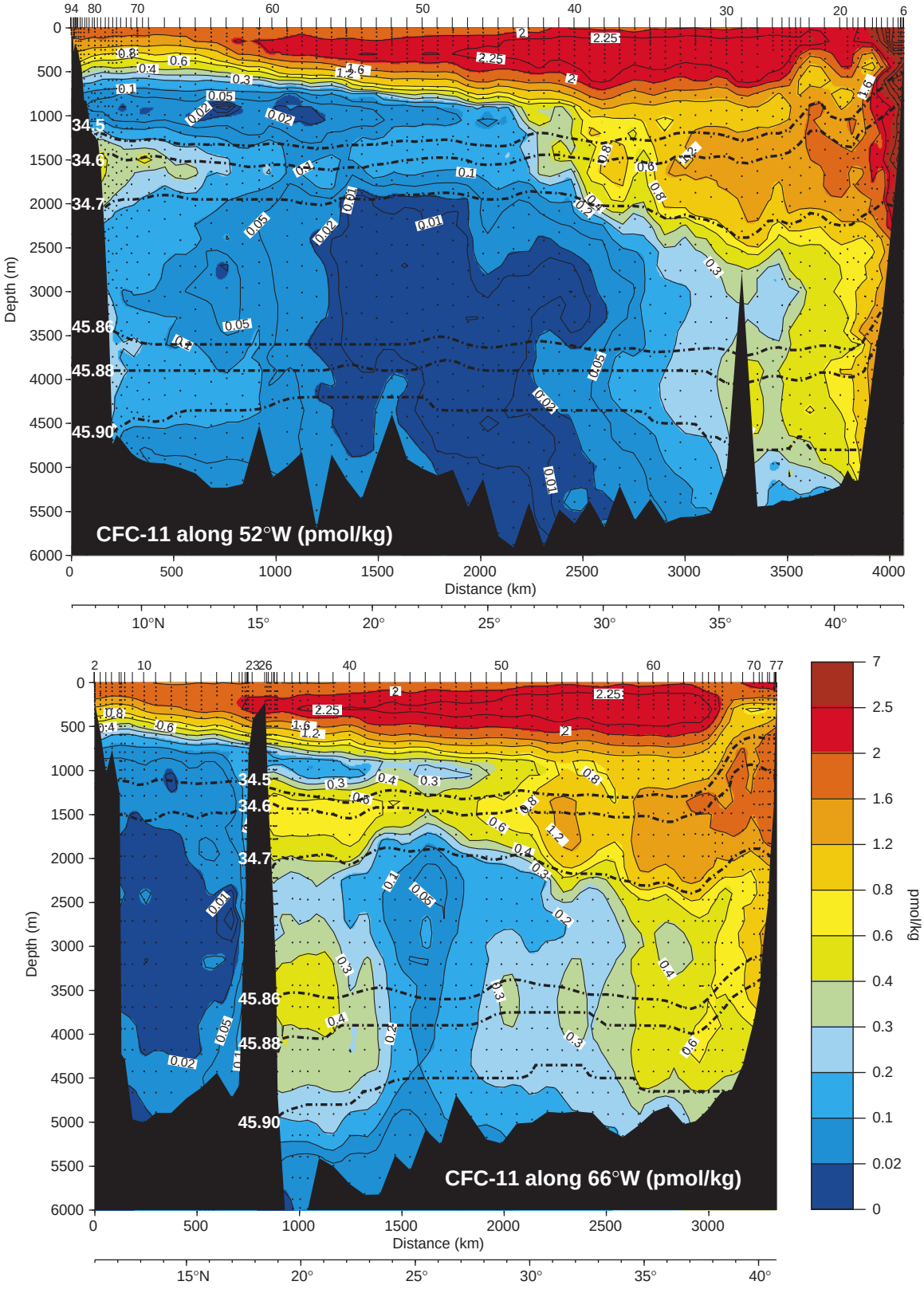

Smethie, page 15, *Figure 2. Vertical sections of CFC-11 (pmol/kg) along the WOCE A20 (52°W) and A22 (66°W) lines. Also plotted are constant density lines for* $\sigma_{1.5} = 34.5,\ 34.6,$ *and* 34.7 *and* $\sigma_4 = 45.86,\ 45.88,$ *and* 45.90. *See Fig. 1 for station locations.*

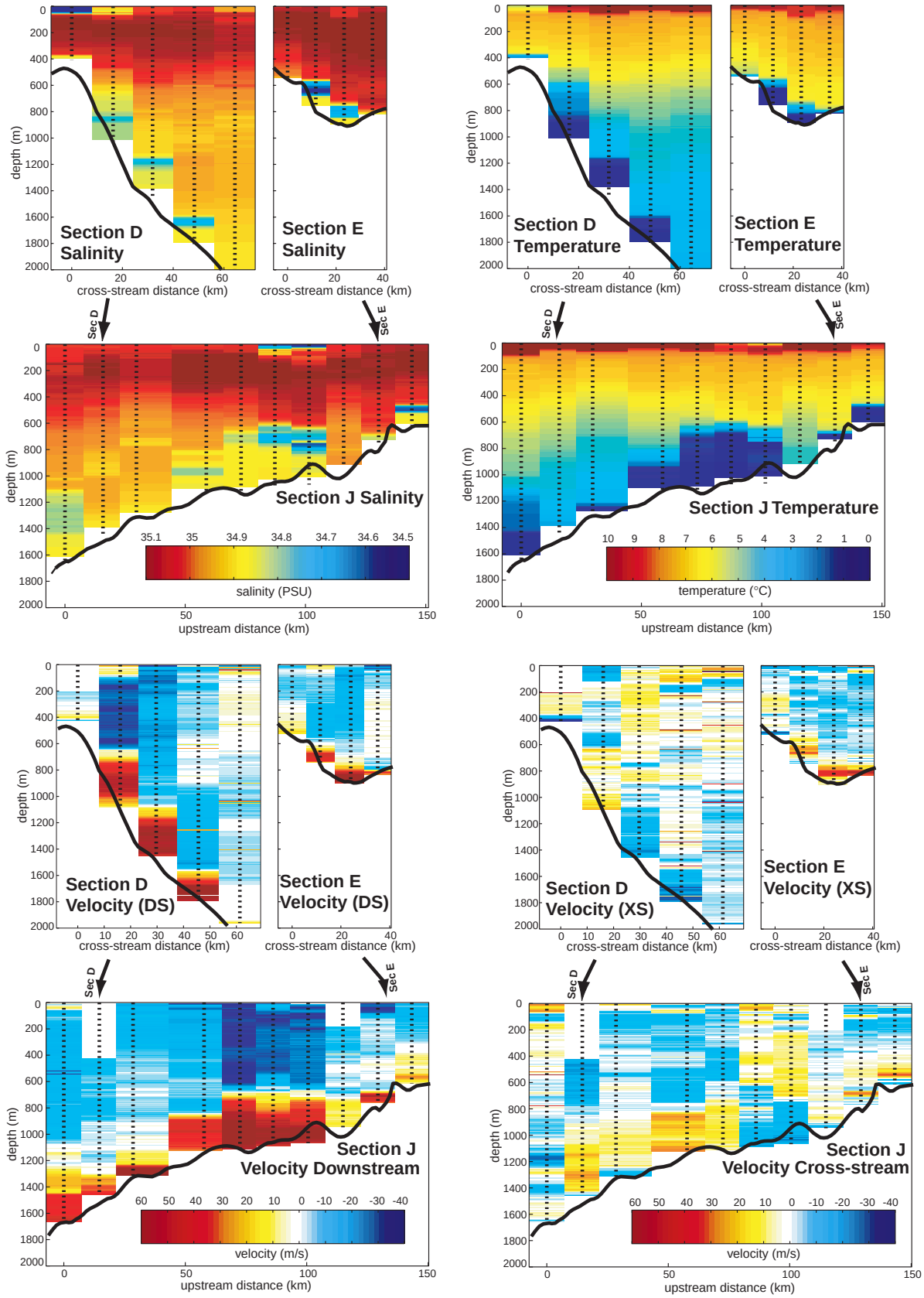

Girton and Sanford, page 28, *Figure 2. Properties measured along each of the three sections, D, E, and J. Profile positions are marked by vertical dotted lines. The mean velocity of each profile has been removed. Approximate bottom depths from Smith and Sandwell (1997) are shown as a heavy black line along each section, but do not always agree with the true depth encountered by the falling probes, as indicated by the extent of the dotted lines. Note that "downstream" is to the south-west, i.e., perpendicular to sections D and E, but parallel to section J.*

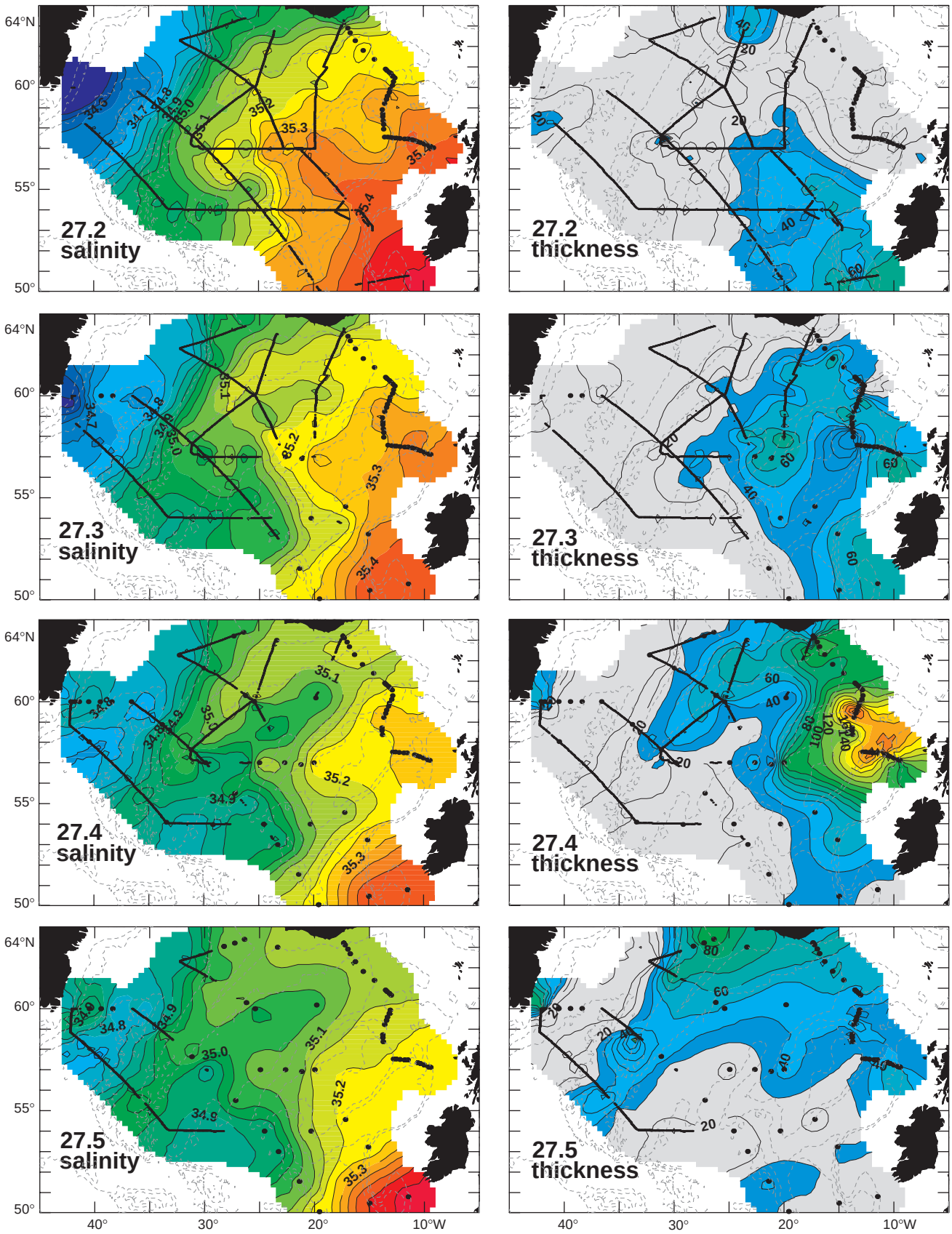

Pollard et al., page 21, *Figure 3. Salinity and thickness are mapped for the isopycnal surfaces σ_0 = 27.2, 27.3, 27.4 and 27.5 kg m^{-3}. Thickness is the separation in dbar of two density surfaces 0.025 kg m^{-3} apart, e.g. 27.175 and 27.2. Thus a thickness of 25 dbar equates to potential vorticity of 10^{-10} m^{-1} s^{-1}. Thicknesses greater than 30 dbar are coloured. Dashed lines are depth contours at 1000 m intervals. Dots and bold lines (which are actually dots at 4 km intervals) show where there are CTD data for each surface.*

with thickness increasing to the north (downstream). On 27.6 (not shown) the largest thicknesses are confined to the northern end of the Irminger Basin, reaching over 80 dbar at CTD 89. Thus the formation of 27.5 and 27.6 mode water is primarily in the Irminger Basin.

This analysis has revealed several interesting parallels between the Irminger and Iceland Basins. In both basins there is a branch of the NAC which first "overshoots" into the next basin to the east, then retroflects around the southern end of bathymetric features (the Reykjanes Ridge and Hatton Bank) before flowing north on the eastern side of each basin hard against the western flanks of those features. There is a marked step in salinity across each of these currents, with more saline water to the east in each case. This change is apparent on several isopycnal surfaces (Fig. 3), identifying a clear change in water mass, most saline in the Rockall Trough (ENAW) and west over Hatton Bank, less saline in the Iceland Basin and over the Reykjanes Ridge, and freshest in the Irminger Basin.

The most weakly stratified mode waters are found to the east of each of the two currents, i.e. over the Reykjanes Ridge and in the Rockall Trough. We believe that there are three reasons for this. The first is that higher salinities in the surface layer weaken the stratification, predisposing the water to deep winter mixing. The second is that both regions are areas of anticyclonic circulation (Fig. 2), which again predisposes the water to winter mixing. The final reason, we suspect, is that mode water is more likely to form where mean currents are weak. We have calculated the density difference between 200 and 300 m (not shown) and found the largest values along 54°N between 25–30°W, where relatively strongly stratified Subarctic Intermediate Water (Arhan, 1990) flows north at the entrance to the Iceland Basin. Similarly the East Greenland Current advects very fresh water down the western side of the Irminger Basin. Thus, where there are strong surface currents there is the potential to maintain the stratification of the surface layer by advection.

In summary, our synoptic data sets (Vivaldi '91 and '96) suggest that mode water property progression round the subpolar gyre is not a gradual, connected process as McCartney and Talley (1982) proposed from the sparse data available to them. Rather, we propose that mode water is most likely to form in areas of weak anticyclonic circulation. (Pollard et al., 1996) found $27.1 – 27.2\ \mathrm{kg\,m^{-3}}$ mode water forming in the large area with such circulation west of Spain and the Bay of Biscay. Here we have shown that $27.4\ \mathrm{kg\,m^{-3}}$ mode water forms in the north Rockall Trough and that $27.5 – 27.6\ \mathrm{kg\,m^{-3}}$ mode water forms over the Reykjanes Ridge and most strongly in the northern Irminger Basin. However, from those formation regions there is a tendency for the mode water to be carried cyclonically round the margins of the Iceland and Irminger Basins.

References

Arhan, M., 1990: The North Atlantic Current and Subarctic Intermediate Water. J. Mar. Res., 48, 109–144.

Arhan, M., A. Colin de Verdière, and L. Mémery, 1994: The eastern boundary of the subtropical North Atlantic. J. Phys. Oceanogr., 24, 1295–1316.

Bacon, S., 1997: Circulation and fluxes in the North Atlantic between Greenland and Ireland. J. Phys. Oceanogr., 27, 1420–1435.

Holliday, N. P., R. T. Pollard, J. F. Read, and H. Leach, 1999: Water mass properties and fluxes in the Rockall Trough; 1975 to 1998. Deep-Sea Res., in press.

Krauss, W., 1995: Currents and mixing in the Irminger Sea and in the Iceland Basin. J. Geophys. Res., 100, 10851–10871.

McCartney, M. S., and L. D. Talley, 1982: The Subpolar Mode Water of the North Atlantic Ocean. J. Phys. Oceanogr., 12, 1169–1188.

Pollard, R. T. , M. J. Griffiths, S. A. Cunningham, J. F. Read, F. F. Pérez, and A. F. Ríos, 1996: Vivaldi 1991 – A study of the formation, circulation and ventilation of Eastern North Atlantic Central Water. Prog. Oceanogr., 37, 167–192.

Read, J. F., and R. T. Pollard, 1992: Water masses in the region of the Iceland–Færoes Front. J. Phys. Oceanogr., 22, 1365–1378.

van Aken, H. M., and G. Becker, 1996: Hydrography and through-flow in the north-eastern North Atlantic Ocean: the NANSEN project. Prog. Oceanogr., 38, 297–346.

Velocity profile measurements of the Denmark Strait Overflow

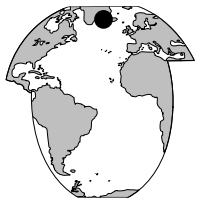

James B. Girton and Thomas B. Sanford, Applied Physics Laboratory and School of Oceanography, University of Washington, USA. girton@ocean.washington.edu

The Denmark Strait Overflow (DSO) is a vigorous and rapidly-varying segment of the North Atlantic thermohaline circulation, transporting convectively-formed cold and dense water southward to become the deep western boundary current and North Atlantic Deep Water (NADW). Because of the importance of this flow to ocean–atmosphere heat transport as well as the possibility that past climate changes have been associated with thermohaline shutdowns, the DSO and other outflows from the Nordic Seas have been the subject of much recent study, including a number of hydrographic sections and moored current meter arrays. We report here on a new approach using instantaneous velocity profiles to gain a greater understanding of the characteristics of the DSO.

In combination, these studies have arrived at estimates of some of the mean and fluctuating characteristics of the DSO. Over the course of the 37 day "OVERFLOW '73" deployment, at the same location as the present study, the mean transport of water colder than 2°C was about 2.9 Sv (Ross, 1984). Longer-term mooring deployments downstream (to the southwest, along the Greenland slope) have suggested that measurements 10 days or more in duration are sufficient to achieve a stable mean transport estimate, and that on longer timescales the rate of NADW formation appears steady despite substantial variability in the convective activity of the source regions (Dickson and Brown, 1994). This view is the subject of current debate (Bacon, 1998; McCartney et al., 1998).

The short-term variability in the flow and hydrographic properties is large – on at least the same order as the mean – and has a dominant period of just a few days. Simultaneous measurements of hydrography show that pulses in transport are often associated with discrete intermediate-depth salinity minima. In addition satellite measurements of surface temperature in the Denmark Strait show a persistent train of cyclonic eddies with similar spatial and temporal scale to transport pulses and salinity minima (Bruce, 1995).

Measurements

With the goal of investigating the connection between the deep layer transport events, intermediate low-salinity patches, and cyclonic surface eddies, as well as gaining a greater understanding of the energy balances at work in the flow, we made a set of velocity profiles (locations shown in Fig. 4) from the Finnish RV Aranda during August 1997. In addition, a set of standard hydrographic stations including CTD and chemical tracers were taken throughout the region on this cruise and have been recently described by Rudels et al. (1999).

In all, twenty-three expendable current profilers (XCPs) were deployed in two sections across (D and E) and one along (J) the path of the overflow, measuring velocity and temperature. Advantages of this technique over previously-used methods for study of the DSO include the use of directly-measured (as opposed to geostrophically calculated) velocity in a closely spaced pattern covering the full water column as well as the ability to measure to within less than a metre from the ocean bottom, allowing resolution of the turbulent boundary layer, as shown in Fig. 1.

The XCP is a self-contained, free-falling profiler

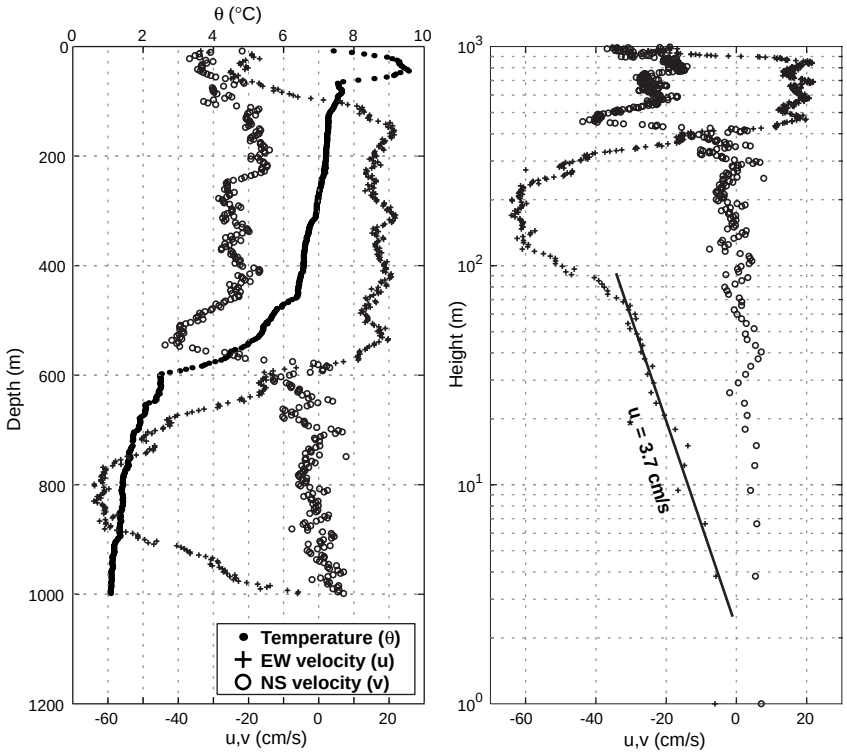

Figure 1. A sample XCP profile from section D showing temperature and relative velocity (magnetic north and east components, left panel) and the logarithmic velocity fit for estimating bottom stress (right panel). In this profile, the shear in the bottom layer happens to lie almost entirely in the magnetic west direction, so that the u_* value obtained is nearly the true one.

based on the principles of geomagnetic induction (Sanford et al., 1993). The instrument consists of a surface float/transmitter and a free-falling probe containing electrodes, a thermistor, and electronics. Data are sent to the ship in real time via an RF link. The autonomous nature of the XCP makes deployment possible in a wide range of weather conditions, and allows for rapid surveying at full vessel speed. Although the survey described here also used a lowered CTD, the XCP can be used in conjunction with expendable CTD (XCTD) probes in situations, like the DSO, where rapid sampling is important. This technique was employed in a later cruise in 1998, which will be reported on in future publications. Since the geomagnetic induction technique yields a profile of relative velocity only, additional information is needed to get absolute flows (as required, for instance, to estimate the volume transport of the DSO). This can be accomplished using near-surface velocity from a vessel-mounted ADCP combined with accurate GPS navigation. In the measurements presented here, however, the profiles have either had their mean velocity removed (Figs. 1, 3 and 2, page 25) or have been referenced to the overlying Atlantic water (Fig. 4). Both methods emphasise features in the shear profile which may be obscured when the (often large) barotropic component of velocity is added in.

Results and discussion

The basic character of the DSO is that of a cold, dense layer flowing to the south-west beneath an interior of warm and salty Atlantic Water (AW). The speed of this bottom layer ranges from $30\,\mathrm{cm\,s^{-1}}$ to $100\,\mathrm{cm\,s^{-1}}$ and the thickness from 40 m to 400 m. Many of the largest overflow speeds and layer thicknesses were seen in conjunction with an overlying salinity minimum (observed in nearly-concurrent CTD casts), indicating the presence of Polar Intermediate Water (PIW, sometimes called upper Arctic intermediate water), distinct from the Arctic Intermediate Water (AIW) and Norwegian Sea deep Water (NSW) which make up the bulk of the overflow. These three water masses give an interior stratification to the overflow which may act to inhibit mixing between its denser parts and the overlying Atlantic water, as suggested by Rudels et al. (1999).

Temperature, salinity and velocity measured along the three sections are shown in Fig. 2, with a 3-D representation of sections D and E shown in Fig. 3. Notice the pronounced veering in the near-bottom velocity of many of the profiles. In addition to the strong bottom-layer plume velocities, section J shows possible evidence of a cyclonic surface eddy, of the sort observed by Bruce (1995), between kilometre 50 and 100, both in the temperature and salinity of the top 50 m and in the cross-stream component of velocity in the top 800 m (above the thick section of the bottom plume). Section D shows a hint of a similar feature. Also interesting to note is the Ekman-type veering in the cross-stream (XS) velocity that sometimes appears as a shift from red to blue approaching the bottom.

In some cases, the profiles reveal strong veering above and within the overflow. Most also resolve part of the bottom turbulent boundary layer and can be used to estimate parameters of this layer, such as bottom stress. A constant-stress turbulent boundary layer (sometimes called a log layer) velocity profile has the form $u = (u_* / k) ln(z / z_0)$, where k is the von Kármán constant (≈ 0.4), z_0 is the roughness length, and u_*, the friction velocity, is related to the bottom stress, τ, by $u_* = \sqrt{\tau / \rho}$ and can be estimated by fitting a straight line to the profile in semilog space. Fig. 1 shows an example of this. The component of velocity giving the greatest u_* by this method is the direction in which the boundary layer stress operates. The distribution of u_* directions and magnitudes over the XCP survey is shown in Fig. 4, along with the direction and speed of the fastest part of the bottom layer (the "nose"). Note that absolute velocities have not yet been determined for these profiles, so the nose velocity estimate has been subjectively determined by referencing to the overlying warm water. The result is that the vectors are in fact indicating the direction and magnitude of the shear, rather than an absolute velocity. The effect of the bottom Ekman layer veering is again apparent here, with the u_* direction almost always lying to the left of the nose velocity, indicating a downslope flow close to the bottom.

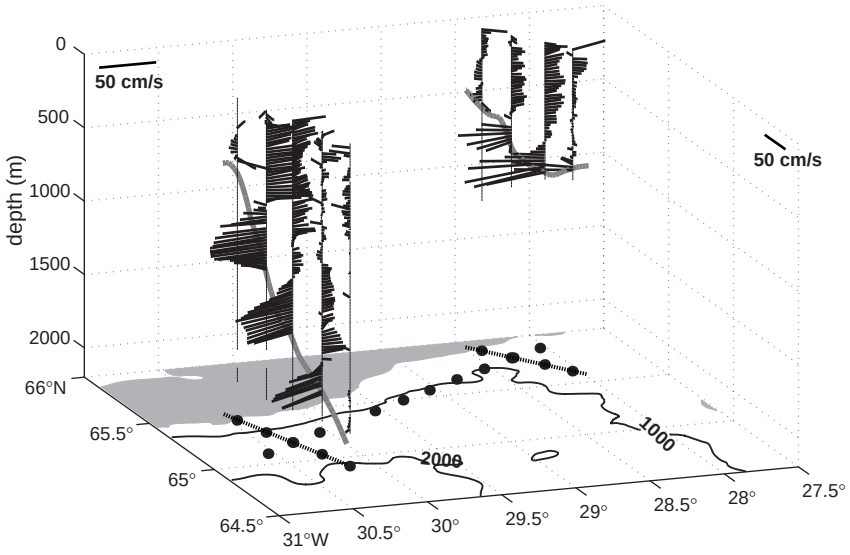

Figure 3. Profiles of relative velocity in cross-overflow sections (D and E). The mean of each profile has been removed. Bathymetry is shown on the lower surface. Water of less than 500 m depth is shaded light grey, and the 1000 m and 2000 m depth contours are shown as solid lines. Heavy grey lines indicate the approximate bottom depth along each section.

Conclusions

The measurements presented here represent some of the first full-water-column velocity profiles made in the Denmark Strait, and show some features of the velocity in and above the overflow plume. Large values of bottom stress are present in the boundary layer, indicating its likely importance to the momentum balance of the plume (as shown for the Mediterranean outflow by Johnson et al., 1994). In addition, Coriolis forces play a strong role in the veering of the near-bottom velocity profile. The plume was observed in a number of different states throughout the 22 profiles, including thick and thin bottom layers, and velocity maxima ranging from 50 to 100 cm s^{-1}. The intermediate salinity minimum appears to be strongly correlated with high velocity and a thick overflow layer, suggesting a possible dynamical significance. In a follow up to these measurements, a more extensive survey was undertaken in September 1998 from the RV Poseidon, deploying 110 XCPs and 76 XCTDs and attempting to characterise the large temporal and spatial variability in the DSO. These recent results will be discussed elsewhere.

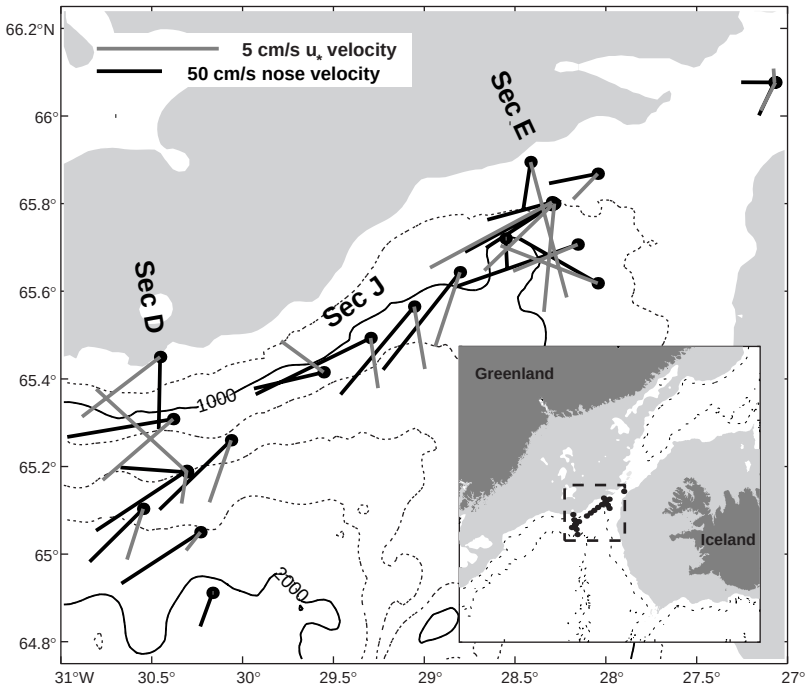

Figure 4. Vectors indicating the overflow plume maximum relative velocity in black and friction velocity (u_*) magnitude and direction in grey for each XCP profile. The inset shows the survey location in a larger geographical context with water depth less than 500m shaded and the 1000m and 2000m contours from Smith and Sandwell (1997) sketched in. In the main figure contours at 250m interval are also shown.

Acknowledgements

The authors would like to thank Bob Dickson, Pentti Malkki, the Finnish Institute of Marine Research, and the VEINS project for providing the time on the Aranda to carry out the measurements, and for allowing the use of data from the ship's CTD instrument. This work was made possible by support from the National Science Foundation (OCE-9712313).

References

Bacon, S., 1998: Decadal variability in the outflow from the Nordic Seas to the deep Atlantic Ocean. Nature, 394(27), 871–874.

Bruce, J. G., 1995: Eddies southwest of the Denmark Strait. Deep-Sea Res., 42(1), 13–29.

Dickson, R. R., and J. Brown, 1994: The production of North Atlantic Deep Water: Sources, rates, and pathways. J. Geophys. Res., 99(C6), 12319–12341.

Johnson, G. C., T. B. Sanford, and M. O'Neil-Baringer, 1994: Stress on the Mediterranean outflow plume, I: Velocity and water property measurements. J. Phys. Oceanogr., 24(10), 2072–2083.

McCartney, M., K. Donohue, R. Curry, C. Mauritzen, and S. Bacon, 1998: Did the overflow from the Nordic Seas intensify in 1996–1997? Int. WOCE Newsl., 31, 3–7.

Ross, C. K., 1984: Temperature–salinity characteristics of the "overflow" water in Denmark Strait during "OVERFLOW '73". Rapp. P.-v. Réun. Cons. int. Explor. Mer., 185, 111–119.

Rudels, B., P. Eriksson, H. Grönvall, R. Hietala, and J. Launiainen, 1999: Hydrographic observations in Denmark Strait in fall 1997, and their implications for the entrainment into the overflow plume. Geophys. Res. Lett., 26(9), 1325–1328.

Sanford, T. B., E. A. D'Asaro, E. L. Kunze, J. H. Dunlap, R. G. Drever, M. A. Kennelly, M. D. Prater, and M. S. Morgan, 1993: An XCP user's guide and reference manual. Technical Report APL/UW 9309, Applied Physics Laboratory, University of Washington, Seattle, WA, USA.

Smith, W. H. F., and D. T. Sandwell, 1997: Global sea floor topography from satellite altimetry and ship depth soundings. Science, 277(5334), 1956–1962.

Satellite tracked surface drifters and "Great Salinity Anomalies" in the subpolar gyre and the Norwegian Sea

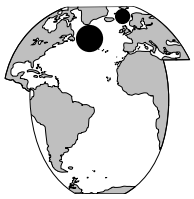

Svend-Aage Malmberg and Hedinn Valdimarsson, Marine Research Institute, Iceland.
svam@hafro.is

The drift of three selected SVP WOCE drifters, drogued at 15 m depth, is described, all deployed in Icelandic waters in August/September 1995, two operating to September–October 1998 and one still operating in August 1999. These drifters were produced by Clearwater Instrumentation and made available by Prof. Peter Niiler at the Scripps Institution of Oceanography (SIO), La Jolla in a programme that was carried out in cooperation with the Marine Research Institute, Reykjavík (MRI).

Altogether 120 drifters were deployed seasonally in Icelandic waters during the years 1995–1998, 60 Clearwater drifters and 60 Technocean drifters (Valdimarsson and Malmberg, 1999). Just a few drifters had a lifetime exceeding one year except those described in the present paper whose lifetime is about 3–4 years.

Result

First, a drifter deployed in August 1995 off West Iceland is considered (23508, Fig. 1). It drifted westwards to Greenland and followed the East and West Greenland Currents along Greenland and around Cap Farewell during 90 days. From there it drifted after some eddy drift in the Labrador Sea southwards to 46°N off Newfoundland where in August 1997, after 360 days drift, it bent eastwards again. It crossed the Mid-Atlantic Ridge 1998 after 600 days just south of the Charlie-Gibbs Fracture Zone at about 52°N and continued northwards in the Icelandic Basin up to 58°N 28°W after 810 days, i.e. on the eastern side of the Mid-Atlantic Ridge, it was trapped in eddy circulation for a while. From there, it crossed the Ridge and continued northwards on the western side to 65°N (June 1998) closing the loop of the "Subpolar Gyre". It turned again southwards with the East Greenland Current and around Cap Farewell into the West Greenland Current (August 1998) and further with the Labrador Current south to 48°N just along the same paths as almost 1000 days or 32 months before, which corresponds to about 6 km per day or 6–7 cm/sec in overall average. The East and West Greenland Currents and the Labrador Current show the highest velocities or 20–30 cm/sec.

In the second round of the drifter it bent eastwards along 48°N (not shown in Fig. 1) or north of the Flemish Cap where it, in the first round, drifted eastwards south of the Cap. In the second turn it then drifted eastwards at a more southerly latitude (48°N) than during the first one (50–52°N), reaching 36°W in August 1999.

Secondly, two other long distance drifters considered in this report drifted eastwards into the Norwegian Sea and Norwegian waters (Fig. 2). They (23525, 23577) were deployed in the waters west of Iceland in August/September 1995 and drifted with the North Icelandic Irminger Current into North Icelandic waters in three to six months. From there, they continued southwards with the East Icelandic Current into the Faroe Current north of the Faroes (1996–1997) and further eastwards into Norwegian waters at 63–64°N. They continued northwards along Norway with the Norwegian Atlantic Current and further into the waters west of Spitzbergen after 1000–1100 days (76–78°N; August 1998). One of these drifters was, for a time, captured by eddies in the Lofoten Basin. The overall mean drift speed corresponds to 3.6 km per day or 4.0 cm/sec, but the highest velocities were obtained in the East Icelandic Current north of the Faroes and in the Norwegian Atlantic Current or up to 15 cm/sec.

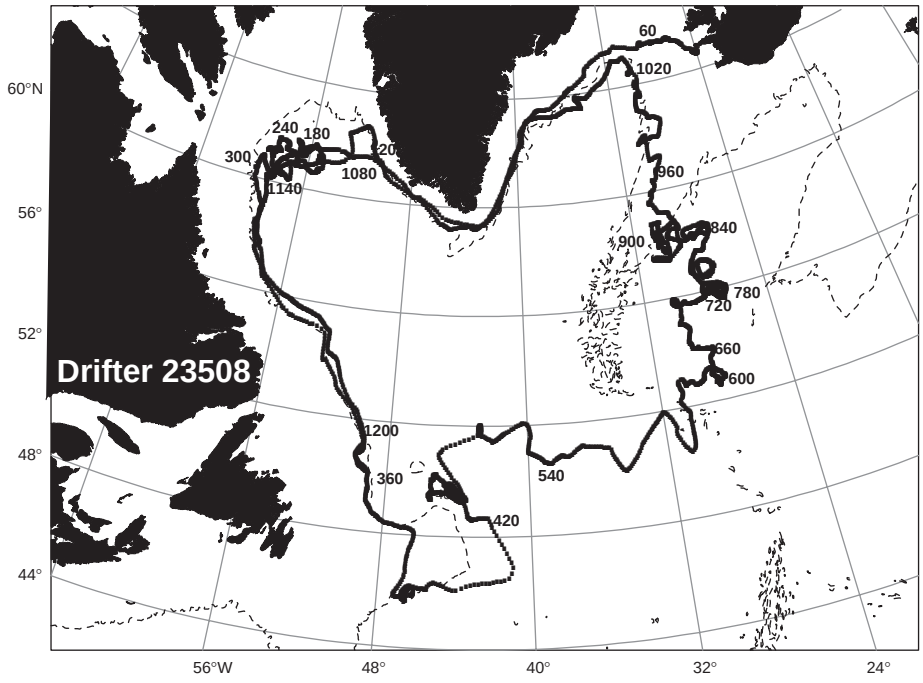

Figure 1. Drift of a satellite tracked surface buoy around the Irminger and Labrador Seas 1995–1999. Number indicates drifting days and depth contours of 2000 m depth.

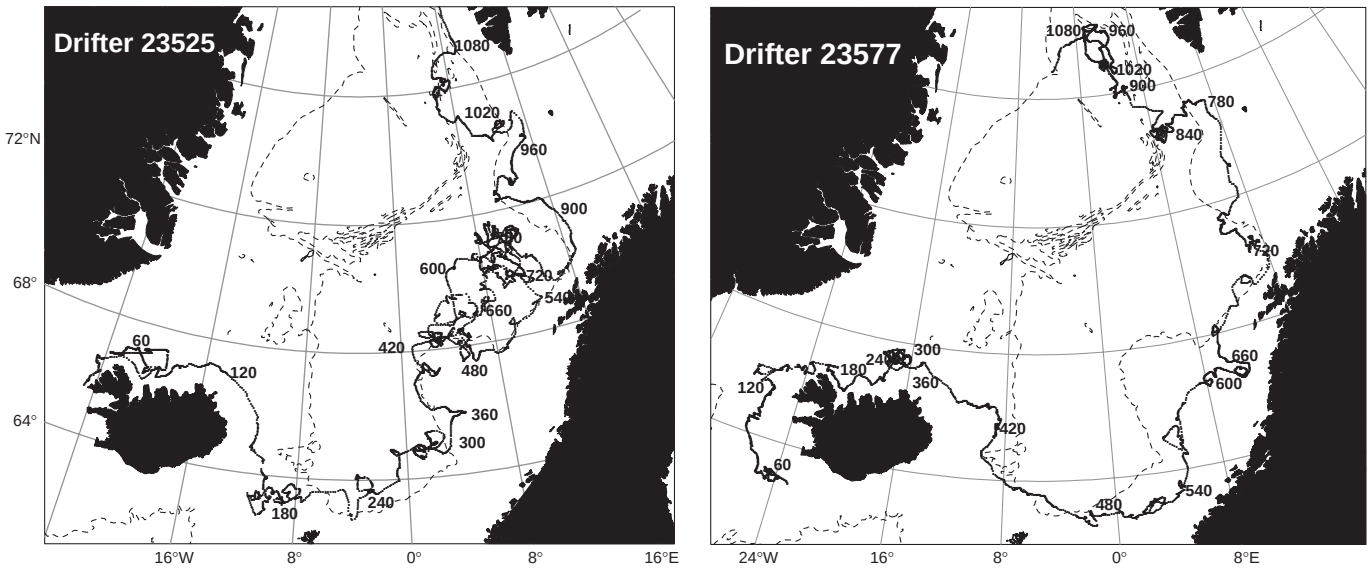

Figure 2. Drift of two satellite tracked surface buoys in the Iceland and Norwegian Seas 1995–1998. Number indicates drifting days and depth contours of 2000 m depth are shown.

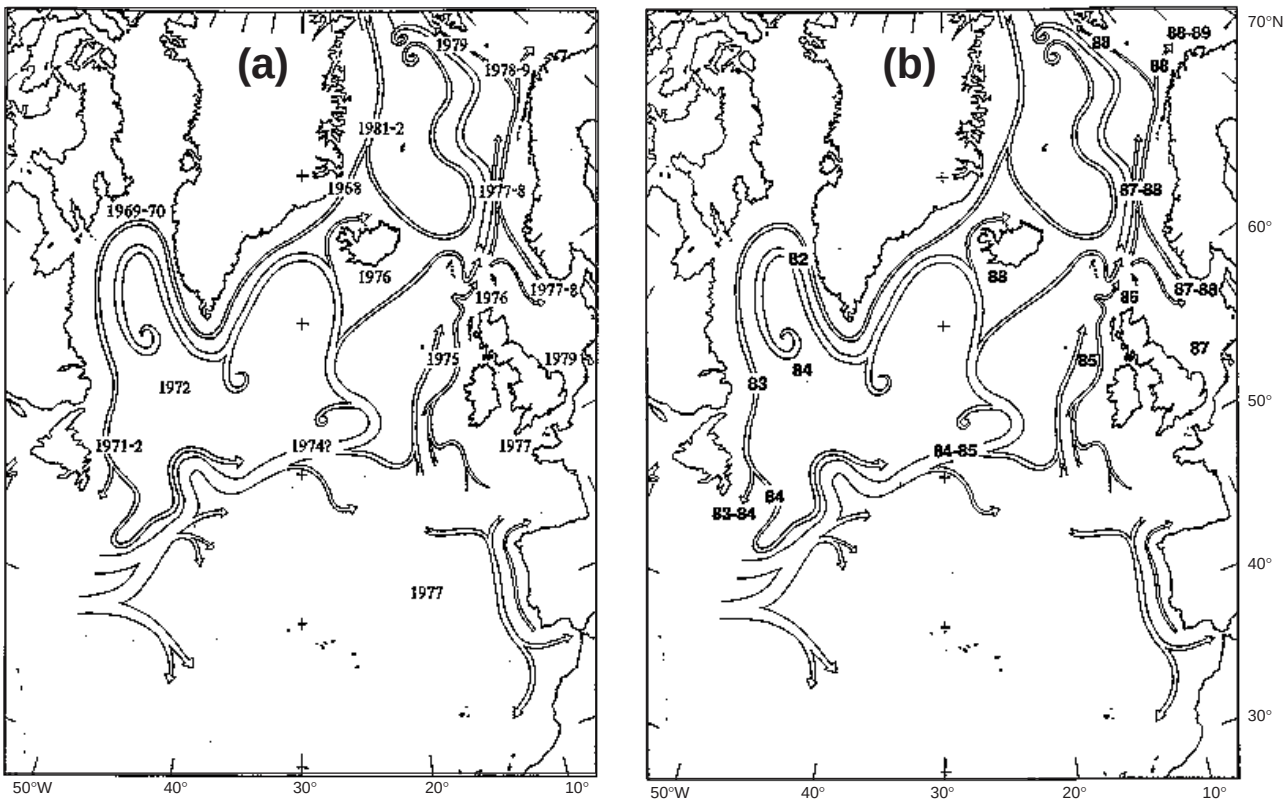

Figure 3. Circulation scheme and transit dates for the minimal values of the GSA of (a) the seventies (Dickson et al., 1988) and (b) the eighties (Belkin et al., 1998).

Discussion and conclusions

These results of drifters deployed in Icelandic waters in August/September 1995 reveal at least two new features, i.e. a long lifetime and a drift around the Subpolar Gyre in the Irminger and Labrador Seas in about 1000 days as well as into the Norwegian Sea northwards to Spitzbergen (Poulain et al., 1996), also in about 1000 days. This drift was along known pathways of ocean circulation in the area (Fig. 3). The steering by the bottom topography is also very evident (Figs. 1 and 2).

At last, comparing the drift velocity of the drifters with the "Great Salinity Anomalies" in the northern North Atlantic in the seventies (Dickson et al., 1988; Fig. 3a) and eighties (Belkin et al., 1998; Fig. 3b) a good agreement is observed for those drifters deployed in Icelandic waters and drifting into Norwegian waters in 2–3 years. This may be due to an advective nature of the circulation in general. The drifter drifting around the Irminger and Labrador Seas reveal a much higher velocity than the salinity anomalies or 2–3 years against up to 8 years respectively. This may be due to the diffusive nature of the salinity anomalies in general vs. an advective nature of the drifter.

References

Belkin, I. M., S. Levitus, J. Antanov, and S. A. Malmberg, 1998: "Great Salinity Anomalies" in the North Atlantic. Prog. Oceanogr., 41–68.

Dickson, R. R., J. Meincke, S. A. Malmberg, and A. Lee, 1988: "The Great Salinity Anomaly" in the northern North Atlantic, 1968–1982. Prog. Oceanogr., 20(2), 103–151.

Poulain, P.-M., A. Warnas, and P. P. Niiler, 1996: Near surface circulation of the Nordic seas as measured by Lagrangian drifters. J. Geophys. Res., 101, 18237–18258.

Valdimarsson, H., and S. A. Malmberg, 1999: Near-surface circulation in Icelandic waters derived from satellite tracked drifters. Rit Fiskideildar, in press.

WOCE/CLIVAR Variability Workshop, 24-27 October 2000, Fukuoka, Japan

The objectives of this workshop are

- To review information gained on seasonal to interannual variability during WOCE,
- To assess information gained on decadal variability from comparison of WOCE and pre-WOCE data,
- To estimate the impact of this variability on the representativeness of the WOCE (particularly WHP) data sets and derived quantities (e.g. heat and fresh-water fluxes),
- To review the ability of models to represent seasonal and longer-term ocean variability and the variation in water mass properties, volumes and formation rates,
- To identify, and take steps to initiate, data analysis and modelling research needed to better assess the representativeness of WOCE data sets and derived quantities,
- To identify the principal mechanisms (e.g. local or remote air-sea exchange, advection, propagation, coupled air-sea processes) behind the oceanic signals of climate variability as measured in WOCE, and
- To make recommendations based on the workshop conclusions for the design of future research (CLIVAR) and operational (GOOS) observing systems.

The workshop will consist of oral presentations, posters, and possible working group discussions. Given the limitations of total attendance, the organisers will attempt to preserve a balance among different ocean basins and scientific foci: measurements vs. models. It is encouraged that large-scale even global, rather than regional, views of data AND models will emerge. Further information will be provided at a later time with a second announcement and via the world wide web.

Members of the organising committee and their general area of responsibility follow:

Name	e-mail	Area of responsibility
T. Joyce	tjoyce@whoi.edu	Chair
S. Imawaki	imawaki@riam.kyushu-u.ac.jp	Co-chair, drifters
D. Roemmich	droemmich@ucsd.edu	repeat XBT/hydrography, Pacific
N. Bindoff	n.bindoff@utas.edu.au	Southern Ocean, S. Pacific, Indian
W. Large	wily@ncar.ucar.edu	air-sea fluxes
P.-Y. Le Traon	letraon@cls.cnes.fr	altimetry
D. Webb	david.webb@soc.soton.ac.uk	models
K. Hanawa	hanawa@pol.geophys.tohoku.ac.jp	N. and Tropical Pacific
P. Koltermann	koltermann@bsh.d400.de	repeat XBT/hydrography, Atlantic

The WOCE North Atlantic Workshop

F. Schott, C. Böning, H. Bryden, R. Molinari, P. Schlosser, C. Wunsch and L. Stramma

The WOCE North Atlantic Workshop was held at Institut für Meereskunde in Kiel during 23–27 August 1999, with the sessions taking place in the Art Gallery located in close proximity to the Institute. It was opened by the Mayor of Kiel, Mr Norbert Gansel, who welcomed the participants and gave a short background on the history of Kiel and of its association with the sea.

Attendance was about 150, with about half coming from Germany, 35 from North America, 15 from the UK, 10 from the Nordic countries and the rest of the participants from other European countries. A reception was held on Monday aboard the Research Vessel Alkor at the Institute dock and a Workshop Dinner on Wednesday in the Kiel Yacht Club.

Scientific sessions and poster presentations

The Workshop was organised into

- four main sessions with a total of 30 invited presentations and general discussion periods at the end of each session to identify and discuss over-arching questions pertinent to session topics,
- poster displays associated with the session format and sequence,
- working group deliberations.

Considering the large observed water mass and circulation variability of the North Atlantic it was decided early in the planning process to put emphasis on the decadal variability aspect while at the same time keeping in mind that a WOCE Variability Workshop is being planned for the fall of 2000.

The four main sessions dealt with the following topics (see March 1999 issue of the WOCE Newsletter for invited presentation titles and speakers):

- N. Atlantic decadal variability and the WOCE period;
- N. Atlantic circulation, pathways and water mass distributions from WOCE observations, altimetry and model results;
- Thermohaline overturning and flux divergences;
- Process studies, which was subdivided into four sub-sessions: Overflows; Labrador Sea convection; deep mixing and role of topography; thermocline ventilation.

In the general discussion periods following each of the sessions, problem areas were identified for further study and taken up subsequently in the Working Group discussions.

The number of posters shown at the Workshop was 78. Poster abstracts were presented on the Workshop Website prior to the Workshop and handed out as a printed collection to participants at registration time. The posters were grouped by session topics, and there were about a quarter of the total for each of the four sessions. Posters were displayed in two batches: for sessions 1/2 during Monday/Tuesday, and for sessions 3/4 on Wednesday/Thursday. Poster presenters were given the opportunity to briefly introduce their posters during the discussion periods at the end of each session.

Working Groups

Four topics were defined ahead of time by the Scientific Organising Committee and the objectives of each of them were presented on the Workshop Website and again to the participants at opening time. The Working Group sessions which were scheduled in pairs on Thursday morning and afternoon were attended by between 30 and 50 people which led to the well-known difficulties to focus the discussion and follow a time table for writing up recommendations. Brief summaries of the WG deliberations follow:

WG 1: WOCE synthesis products (chaired by J. Marotzke, L. Talley)

The group reviewed ongoing atlas and data assembly activities, based on a summary table provided by Kai Jancke. The general conclusion was that the production of basic WOCE synthesis products is well under way, and that no additional initiatives besides ongoing efforts are required.

WG 2: Improved parameterisations for large scale models (chaired by C. Böning, A. M. Treguier)

Improved parameterisation of WOCE synthesis models was considered a top priority of the overall Workshop discussions. The WG compiled a list of critical processes and discussed strategies how to parameterise them. Main emphasis was on improving model representations of the overflows and downslope entrainments along the topography, and an intercomparison study for the evaluation of different parameterisation schemes was suggested by representatives of different modelling teams. The second major issue of that WG was deep convection in the Labrador Sea, a remaining puzzle that was addressed for further work was that although the models generally reproduce deep mixing by local surface-flux forcing quite well, different models forced with similar forcing reveal large differences in convection depths and patterns. As a second major convection issue the dynamical effect on the overturning circulation was identified and quantitative model evaluations were recommended. The WG further discussed the various deep mixing processes over rough topography for which the potential effects on model mean and variability fields need further study.

WG 3: North Atlantic decadal variability (chaired by M. Latif, J. Willebrand)

A major discussion point in session 1 had been the contrast between fairly small (~10%) model variations of the overturning circulation, both in realistically forced ocean-only and in coupled models, and fairly large (~50%) derived changes in a recent analysis of basin-wide repeat hydrography section data as well as in historical data evaluations of deep geostrophic boundary section transports. To address this issue, the WG recommended evaluation of model output fields in similar ways as observed ocean section data are dealt with, where barotropic flows pose the major problem. As regards model decadal variability, the WG noted that while SST patterns in most coupled models are rather similar, and in rough agreement with observations, the time scales of THC variations are very different. Sensitivity and model intercomparison studies were proposed to investigate this issue. Regarding forcing mechanisms, a high priority research topic is the role the ocean plays in NAO related variability, and more generally, the degree of feedback to the atmosphere by oceanic variability at different time scales. Another important future research objective discussed were possible mechanisms relating subpolar and tropical–subtropical decadal variability and the potential role of oceanic advection in it. As a specific North Atlantic question the possible effect of LSW formation on Gulf Stream variability was brought up and whether or not this might be of importance for understanding decadal variability at the larger scale. Participants saw an urgent need in establishing continued observations of key variables to be compared with model results, with a monitoring effort of THC variability being of top priority.

WG 4: Requirements for future observations (chaired by U. Send, M. Visbeck)

The WG started off by taking note of the fact that various other groups, in the context of CLIVAR or GOOS, had already previously drafted recommendations on what might be needed for future ocean-climate research. Therefore the discussion was started from the current state of the observation system. Concerning upper-ocean observations, the float project ARGO was endorsed while cautioning at the same time against removing elements of the present observing network prior to establishing how well ARGO will actually perform the tasks it is envisioned for. The great importance of continuing and expanding existing ocean time series was stressed and a number of possible future sites were discussed. An essential requirement from future near-surface observations will be salinity measurements in the subpolar North Atlantic, conveniently taken via cooling water intakes of vessels of opportunity. Concerning air-sea fluxes, two modes of using moored observations were recommended: flux process calibration studies by moving moorings around in sub-regions typical of certain flux conditions; and longer-term deployments for cross-checking time series from other observations. Much of the WG 4 discussion focused on potential ingredients of a THC observing system, and specific proposals for applying boundary arrays, geostrophic moorings and acoustic tomography towards this central objective were put forward. Regarding the input from observational networks into model synthesis, such as planned in GODAE, the WG determined the need for impact assessment studies to determine which mix of data will be most effective for observing the important space-time scales of North Atlantic variability.

Closure discussions and outlook

In plenary session on Friday morning, the WG reports were received and discussed. It was found that the immediate main objective of a WOCE/AIMS synthesis activity, i.e. the production of atlas and map products that can serves as bases for model and inverse analysis studies in the future was considered well under way based on the activities presented in WG 1. As to the model development and parameterisation reviewed by WG 2, active group co-operations are under way and co-ordinated activities continue in the WOCE Ocean Model Development WG (chaired by C. Böning). The model comparisons and evaluations recommended by WG 3 were endorsed and the need expressed by modelling participants of WG 3 for establishing decadal ocean observations was noted. WG 4 recommendations were developed from existing plans and expanded based on requirements derived from Workshop topics with the intent to merge this into the papers to be prepared for the OceanObs99 Conference in St Raphael. In relation to future observations, some participants expressed concern about the fact that a data management structure for such observations still needs to be established. It was emphasised that existing WOCE structures should be reviewed and maintained if suitable for CLIVAR/GOOS purposes.

A number of group co-operations for model-observation synthesis were established during the Workshop, in particular on Labrador Sea convection and resulting large-scale effects on the overturning circulation. Regarding future observations, a group meeting was organised on Wednesday by Y. Desaubies to work out a co-ordinated proposal for profiling float deployments within ARGO in the context of the EC 5th Framework funding initiative.

Several possible milestones for more formal future co-operations and interactions were discussed such as special sessions at AGU or EGS and presentations in relevant sessions of the upcoming Ocean Sciences Meeting. Concerning focused publications on Workshop topics, participants were made aware that a special issue of JPO on Labrador Sea convection is being assembled with an end 1999 deadline, but other possible options for collections of future synthesis papers were also discussed.

A more complete report of the WOCE North Atlantic Workshop will appear as part of the WCRP series. It will also be available on

www.ifm.uni-kiel.de/ro/naws/naws.html

Volume transports and structure of the Leeuwin Current at 22°S – WOCE ICM6

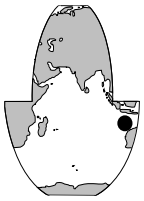

Catia M. Domingues, FIAMS, Flinders University; Susan Wijffels, CSIRO Division of Marine Research and Antarctic CRC; Matthias Tomczak, FIAMS; and John A. Church, CSIRO Division of Marine Research and Antarctic CRC, Australia.
Catia.Domingues@flinders.edu.au

The WOCE Current Meter Array 6 (ICM6) was deployed in August 1994 to estimate the variability of the transport of the anomalous poleward eastern boundary current of the Indian Ocean, the Leeuwin Current, at 22°S. It consisted of six moorings in water depths ranging from 250 to 3050 m, along a line extending 110 km westwards off the southern end of the Northwest Shelf of Australia (Fig. 1, top). The current meters, which included 4 upward looking ADCPs (3 broadband and 1 narrowband), 5 Neil Brown ACM2s and 13 Aanderaa RCMs (Fig. 1, bottom), were recovered in June 1996. Geostrophic velocities were calculated from CTD sections completed during three repeat WOCE hydrographic surveys (Table 1) while a snapshot of the upper-ocean currents structure was derived from a shipborne ADCP section completed during the recovery cruise.

Table 1. Cruise surveys and respective CTD stations bracketing moorings 1, 2 and 3

Cruise	Date	Station No.	Water Depth (m)
FR 03/95	22 Apr 95 17:14h	71	160
	22 Apr 95 16:14h	70	384
	22 Apr 95 14:36h	69	866
	22 Apr 95 12:17h	68	1310
KN 145/8	26 Apr 95 10:06h	444	153
	26 Apr 95 11:10h	445	414
	26 Apr 95 12:42h	446	863
	26 Apr 95 14:51h	447	1293
FR 05/96	28 May 96 21:10h	92	66
	28 May 96 19:33h	91	396
	28 May 96 17:31h	90	864
	28 May 96 15:14h	89	1290

The current meter data

All current meter data were individually examined to detect errors and to remove spikes before filtering. Short gaps were filled linearly (up to 3 h) or were interpolated using a cubic spline (up to 24 h). For longer gaps (up to 12 days), spectral interpolation was used as described in Andersen (1974). A cosine Lanczos-6 low-pass filter, with a cut-off period of 40 h, was applied to suppress inertial (32 h at 22°S), tidal and other higher-frequency signals. The valid low-passed data were decimated to a 6 hourly series. Further information are detailed in Domingues et al. (1999). The original *v* component was rotated 9° clockwise from the true north to coincide with the *v* component derived from the geostrophic estimates. However, the principal orientation of the local bathymetry (200 m isobath) is tilted 18° clockwise from the true north. Owing to the shorter length of the ADCP data in mooring 3, until December 1995, a multiple linear regression was used to extrapolate the velocity integrated from 50 to 210 m, based on the records of velocity at 50 m in mooring 2 and velocity at 248 m and temperature at 244 m in mooring 3.

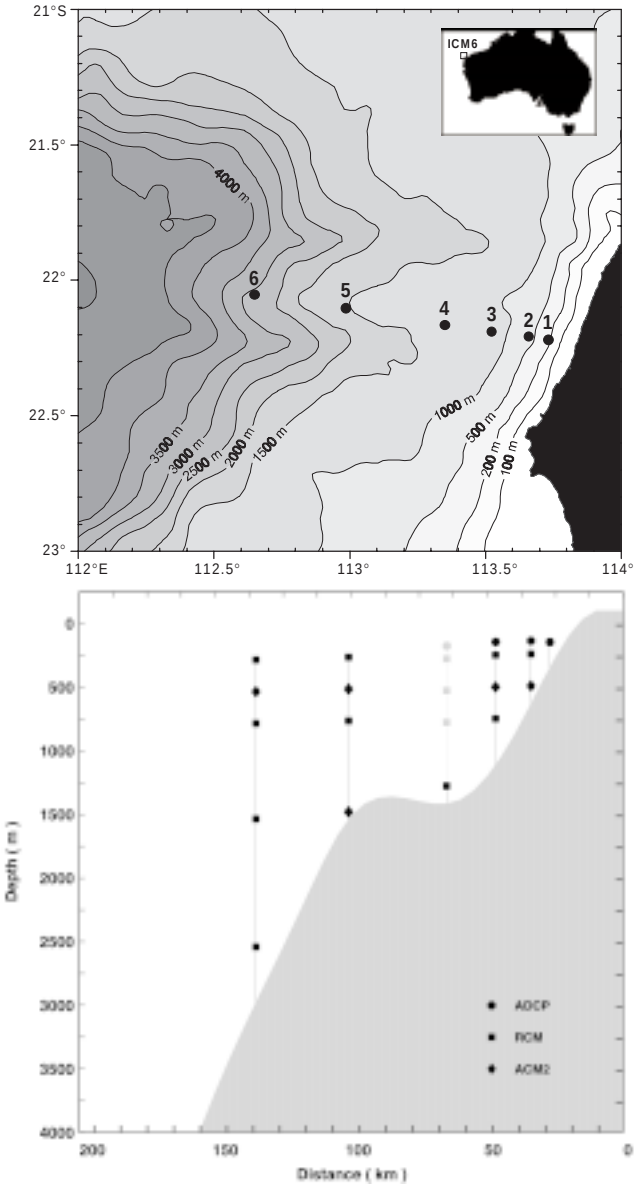

Figure 1. ICM6 mooring sites (top) and current meters distribution (bottom).

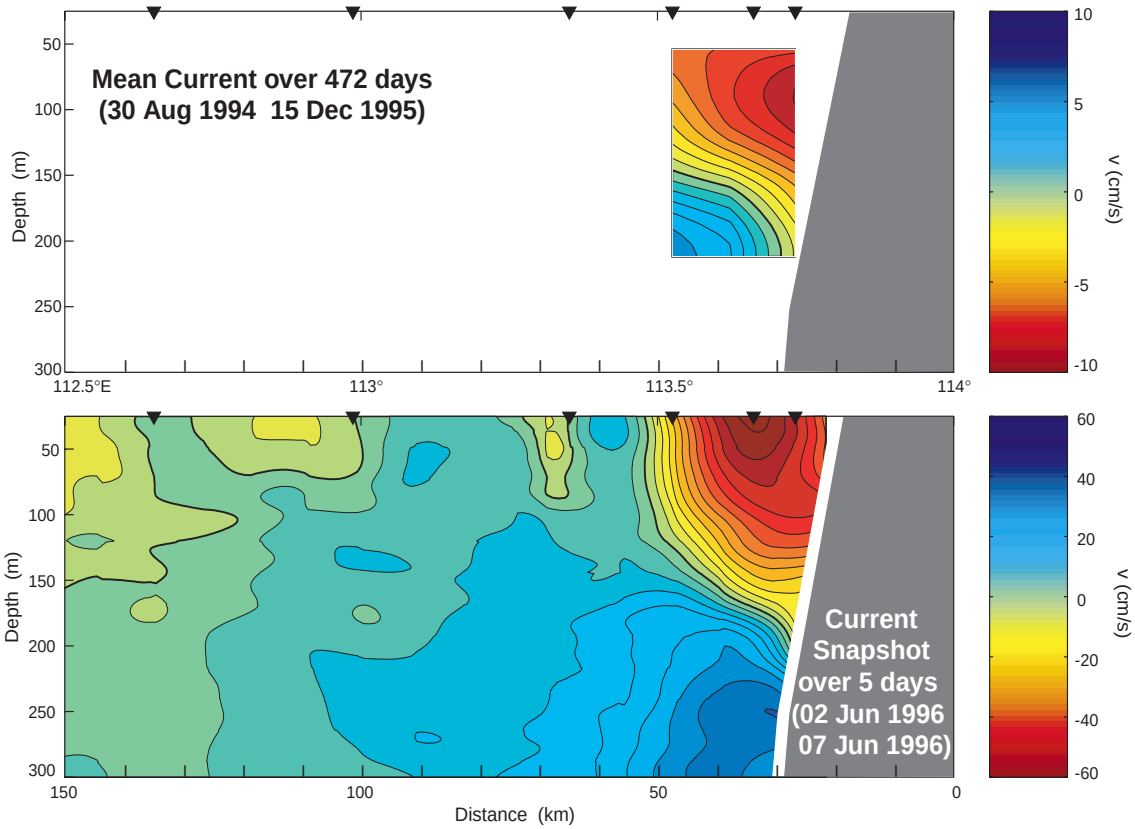

Domingues et al., page 36, *Figure 2. Leeuwin Current mean velocity structure (August 1994–December 1995) on top and Leeuwin Current snapshot structure (2–7 June 1996) on bottom across ICM6 array. From right to left, the black triangles correspond to the location of the moorings 1 to 6. Contours intervals are* $1\,cm\,s^{-1}$ *and* $5\,cm\,s^{-1}$ *for the mean and snapshot respectively. Positive equatorward.*

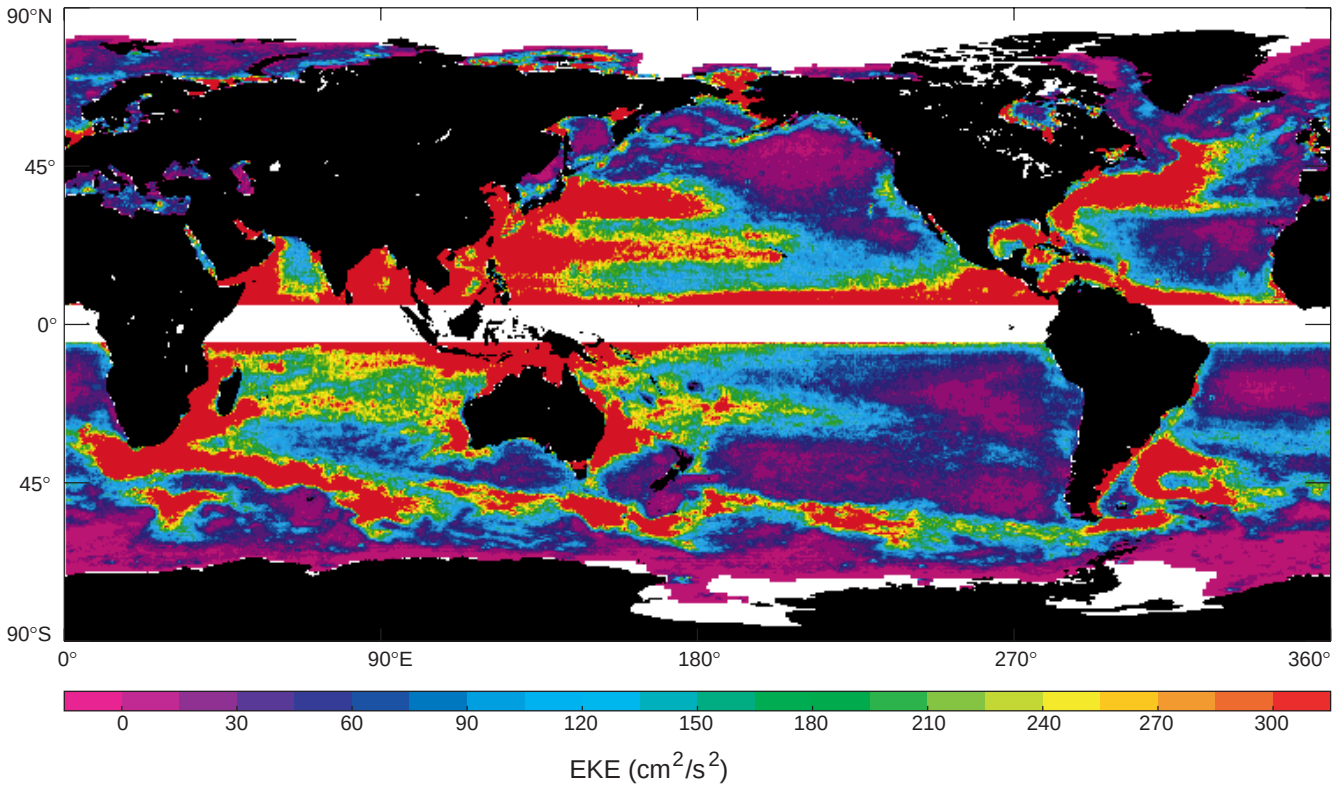

Ducet et al., page 40, *Figure 3. Eddy kinetic energy from both components of the geostrophic velocity variance inferred from the combined T/P+ERS maps from October 1992 to October 1997.*

Current structure

To estimate the structure of the upper-ocean currents across the ICM6 array, we used five days of shipborne ADCP data collected during the recovery cruise (FR 06/96, Fig. 2, bottom, page 37). Both the Leeuwin Current and the Leeuwin Undercurrent are trapped on the slope, with the core of the Leeuwin Current at the surface near mooring 2 and the Leeuwin Undercurrent core around 250-300 m depth. The southward flowing Leeuwin Current and the northward flowing Leeuwin Undercurrent have peak speeds of over $60\,cm\,s^{-1}$ and $35\,cm\,s^{-1}$ respectively.

A similar estimate of the current structure from the ICM6 direct measurements was not possible because there were no data from mooring 4‡ (and in the upper 250 m from moorings 5 and 6. Nevertheless, the 472 days mean of the *v* component derived from the ADCPs at the inner moorings reflects a structure resembling that obtained during the snapshot (Fig. 2, top). However for the mean, the core of the Leeuwin Current is subsurface, around 100 m depth, and near mooring 1. The currents of the outer moorings (5 and 6, not shown) seem to be dominated by a different system with a lower frequency variability, possibly mesoscale eddies.

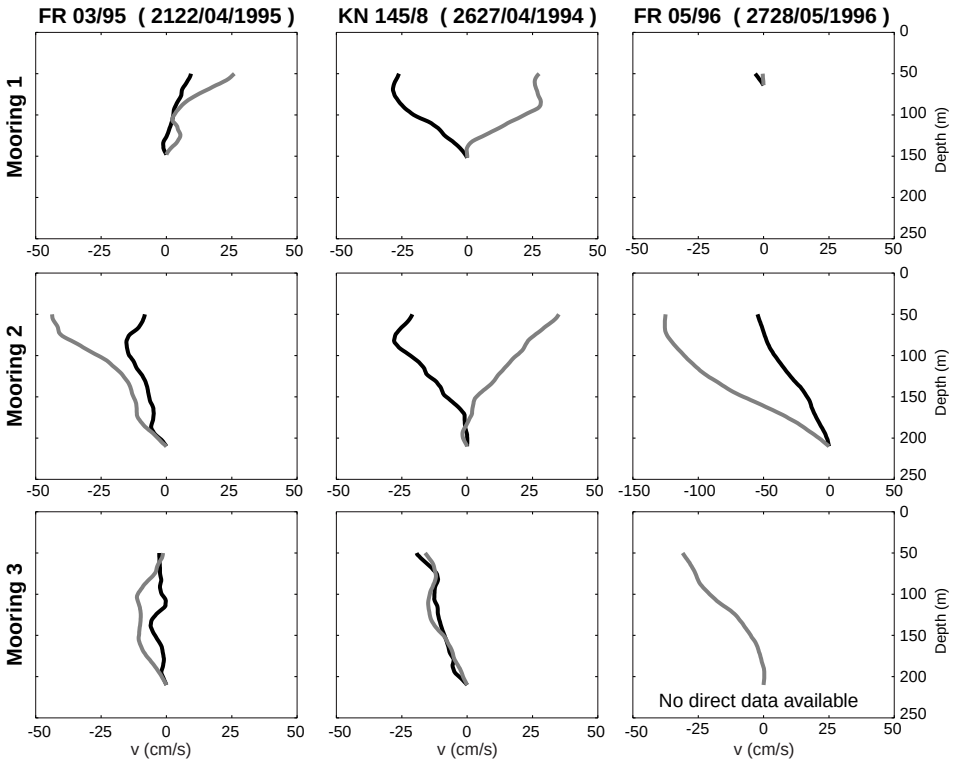

Figure 3. Bottom-referenced geostrophic (grey) and direct (black) velocity shears of moorings 1, 2 and 3 (from top to bottom) and in each cruise survey (from left to right). Positive equatorward.

Table 2. Bottom-referenced geostrophic and direct transport estimates (Sv)

Cruise	Geostrophic (relative to 210 m)	Direct (relative to 210 m)
FR 03/95	-0.51	-0.20
KN 145/8	0.05	-0.59
FR 05/96	-1.32*	-0.47*

* Included only moorings 1 and 2

Both data sets indicate the Leeuwin Current as a 30 km wide and 150–200 m deep southward jet. The Leeuwin Current and the Leeuwin Undercurrent have high variability and as a result the mean velocities are much weaker than those from the snapshot.

‡ Four of five instruments were lost and the sole instrument recovered had no good data (Fig. 1, bottom).

Comparison of geostrophic and direct transport estimates

The velocity shears measured by the three inshore ADCPs and calculated from the CTD data, both relative to the current at 210 m, are compared in Fig. 3. In all cruises (Table 1), the vertical profiles of the geostrophic velocities near mooring 1 were shallower than 210 m. Therefore, there we set both shear profiles to zero at the maximum depth of the CTD profiles. The noticeable discrepancies in the geostrophic estimates appear to be associated with the presence of strong internal tides in the study area, which causes a large variability of the temperature (and presumably of the salinity) at tidal frequencies. These internal tides affect the density field and consequently the geostrophic calculations. To illustrate them, the temperature variability during April/May 1995, including the days of the first two cruises, are shown in Fig. 4. The temperature can change by as much as 2°C from the low-passed values in periods as short as 6 h. As a result, the geostrophic vertical velocity shears can be very different from the direct measurements and hence transport estimates from CTD sections can be inaccurate, as shown in Table 2.

Transport variability

The volume transport estimates obtained from the ADCP data were depth-integrated from 50 to 210 m and filtered to remove oscillations less than 30 days. These estimates

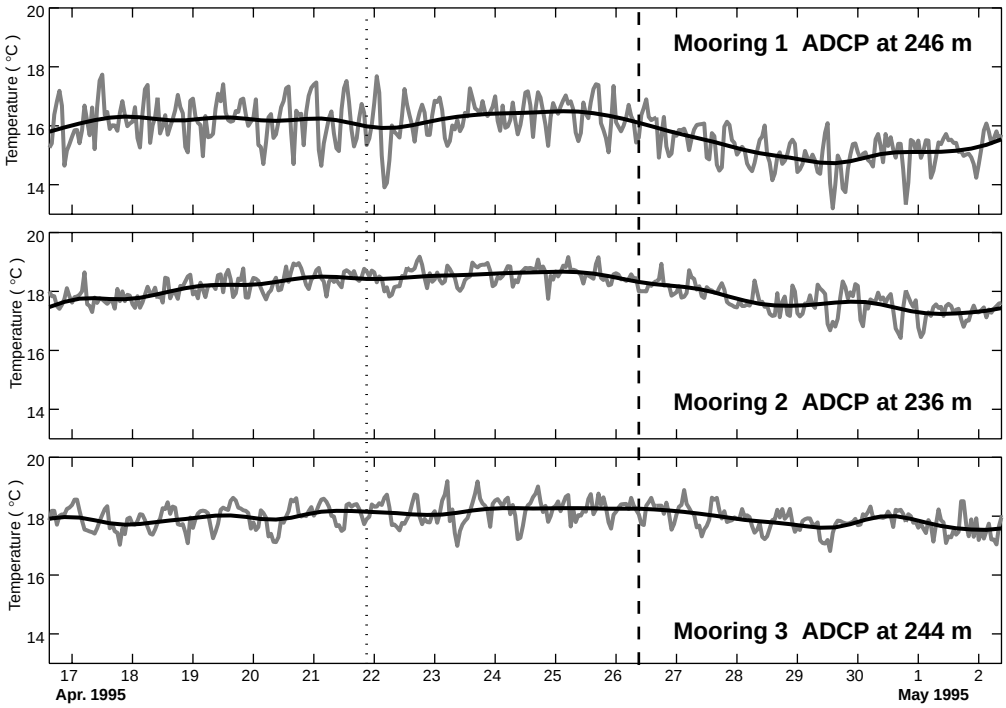

Figure 4. Raw (grey) and low-pass filtered (black) temperature time series during 17 April to 2 May 1995. The vertical lines correspond to the cruises FR 03/95 (dotted) and KN 145/8 (dashed). From top to bottom, moorings 1, 2 and 3.

were also split in two components based on information from the 472 days mean velocity. The area above the zero line in Fig. 2 (top) was termed the Leeuwin Current and the component below the zero line the Leeuwin Undercurrent. The transport time series between August 1994 and June 1996 is presented in Fig. 5 and the statistics are given in Table 3. The black shading at the end of the record (after December 1995) includes extrapolated estimates for mooring 3 (r.m.s. 0.03 Sv), and the grey shading is actual data.

As well as the distinct intraseasonal variability, the transport time series also indicates an interannual variability, with a progressive intensification of the Leeuwin Current towards 1996. This strengthening of the southward flow is accompanied by a warming trend in the temperature records at depths of the Leeuwin Undercurrent (not shown), suggesting a deepening of the thermocline (no temperature records in the upper 240 m). Indeed, Morrow and Birol (1998) found a general warming of the upper 150 m and an increase in the dynamic heights, as calculated from XBT and T/P data, for the same region during 1993 to 1995. Meyers (1996) reported that these variations on the north-western coast of Australia are associated with the ENSO signal. In general, anomalously low SST and dynamic height occur at the same time as anomalously shallow thermocline (El Niños) and vice-versa for opposite anomalies (La Niñas).

Although the Leeuwin Current can reach speeds of 100 $cm\,s^{-1}$ or more, the low transport values are a consequence of its narrowness and shallowness as well as of its high variability. The synoptic, intraseasonal and long-term variabilities are currently under investigation.

Conclusions

At 22°S, the Leeuwin Current is a 30 km wide and shallow (150–200 m deep) poleward jet close to the slope. Its 472 days mean

Table 3. Simple statistics of the volume transport series (Sv)

Transport	Period	Mean	Std
Total (50-210 m)	Aug 1994-Jun 1996 (640 days)	-0.23	0.55
Total (50-210 m)	Aug 1994-Dec 1995 (472 days)	-0.14	0.51
Leeuwin Current	Aug 1994-Dec 1995	-0.19	0.35
Leeuwin Undercurrent	Aug 1994-Dec 1995	0.05	0.16

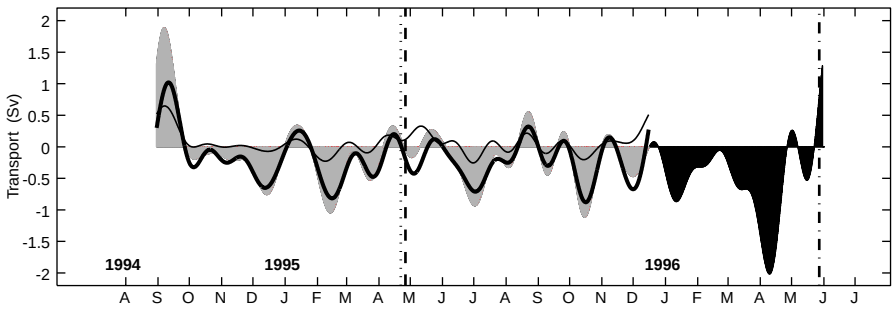

Figure 5. Leeuwin Current volume transport time series across ICM6 array. The vertical lines correspond to the cruises FR 03/95 (dotted), KN 145/8 (dashed) and FR 05/96 (dotted-dashed). Grey shading indicates actual estimates while black shading indicates the period when the extrapolated velocities for mooring 3 were used (r.m.s. 0.03 Sv). The bold line is the Leeuwin Current transport and the thin line is the partial contribution of the Leeuwin Undercurrent. Positive equatorward.

southward core velocity is around $8-10\,\mathrm{cm\,s^{-1}}$ at 100 m depth. Its transport time series, with a mean value of 0.19 Sv, indicates considerable synoptic (not shown), intraseasonal and interannual variability. While earlier studies (Holloway and Nye, 1985; Smith et al., 1991) found a marked seasonal pattern for the transport of the Leeuwin Current with strongest flow during March/May, the time series comparatively presents only a weak seasonal signal. Discrepancies in the Leeuwin Current transport estimates that might exist using geostrophic calculations seem to be associated with strong internal tides.

References

Andersen, N., 1974: On the calculation of filter coefficients for maximum entropy spectral analysis. Geophysics, 39, 69–72.

Domingues, C. M., M. Tomczak, S. Wijffels, H. Beggs and J. A. Church, 1999: Direct observations of the Leeuwin Current at 22°S, 1994–1996. CSIRO Marine Research Report Series/FIAMS Tech. Report 235/17, 49 pp.

Holloway, P. E., and H. C. Nye, 1985: Leeuwin Current and wind distributions on the southern part of the Australian Northwest shelf between January 1982 and July 1983. Aust. J. Mar. Freshwater Res., 36, 123–137.

Meyers, G., 1996: Variation of Indonesian Throughflow and El Niño-Southern Oscillation. J. Geophys. Res., 101, 12255–12263.

Morrow, R., and F. Birol, 1998: Variability in the southeast Indian Ocean from altimetry: Forcing mechanisms for the Leeuwin Current. J. Geophys. Res., 103, 18529–18544.

Smith, R., A. Huyer, J. S. Godfrey and J. A. Church, 1991: The Leeuwin Current off Western Australia, 1986–1987. J. Phys. Oceanogr., 21, 323–345.

How accurately can we map the mesoscale ocean surface variability from the combination of T/P and ERS-1/2 altimetric data?

Nicolas Ducet and Pierre-Yves Le Traon, CLS Space Oceanography Division, France; and Gilles Reverdin, LEGOS, France. Nicolas.Ducet@cls.fr

Altimeter data processing and merging

The same geophysical corrections are used for T/P and ERS-1/2 altimeter data sets and a global crossover adjustment of ERS orbit is performed by using the more precise T/P data as a reference (Le Traon and Ogor, 1998). To reduce measurement noise, the along-track data are filtered (using a Lanczos low pass filter). The filter cut-off wavelength depends on latitude, taking into account variations in the typical spatial scales of the ocean signal. The data are then merged through an improved global objective analysis method that allows us to correct for residual long wavelength errors (Le Traon et al., 1998) and uses realistic correlation scales of the mesoscale ocean circulation (e.g. 175 km at 30°N/S and 100 km at 60°N/S). Merged Sea Level Anomaly maps have a global high resolution of $\frac{1}{4}°$ and can be used directly for signal analysis and in comparison with numerical models and in situ measurements or for data assimilation.

Ducet et al. (1999) give a detailed statistical analysis of the contribution of the merging and assess its interest for further investigations on the mesoscale ocean dynamics. They show that T/P and ERS intercalibrated data sets have an excellent global compatibility, the r.m.s. of their difference being less than 3 cm in low ocean variability regions. The a posteriori mapping error is spatially homogeneous and significantly reduced by the combination. This confirms that for a realistic mapping of the mesoscale ocean variability, T/P data are not sufficient on their own, owing to the too large spatial sampling of the satellite tracks (2.8°). Combining T/P and ERS data enables us to get a better estimation of the meridional geostrophic velocity and to observe about 30% more energy in both velocity components than T/P data alone.

Because the energy level contained in the combined maps could be affected by the spatial filtering and the mapping procedure, we carried out a careful validation of the geostrophic velocity calculation.

Comparison with surface drifters

The data set used here contains data of 1159 WOCE SVP drifters drogued at 15 metres from 1991 to January 1999 in the North Atlantic Ocean. The data have been processed at the Atlantic Oceanographic and Meteorological Laboratory (AOML) and time series resulting from a krigging analysis are provided at 6-hourly intervals (Hansen and Poulain, 1996). Detection of drogue loss is automatically done at AOML, and these data are removed. The drifters are likely to be representative of the ocean currents at 15 m to within 1 to 2 cm/s (Niiler et al., 1987; 1995). In addition, we included 60 drifters drogued at 50 metre depth and deployed in the Labrador Sea for the Ice Patrol. Filtering of inertial motion and other high-frequency non-geostrophic motions was done by applying a Lanczos filter with cut-off at 2 days. The variance associated with the Ekman component of the drifts was estimated according to Van Meurs and Niiler (1997) who illustrated how the stationary wind-

driven component of the buoy drift could be estimated from the wind stress. We have applied their formula with an additional scaling in latitude as the square root of the Coriolis parameter (P. Niiler and E. Ralph, pers. comm., 1997) on 1989–1993 daily fields of the ECMWF reanalysis. The variance in this component of the current corresponds to EKE levels smaller than $20\ \mathrm{cm}^2\mathrm{s}^{-2}$ everywhere and was removed from the EKE estimates. This is rather uncertain, but is small compared to the surface EKE in most of the Atlantic, and therefore has a small effect on the comparison with the TP+ERS combined maps.

The number of data included in this set is much higher than in earlier analyses based on the order of a hundred floats (Richardson, 1983; Brügge, 1995). The data were gridded on a $0.5° \times 1°$ grid to retain the fine resolution that the number of observations permits in a large part of the North Atlantic. The data distribution is not homogeneous (more drifters having been deployed north of the Gulf Stream, close to Iceland, and in the Azores Current). Drifters will also tend to sample preferentially convergent features, and therefore also fronts. These effects will result in biases in the mean field. In that sense, it is reassuring to find similar features in the average circulation to the ones presented in Brügge (1995) using a different set of drifters, all drogued at 100 metres. The effect should be much less severe for the variability, and here we will assume that the data set provides a quasi-Eulerian sampling of the eddy field. Uncertainty due to the sampling of the variance field is large, often a factor 2, as was found when comparing estimates based on half the floats or separated seasons. The large-scale features of the field are nonetheless robust except in the southern and south-western parts of the subtropical gyre, Gulf of Mexico and in the Gulf Stream south of 36°N and shortly downstream of Cape Hatteras (the drifters enter the stream mostly from the slope current to the north).

The EKE values found in this drifter set (see left panel of Fig. 1) are comparable to the values in Brügge (1995) for the North Atlantic Current branches and in the subpolar gyre. The maximum values we have in the Gulf Stream are larger by up to a factor 2 compared to Richardson (1983). This might be caused by the coarse resolution of this earlier product.

The maps of r.m.s. variability from the drifter data sets present striking similarities with the ones in the combined product for both geostrophic velocity components, even at a fairly high level of detail. The maxima of variance in the Gulf Stream are comparable, being only 20% larger in the drifter set, part of this resulting from the noise in the drifter set related to insufficient sampling. Visually, variance in the Gulf Stream seem larger for *u* in the drifter set and for *v* in the TP+ERS mapped product. There is also a tendency for variance to be larger in the drifter set in the subpolar gyre (see for example, the patch of large values in the drifter product near 61–62°N off west Greenland). We also present the comparison as a scatter

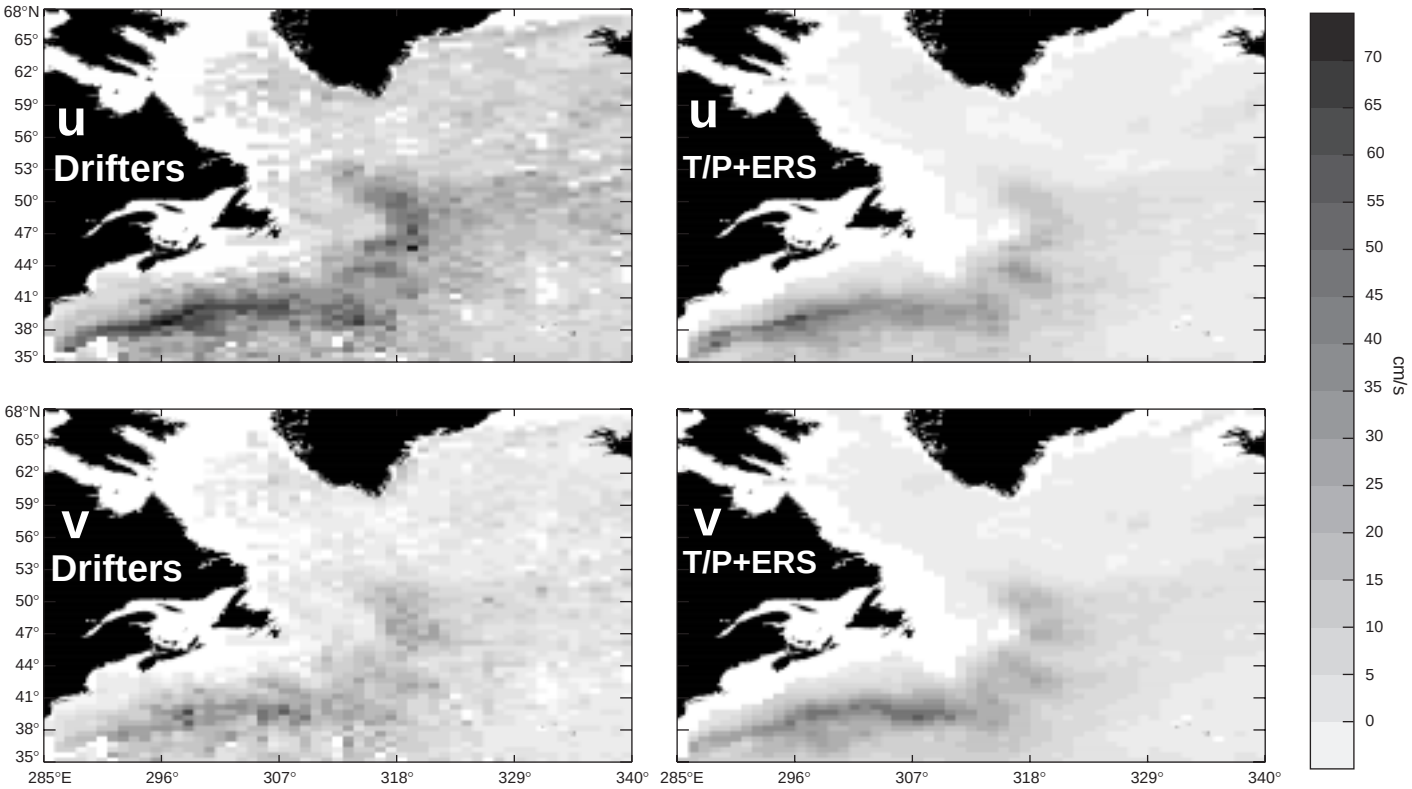

Figure 1. R.m.s. of the zonal u (top) and the meridional v (bottom) components of the geostrophic surface velocity for the WOCE drifters (left) and the combined T/P+ERS maps (right). Boxes with at least 25 days of data were kept for the drifters. Altimetric data over water depths greater than 500 m are shown.

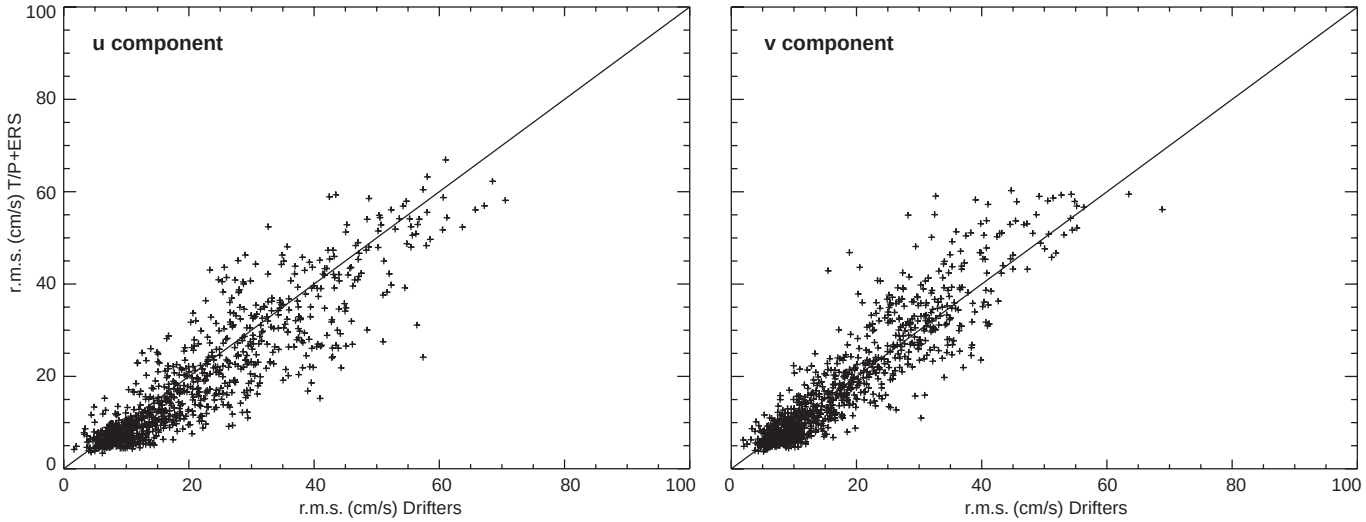

Figure 2. Scatter diagram of the r.m.s. of u (left) and v (right) between the WOCE drifters and T/P+ERS-1/2 product.

diagram both for the zonal and meridional components (Fig. 2). The figure presents a clear correlation between the two sets with an alignment of the data along the axis of equal values (we have retained only values with more than 25 days of drifter observations). The visual tendency for more *v* variance and less *u* variance in the T/P+ERS maps for large velocity r.m.s. variability is confirmed by Fig. 2 and is not yet fully explained.

EKE spatial distribution

Fig. 3 (page 37) presents the spatial distribution of the surface EKE inferred from the merged altimetric data over the whole ocean. As expected, the maximum levels of EKE are concentrated in the vicinity of the major current systems, and can reach values of up to $4500\,cm^2s^{-2}$. The largest value is in the Agulhas region, with secondary maxima in the Kuroshio, the Gulf Stream, the Brazil/Malvinas Confluence Zone, and finally the Antarctic Circumpolar Current. We have saturated the colour scale at $300\,cm^2s^{-2}$ to concentrate on the many intriguing regional features revealed by this map. This also enables us to characterise the background noise variance on the EKE field, which is only on the order of $15\,cm^2s^{-2}$ (see the north-eastern Pacific and the northern South Atlantic).

In the North Pacific Ocean, the south-westward flowing Oyashio Current as well as the Alaskan gyre can be clearly identified with EKE levels of up to $400\,cm^2s^{-2}$. Further east, the California Current shows a maximum energy level of $250\,cm^2s^{-2}$ (near 125°W) in excellent agreement with results of Strub et al. (1997). Also note the well defined tongue of high EKE extending from 130°E to 170°W, near 20°N, associated with the Subtropical Countercurrent.

In the northern North Atlantic Ocean, the main variable oceanic features are also clearly reproduced, notably the north-eastward deflection of the North Atlantic Current and its splitting into two branches flowing north-eastward on both eastern and western flanks of the Rockall Plateau (near 58°N, 20°W), or the beginning of the Norway current, near 60°N, 5°W, as it passes northward through the Faeroe–Shetland Channel. The Irminger current, flowing north-eastward along the western flank of the Reykjanes ridge and then veering cyclonically to the south-west along east Greenland, exhibits EKE levels of about $80\,cm^2s^{-2}$. EKE values of up to $150\,cm^2s^{-2}$ are also found in the subpolar gyre, at about 60–62°N and west of 50°W, where the West Greenland Current separates from the coast, and generates eddies. Even rather stable and not highly turbulent feature like the Labrador Current can be identified, as it follows the eastern slope of the Grand Banks, by EKE values around $50\,cm^2s^{-2}$. In contrast, the Azores front, flowing along 33°N, is well observed by the combined map with energy ranges from more than $300\,cm^2s^{-2}$ at 40°W to $150\,cm^2s^{-2}$ at 20°W.

In the interior of the subtropical gyre of the South Atlantic, a zonal band of EKE values of up to $150\,cm^2s^{-2}$ extends across the entire gyre at about 33°S. This oceanic feature corresponds to a r.m.s. sea level variability of up to 10 cm, and to our knowledge has not previously been discussed in the literature.

In the western Mediterranean, the time varying Alboran gyres in the Strait of Gibraltar and further east, the Algerian Current eddies off the North African coast are also detected, as well as the Ierapetra gyre (35°N, 27°E).

A more complete description of this map is given by Ducet et al. (1999) and reveals a very high level of detail presumably never previously achieved so far at a global scale.

Conclusion

The combination of T/P and ERS-1/2 provides an accurate description of the ocean circulation, retaining the accuracy of T/P data but with a finer spatial resolution. R.m.s. velocity variability derived from the combination of T/P

and ERS-1/2 data was found in close agreement with the one estimated from surface drifters. We now have a powerful altimetric product to perform detailed global mesoscale ocean analyses, study the variance of the zonal and meridional velocities independently and thus get better insight into the ocean isotropy.

Acknowledgements

This work was realised as part of the Environment and Climate EU AGORA (ENV4-CT9560113) and DUACS (ENV44-T96-0357) projects. These 5½ years of sub-optimally mapped data used in this study have recently been released and made available by AVISO to the scientific community on two separate CD-ROMs (one for T/P, the other for TP+ERS).

References

Brügge, B., 1995: Near-surface mean circulation and kinetic energy in the central North Atlantic from drifter data. J. Geophys. Res., 100, 20543–20554.

Ducet, N., P. Y. Le Traon, and G. Reverdin, 1999: Global high resolution mapping of ocean circulation from TOPEX/POSEIDON and ERS-1/2. Submitted in a revised form to J. Geophys. Res.

Hansen, D. V., and P.-M. Poulain, 1996: Quality control and interpolations of WOCE/TOGA drifter data. J. Atm. Ocean. Tech., 13, 900–909.

Le Traon, P.-Y., and F. Ogor, 1998: ERS-1/2 orbit improvement using TOPEX/POSEIDON: the 2 cm challenge. J. Geophys. Res., 103, 8045–8057.

Le Traon, P.-Y., F. Nadal, and N. Ducet, 1998: An improved mapping method of multi-satellite altimeter data. J. Atm. Ocean. Tech., 15, 522–534.

Niiler, P. P., R. E. Davis, and H. J. White, 1987: Water-following characteristics of a mixed layer drifter. Deep-Sea Res., 31, 1867–1881.

Niiler, P. P., A. S. Sybrandy, K. Bi, P. M. Poulain, and D. Bitterman, 1995: Measurements of the water-following capability of holey-sock and TRISTAR drifters. Deep-Sea Res., 42, 1951–1964.

Richardson, P. L., 1983: Eddy kinetic energy in the North Atlantic from surface drifters. J. Geophys. Res., 88, 4355–4367.

Strub, P. T., T. K. Chereskin, P. P. Niiler, C. James, and M. D. Levine, 1997: Altimeter-derived variability of surface velocities in the California Current System. 1. Evaluation of TOPEX altimeter velocity resolution. J. Geophys. Res., 102, 12727–12748.

Van Meurs, P., and P. P. Niiler, 1997: Temporal variability of the large-scale geostrophic surface velocity in the northeast Pacific. J. Phys. Oceanogr., 27, 2288–2297.

Subduction of water into the thermocline of the subtropical Indian Ocean

Johannes Karstensen, IfM Hamburg; and Detlef Quadfasel, NBI/APG Copenhagen, Denmark. J.Karstensen@omnet.com

Thermocline ventilation

Vertical Ekman pumping and lateral advection through the base of the mixed layer both contribute to the transfer of near surface waters into the oceanic thermocline. This so called subduction controls the overall rate at which the thermocline is ventilated (Woods, 1985), but locally the ventilation is also influenced by the wind-driven circulation and the mixing of the water masses. Time-scales associated with the ventilation range from years to decades. The fluxes of heat, freshwater and dissolved gases, like oxygen and anthropogenic carbon, determine the hydrographic structure of the thermocline and a quantification of the subduction rates is thus essential for estimating the capability of the oceans to buffer climate variability associated with greenhouse gases.

The thermocline of the Indian Ocean in both hemispheres is mainly ventilated from the south. The overflows from the Red Sea and the Persian Gulf and the inflow from the Indonesian archipelago play only a minor role. Buoyancy fluxes through atmospheric heat loss in the Agulhas retroflection region and through an

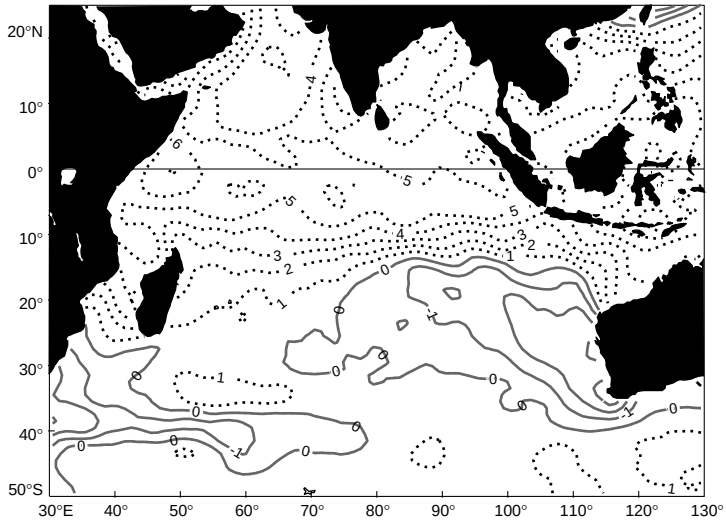

Figure 1. Annual mean buoyancy flux (units: 10^{-6} kg m^{-2} s^{-1}) in the Indian Ocean calculated from SOC heat and momentum flux climatology (Josey et al., 1996). Positive values (dotted line) indicate flux into the ocean.

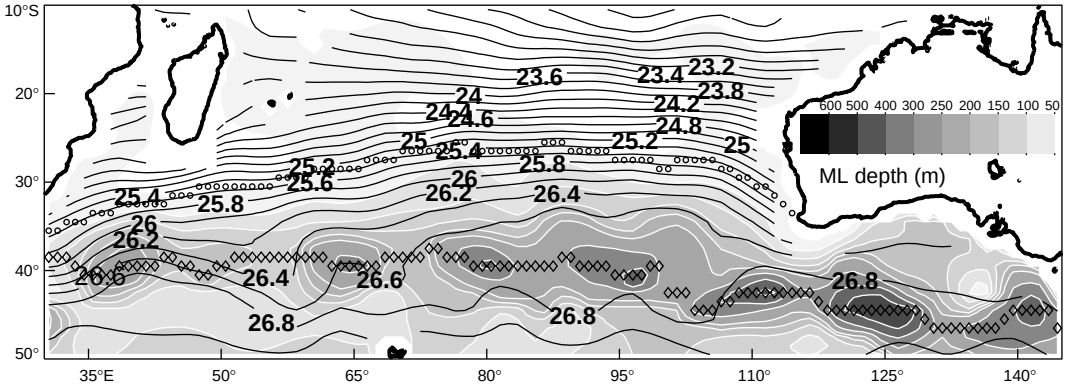

Figure 2. Winter mixed-layer depth and density from WOA98 data defined as the depth where the surface density increased by $0.125\,kg\,m^{-3}$. Circles denote the salinity maximum at the base of the mixed-layer, diamonds denote the deepest mixed-layer depth.

excess of evaporation over precipitation on the eastern side of the subtropical gyre lead to a deepening of the mixed layers and the formation of water masses (Fig. 1). In these two regions Mode Waters and Central Waters are formed (England et al., 1993, Sverdrup et al., 1942). After being subducted into the Indian Ocean thermocline, these waters circulate in the anticyclonic subtropical gyre, and also spread further north into the cyclonic tropical gyre (Woodberry et al., 1989). Via the western boundary currents off East Africa and Somalia part of the thermocline waters also advect into the northern hemisphere.

Table 1. Subduction (transport in Sv = 10^6 m^3/s) of water into the permanent thermocline from analysis of hydrographic and meteorological data. The rates for the North Atlantic and Pacific Oceans are taken from Qiu and Huang (1995)

	South Indian	North Atlantic	North Pacific
Ekman pumping (surface)	13 Sv	22.2 Sv	30.8 Sv
Ekman pumping (mixed layer base)	11 Sv	17.5 Sv	25.1 Sv
Lateral injection	21 Sv	9.5 Sv	10.1 Sv
Total subduction	32 Sv	27.0 Sv	35.2 Sv

As a first step towards quantifying the impact of changing subduction rates in relation to climate variability we present here an estimate of the annual mean subduction rate into the Indian Ocean subtropical gyre, using climatological hydrographic data (World Ocean Atlas, 1998, hereafter WOA98) and recent WOCE data (I3, I5, I8). We compare estimates derived from two different approaches and discuss the characteristics of the subducted waters.

Methods

We use two methods to calculate subduction rates from hydrographic and meteorological data, the "kinematic approach" and the "water age approach". In the kinematic approach (e.g. Qiu and Huang, 1995) the flux of water from the upper layer into the thermocline through the base of the mixed layer is calculated directly. The vertical Ekman pumping contribution is estimated from the rotation of the

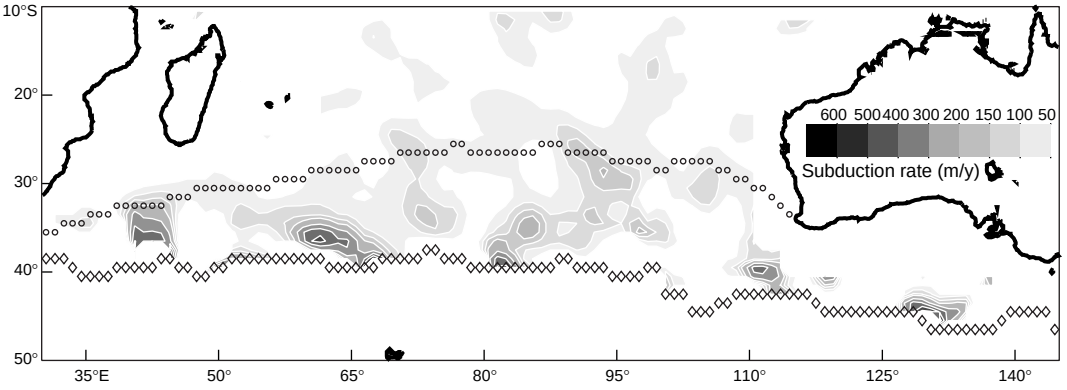

Figure 3. Annual mean subduction rate S_{ann} calculated from WOA98 data and SOC wind stress data. Circles and diamonds denote the boundaries where subduction into the ventilated thermocline occur (see text and Fig. 2 for details).

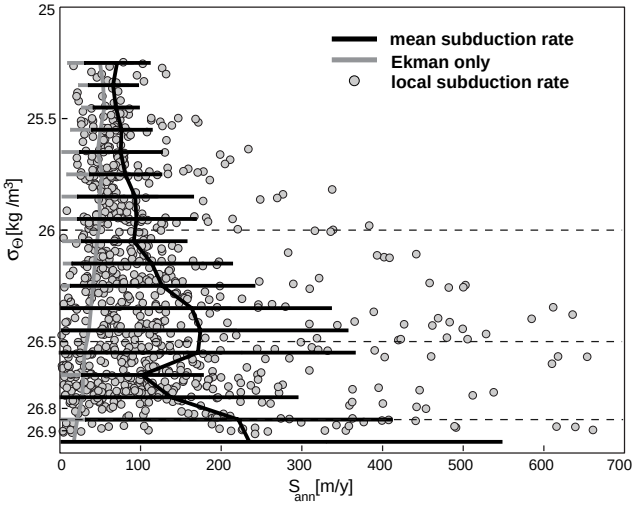

Figure 4. Subduction rate S_{ann} versus density at the base of the winter mixed-layer derived from the kinematic approach (see Fig. 3). The black line indicates the mean and standard deviation of the annual mean subduction rate, the grey line the Ekman pumping velocity as calculated from the wind field.

wind stress field, taking the forcing of the mixed-layer into account and correcting for it. The horizontal velocities at the base of the mixed-layer are calculated assuming geostrophy and using a deep layer of no motion. The fluxes across this surface are then calculated from the tilting of the mixed-layer base and the horizontal velocities. This approach allows the calculation of the spatial distribution of subduction rates.

The "water age approach" (e.g. Jenkins, 1987) uses the vertical gradient of water ages in the interior of the thermocline. The ages are projected back to an outcrop latitude of the respective density surface. Subduction rates can so be calculated for every data point in the interior. A spatial distribution of the subduction rates cannot be derived with this method. The vertical gradient of water ages is obtained from transient tracer data taking the influence of mixing on the tracer field into account. To enlarge the data base for water ages we also use a density dependent oxygen utilisation rate (AOU), introducing "oxygen apparent ages" (Karstensen, 1999).

Subduction rates

The mean winter temperature and annual salinity, averaged on a 1 by 1 latitude–longitude grid, are used to calculate the deepest mixed-layer depth (Fig. 2). The distribution of tracers on this surface determines the characteristics of the interior hydrographic field (salinity, oxygen, CFC, etc.). As expected, the isopycnals are oriented in an almost zonal direction. South of about 35°S a band of low gradients indicates homogenous waters associated with the Mode Water, between 26.2 and 26.8 kg m^{-3} This density range agrees with the volumetrically strongest Mode Waters identified by Fine (1993) along WOCE section I5 at about 32°S. The two boundaries for the subduction of waters into the permanent thermocline of the subtropical gyre can now be identified: the southern boundary coincides with the deepest mixed-layer depth. Waters formed further south can not subduct into the gyre without being again part of the mixed-layer in the trough. We defined the northern boundary as the salinity maximum at the base of the winter mixed-layer. It marks the transition zone between the permanent thermocline of interest here and the seasonal (tropical) thermocline and nearly coincides with the region of maximum wind stress curl (Sprintall and Tomczak, 1993).

The spatial distribution of the annual mean subduction rates into the Indian Ocean permanent thermocline calculated from the kinematic method is shown in Fig. 3. The vertical transfer generated by the curl of the wind stress

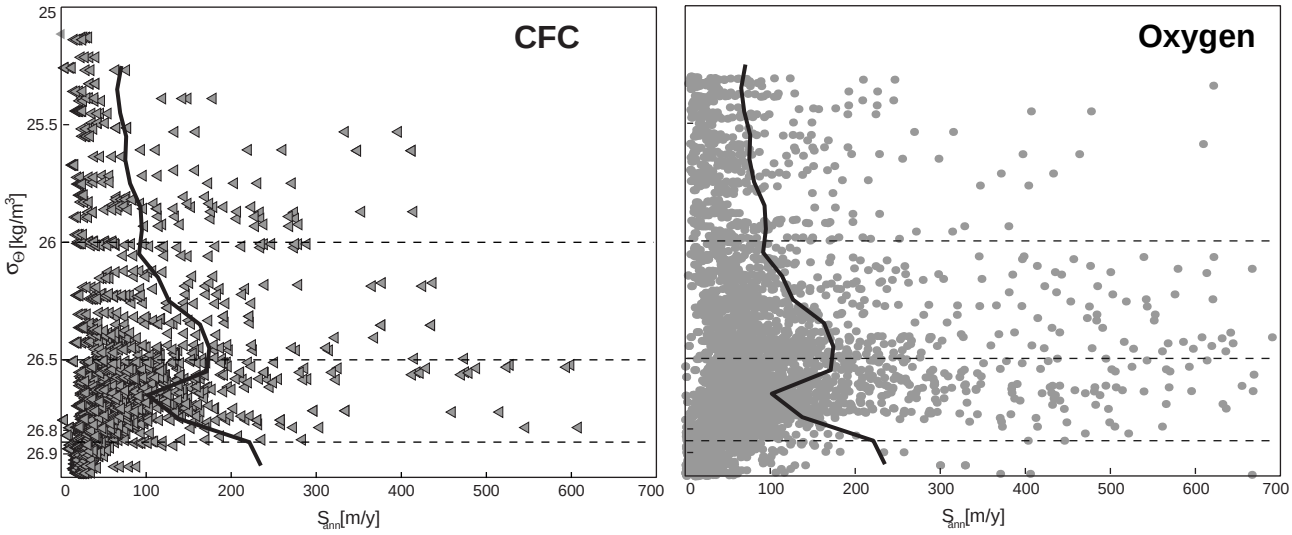

Figure 5. Subduction rate S_{ann} derived from water age approaches. (left) based on CFC data from WOCE I3, I5 and I8 in the interior subtropical gyre, (right) based on oxygen using a density dependent oxygen utilisation rate and historical data. The black line is the mean subduction rate from the kinematic approach (see Fig. 4).

dominates the subduction rate in the central and eastern subtropical gyre and coincides with the formation site of water through the freshwater buoyancy flux (Fig. 1). At the southern rim of the subtropical gyre, along the Subtropical Front, Mode Waters are formed through mid-latitude thermal convection (Fig. 1) and are transferred laterally into the gyre through the horizontal flow across the tilted base of the mixed-layer. When plotting the subduction rates at each individual grid point in relation to the winter mixed-layer density it becomes clear that the lateral transfer of Mode Waters in the density range 26.2 to 26.9 $kg\,m^{-3}$ contributes most to the subduction (Fig. 4). Largest rates are found at 26.5 $kg\,m^{-3}$ and 26.85 $kg\,m^{-3}$. At low densities the transfer is mainly driven by Ekman pumping (grey line). Note that the uncertainty bars on the mean curve indicate the spatial variability of the field and not temporal variability.

These rates calculated from the kinematic approach can be directly compared with those from the water age approach (Fig. 5). For the plot on the left hand side we calculated the vertical age gradients using CFC data in the subtropical gyre. The apparent ages are corrected for effects of mixing, which underestimates the age by about 5%, with the aid of a pipe flow model (Karstensen and Tomczak, 1998). Vertical current shear is assumed to be negligible. The input of water is largest at high densities, reaching a maximum at about 26.7 $kg\,m^{-3}$. The density dependent subduction rates based on oxygen utilisation rates to determine the water mass ages are shown in Fig. 5 (right). Here the scatter is larger, but the general pattern is the same as for the CFC ages. Both water age tracer approaches do not confirm the maximum in rates at about 26.85 $kg\,m^{-3}$. This might be an effect of the coarse vertical resolution of the bottle samples from which the age gradient is calculated.

To compare the subduction rates of the Indian Ocean with those determined for the North Atlantic and Pacific Oceans (Qiu and Huang, 1995) we have integrated the individual contributions (Ekman only, vertical, and lateral) over the region enclosed by the northern and southern boundaries (see Fig. 3). The comparison is summarised in Table 1. The total amount of subducted water in the Indian Ocean is comparable to those of the northern hemisphere oceans even though the area of subduction is much smaller. There is, however, a strong qualitative difference. Whereas Ekman pumping dominates the subduction in the northern hemisphere, the lateral injection is about twice as large as the vertical transfer in the southern Indian Ocean. We attribute this to the comparatively strong eastward velocities along the subtropical front, in combination with the slight southward tilt of the subtropical front.

Acknowledgements

This work was supported from the Bundesministerium für Bildung, Wissenschaft, Forschung und Technologie (BMBF) under research grant 03F0157A (WOCE IV).

References

England, M. H., J. S. Godfrey, A. C. Hirst, and M. Tomczak, 1993: The mechanism for Antarctic Intermediate Water renewal in a world ocean model. J. Phys. Oceanogr., 23, 1553–1560.

Fine, R. A., 1993: Circulation of Antarctic Intermediate Water in the South Indian Ocean. Deep-Sea Res., 40(I), 2021–2042.

Jenkins, W. J., 1987: ^{3}H and ^{3}He in the beta triangle: Observations of gyre ventilation and oxygen utilisation rates. J. Phys. Oceanogr., 17, 763–783.

Josey, S. A., E. C. Kent, D. Oakley, and P. K. Taylor, 1996: A new global air-sea heat and momentum flux climatology. Int. WOCE Newsl., 24, 3–5.

Karstensen, J., and M. Tomczak, 1998: Age determination of mixed water masses using CFC and oxygen data. J. Geophys. Res., 103(C9), 18599–18610.

Karstensen, J., 1999: Über die Ventilation der Thermokline im Indischen Ozeans. PhD thesis, Fachbereich Geowissenschaften, Universität Hamburg, Germany.

Qiu, B., and R. X. Huang, 1995: Ventilation of the North Atlantic and North Pacific: subduction versus obduction. J. Phys. Oceanogr., 25, 2374–2390.

Sprintall, J., and M. Tomczak, 1993: On the formation of Central Water and thermocline ventilation in the southern hemisphere. Deep-Sea Res., 40, 827–848.

Sverdrup, H. U., M. W. Johnson, and R. H. Fleming, 1942: The oceans: Their physics, chemistry, and general biology. Prentice-Hall, Englewood Cliffs, N.Y., 1060 pp.

Woodberry, K. E., M. E. Luther, and J. J. O'Brien, 1989: The wind-driven seasonal circulation in the southern tropical Indian Ocean. J. Geophys. Res., 94(C12), 17985–18002.

Woods, J. D., 1985: Coupled Ocean-Atmosphere models, chapter Physics of thermocline ventilation, pp 543–590, J. C. J. Nihoul, Elsevier, Amsterdam.

World Ocean, 1998: 1998 Atlas, Objective Analysis and Statistics. U.S. Department of Commerce, NOAA, NESDIS, NODC, OCL, WDC-A.

Errata Corrige

In Table 1 of P.S. Ridout's article "The Development of Seawater Standards for Dissolved Nutrients" (Issue No. 35, pp. 38–39), the units of marine nutrient concentration are **micro-Molar**. Apologies to the author and readers.

WOCE Young Investigator Workshop

12–30 June 2000, Boulder, CO, USA

Programme

The University Corporation for Atmospheric Research will host the first World Ocean Circulation Experiment (WOCE) Young Investigator Workshop in Boulder, Colorado. The goals of the Workshop are to familiarise Young Investigators with WOCE models, datasets and estimation procedures; to offer intensive hands-on exposure to these models and methods; to build collaborations among junior scientists and more senior WOCE investigators; and finally to generate ideas and projects leading to fundable WOCE synthesis projects. The Workshop will offer a mixture of tutorial lectures on numerical models and estimation procedures, advanced seminars on current WOCE synthesis activities and related projects, and hands-on projects emphasising current practices in large-scale modelling and estimation.

Organisation

An Organising Committee composed of representatives from the university and research community is co-ordinating the workshop. Members of the Organising Committee include Carl Wunsch from Massachusetts Institute of Technology, Dale Haidvogel from Rutgers University, Robert Hallberg from the Geophysical Fluid Dynamics Laboratory, and Nelson Hogg from Woods Hole Oceanographic Institution. The Organising Committee has the responsibility for programme development and applicant screening.

Drs Wunsch and Haidvogel are the main lecturers for the Workshop. Special speakers also include Lynne Talley (Scripps Institution of Oceanography), Aike Beckmann (Alfred-Wegener Institut für Polar- und Meeresforschung), Frank Bryan (National Center for Atmospheric Research), Ichiro Fukumori (Jet Propulsion Laboratory), and Detlef Stammer (Massachusetts Institute of Technology).

Lectures will be presented in the morning, with free time in the early afternoon for computer demonstrations and/or independent projects, and lastly, a late-afternoon seminar devoted to examples of WOCE-related applications. Workstations will be provided to allow participants to construct and run forward and inverse models, to try various assimilation methods, and in general to be able to experiment with the course elements.

Two of the organisers will provide a series of morning lectures, and will be present at the Workshop for its entire three-week duration. Four or five additional faculty will be in residence at the Workshop for approximately one week each, and are responsible for giving two or three guest lectures on relevant topics. All faculty will participate in the formulation of project topics suitable for pursuit by the Young Investigators. Lecture notes will be prepared by the students working interactively with the lecturers, and distributed following the conclusion of the workshop.

Participants and support

It is anticipated that approximately 20 scientists will participate in this programme. Participants are expected mainly to be recent PhDs in an oceanographic subject, but students within about a year of completion of their doctorates will also be considered, as will more senior scientists with an interest in learning these techniques. Each participant will receive air travel, lodging and per diem. Participants will be housed in University of Colorado dormitories and will be invited to several planned social events during the workshop. Breakfast is served at the dormitories each day and some lunches and dinners will be provided.

Application procedures

To apply, please send a letter of application stating your interest in the WOCE AIMS. The application materials should include:

- Covering letter stating name of this workshop
- Resume including publications, fellowships, awards
- Transcripts and/or PhD thesis abstract and title
- Names and addresses of three recommendations from faculty members who know your work well. (Applicant should request that letters be sent to UCAR by the application deadline.)
- One to two page statement explaining your interests and qualifications for participation in this programme.

The deadline for applications is 15 March 2000. Application materials should be sent directly to:

UCAR Visiting Scientist Programs
P.O. Box 3000
Boulder, CO 80307-3000
USA.

Invitations will be mailed beginning 1 April 2000.

This workshop is being sponsored by the National Science Foundation (Division of Ocean Sciences) and the NASA (Polar Programs).

Visit the Web site: http://www.vsp.ucar.edu/ for more information.

The WOCE International Newsletter is published by the WOCE International Project Office.

Editor:
Roberta Boscolo

Compilation and layout:
Sheelagh Collyer

The International WOCE Newsletter is distributed free-of-charge upon request thanks to the funding contributions from France, Japan, UK, and WCRP.

This Newsletter provides a means of rapid reporting of work in progress related to the Goals of WOCE as described in the WOCE Scientific and Implementation Plan.

Requests to be added to the mailing list and changes of address should be sent to:
WOCE IPO
Southampton Oceanography Centre
Empress Dock
Southampton SO14 3ZH
United Kingdom
Tel. +44 23 8059 6205
Fax. +44 23 8059 6204
e-mail: woceipo@soc.soton.ac.uk

Contents of past issues together with the electronic PDF version can be found at:
http://www.soc.soton.ac.uk/OTHERS/woceipo/acrobat.html

Articles, letters, announcements and reviews are welcome and should be addressed to the editor.

Printed by Technart Ltd.
Southern Road
Southampton SO15 1HG
United Kingdom.

If undelivered please return to:

WOCE IPO
Southampton Oceanography Centre
Empress Dock
Southampton SO14 3ZH
United Kingdom.

CONTENTS OF THIS ISSUE